

ASSOCIATION OF AN ELECTRICAL NETWORK WITH DIGITAL
COMPUTERS FOR DETERMINATION OF ELECTRON TRAJECTORIES
Application to Ionic Propulsion.

Christian Lérin

N 65-21628

(ACCESSION NUMBER)
782
(PAGES)
(NASA CR OR TMX OR AD NUMBER)

(TRU)

(CODE)

28
(CATEGORY)

Translation of "Association du réseau électrique et des calculatrices
arithmétiques pour la détermination des trajectoires
électroniques. Application a la propulsion ionique"
Office National d'Études et de Recherches Aéronautiques
Chatillon-sous-Bagneux, France, [ONERA TN-73]

GPO PRICE \$

OTS PRICE(S) \$

Hard copy (HC) \$5.00

Microfiche (MF) \$1.25

NATIONAL AERONAUTICS AND SPACE ADMINISTRATION
WASHINGTON NOVEMBER 1964

ASSOCIATION OF AN ELECTRICAL NETWORK WITH DIGITAL
COMPUTERS FOR DETERMINATION OF ELECTRON TRAJECTORIES

Application to Ionic Propulsion

by

Christian Lerin

ASSOCIATION OF AN ELECTRICAL NETWORK WITH DIGITAL COMPUTERS FOR DETERMINATION OF ELECTRONIC TRAJECTORIES. APPLICATION TO IONIC PROPULSION. (Association du réseau électrique et des calculatrices arithmétiques pour la détermination des trajectoires électroniques. Application à la propulsion ionique.) C.Lérin. Office National d'Etudes et de Recherches Aérospatiales (ONERA TN-73), 1963.

21628

#137

In an ionic propulsor, determination of the trajectories of the particles from the emitting electrode is required to define the efficiency and - if necessary - to modify the relative configuration of the electrodes. For solving this problem, an iterative calculation method, combining analog and digital computers, is presented: The electric potential inside the drive is simulated by the voltage of a resistance network whose elements and boundary conditions are adjusted, while the trajectories and the space charges are defined from the voltage distribution by means of a digital computer. The principle of the method is checked on an analytically computable example, after which a special design of an axially symmetrical drive is described.

Fuller

TABLE OF CONTENTS

	Page
SYMBOLS	vi
INTRODUCTION	1
CHAPTER I - Local Equations of Stationary Fields and their Application	6
1.1 - Local Equations of Stationary Fields	6
1.2 - Differential Equation of Trajectories	8
1.3 - Analog Solution of Poisson's Equation	10
1.3.1 - Relations with Finite Differences	10
1.3.2 - Electrical Networks	11
1.4 - Solution of the Differential Equation of Trajectories on Digital Computers	14
1.5 - Calculation of the Space Charge	17
1.6 - Iterative Solution Method	19
CHAPTER II - Limit Conditions	22
2.1 - Physical Limit Conditions	22
2.1.1 - On the Electric Potential	22
2.1.2 - On the Initial Velocity of Electric Particles ..	24
2.1.2.1 - Zero Velocity U_0	24
2.1.2.2 - Nonzero Velocity U_0	27
2.1.3 - Influence of the Emitter Shape on Calculation of the Space Charge	27
2.1.3.1 - Spherical Emitter	28

* Numbers in the margin indicate pagination in the original foreign text.

	Page
2.1.3.1.1 - Zero Initial Velocity	29
2.1.3.1.2 - Nonzero Initial Velocity	30
2.1.3.2 - Plane Emitter	30
2.2 - Analog Representation of the Limit Conditions	31
2.2.1 - Dirichlet Problem	31
2.2.2 - Neumann Problem	35
2.2.2.1 - Case of the One-Dimensional Problem	35
2.2.2.2 - Case of the Problems of Revolution	36
CHAPTER III - Analog Realization	38
3.1 - Electrical Network	38
3.2 - Cutting of the Domain	39
3.3 - Electric Feed of the Network	40
3.4 - Application of Current: Method of High Resistances	42
CHAPTER IV - Application to the Three-Dimensional Problem of Axial Symmetry	45
4.1 - Verification of the Method on the Theoretical Case of a Plane Diode	45
4.1.1 - Theoretical Investigation	45
4.1.2 - Solution of Poisson's Equation at the Electrical Network	46
4.1.3 - Solution Methods	49
4.1.3.1 - First Method	50
4.1.3.2 - Second Method	53
4.1.3.3 - Third Method	54
4.2 - Application of the Various Methods to the Revolution Problem	56

	Page
4.2.1 - Laplace's Field	57
4.2.2 - Poisson's Field	58
4.2.2.1 - First Method	58
4.2.2.2 - Second Method	60
4.2.2.3 - Third Method	61
CHAPTER V - Estimation of Errors	64
5.1 - Errors Linked to the Network	64
5.1.1 - Cutting Errors	64
5.1.2 - Errors of Material Limitation	68
5.1.3 - Electric Errors	70
5.1.4 - Errors of Quantification	70
5.2 - Errors Due to Computation on Digital Computers ...	71
5.3 - Errors Introduced by the Method of Calculating the Space Charge	73
CONCLUSION	79
APPENDIX I	82
APPENDIX II	88
Bibliography	92
Tables I to XIV	96 - 105
Field I	106
Field II	107
Charts I to IV ₁₉	108 - 132
Figures 1 to 53	133 - 168

SYMBOLS

1 - GEOMETRY OF THE ELECTROSTATIC PROPULSOR:

- r, θ, z cylindrical coordinates
 R radius of the spherical emitter
 d distance between emitter and accelerating electrode
 h_0 height of a spherical segment

2 - KINEMATIC QUANTITIES:

- \vec{U} velocity of the electric particle
 u, v, w components of \vec{U}
 \vec{Y} acceleration of the electric particle
 t time
 λ constant (theorem of living forces)
 $r' = \frac{dr}{dz}$
 $r'' = \frac{d^2 r}{dz^2}$
 U_0 initial velocity of the electric particle
 r_0, z_0 initial coordinates of a trajectory
 r'_0 initial slope of a trajectory
 $\alpha = \sqrt{\frac{2e}{m}} V_s$ maximum velocity of an electric particle

3 - ELECTRIC QUANTITIES:

- V electric potential
 ρ space charge
 ϵ_0 absolute permittivity of the void

\vec{E}	electric field
\vec{E}'	electric field induced by the space charge
\vec{D}	electrostatic induction
V_a	accelerating potential
m	mass of the electric particle
q	charge of the electric particle
e	elementary charge of an electron
j_0	ionic emission density, in amp/m ²
j_s	emission density at saturation
χ	surface density of emission or number of particles emitted per second and per unit surface

p.2

4 - ANALOG QUANTITIES:

Φ	analog potential ("analog field")
k	analog coefficient defined by $\Phi = kV$
$\varphi = \Phi_P - \Phi_L$	analog potential, created by the space charge
$\frac{\alpha p}{j_0}$	reduced space charge
E, E'	electrodes
C	electric conductances
$\nu = -k\lambda$	constant
$\Delta r, \Delta z$	cutting step in direction of the axes r and z
i_0	intensity applied to one node of the network
R^*, R_j, R_n	electric resistances
R	variable resistance
R_v	true resistance
i_p, i_L, i_φ	intensity discharged by the emitting electrode

5 - SUBSCRIPTS:

e, f, a	quantities related to the emitting, focusing, and accelerating electrodes
o	referring to a node of the network
L, P	quantities of the solutions of Laplace's and Poisson's equations
i, j, l	indices of position and summation
g	quantities referring to a grid

6 - MISCELLANEOUS:

p.3

(V)	volume	
$(\Sigma), (S)$	surface	
$d\tau, d\sigma$	elements of volume, of surface.	
$x, y; X, Y$	auxiliary coordinates	
ξ, η, ζ	auxiliary coordinates	
\vec{n}	vector normal to a surface	
$\vec{\tau}$	vector tangent to a curve	
δ	thickness of the beam	
Δ	increment	
Δ	Laplacian operator	
T	absolute temperature	
Log	Napierian logarithm	
\log	decimal logarithm	
I	intensity	
$r_0, r_1, r_2, \rho_1^*, \rho_2^*$	radii	
(Γ)	boundary of a domain.	$E\%, e\%$ partial, total errors.
R_0	error introduced by the method of finite differences	

INTRODUCTION

Electronic optics and its technical applications involve a study of the motion of an electron beam in an electric field, produced by electrodes brought to a given voltage. The problem is divided into two parts: first, definition of the distribution of the voltage V and, then, determination of the electronic trajectories in the thus defined electrostatic field.

In certain cases, the function V can be obtained by using conformal geometry or methods based on certain expansions in series (Bibl. 19, 20, 21, 22) but, in general, the problem cannot be solved directly. Then, for determining the voltage chart, numerical approximation methods (Bibl. 23, 24, 25), graphic methods (Bibl. 26), or - more generally - analog procedures are used of which the most practical, and probably the most accurate one, requires an electrolytic cell.

In an electrolyte, for permanent operation, the potential V verifies the Laplace equation $\Delta V = 0$. The same holds true for the inside of a vacuum tube, where the space charge can be neglected. This approximation and the characteristics of the Laplace equation were used for studying, on an enlarged model, in the electrolytic cell the voltage distribution taking place in a vacuum tube. Unfortunately, in numerous cases, of interest, this method constitutes only a very rough first approximation, specifically in the vicinity of a cathode operating under space charge.

For bodies of revolution and in the case in which the electrons travel in the vicinity of the axis, their velocity making an infinitely small angle with this axis (Gaussian approximation of optics), it is readily possible to determine the electronic trajectories by calculation based on the voltage distribu-

tion V. Various authors (Bibl.27, 28) have developed complicated equipment which permits an automatic tracing of the trajectories, with satisfactory accuracy. More recently, other authors (Bibl.1,5), invented simpler equipment which also gave satisfactory results. However, the graphical methods, compiled by Musson-Genon (Bibl.1), are useless if the initial velocity of the electric corpuscles is zero.

The electrostatic interactions, existing between the charged particles of a beam, influence the voltage distribution and thus also the shape of the electronic trajectories. The voltage distribution V , in the zone occupied by the beam, thus is controlled by Poisson's equation $\Delta V = -\rho/\epsilon_0$.

A study made by the C.N.E.T. (Bibl.2) develops an interesting solution method for Poisson's equation. By means of integrals, one obtains the voltage and the electric field produced, at a given point P , by the charges placed at a point M or contained in a sector of the beam limited by a curve Γ . The semi-analog process requires determination, in the electric cell, of the electric field E_L on the cathode. The computations appear long and involved for simple electrode shapes, which hardly makes it desirable to generalize them for more complex shapes.

R.Fox (Bibl.3), in studying vacuum tubes of revolution, used a paper conductor whose resistance is uniform in one direction and inversely proportional to the distance in the orthogonal direction. The direct injection into the paper of the intensities representing the space charge obviously increases the inaccuracy of the method, which might lead specifically to a roughening of the problem.

G.R.Brewer, J.E.Etter, and J.R.Anderson (Bibl.4) have developed a complex unit which, on the basis of data collected in a galvanometric tank, automat-

ically plots the trajectories and computes the space charge. The charge is directly simulated in the plane-bottom cell, by injecting electric currents. This process poses complex technical problems which apparently have not yet been solved in France.

R.Musson-Genon (Bibl.1) proposes an elegant method for solving the Poisson equation, using a suitably shaped bottom of the cell and also operating by successive approximations (the space charge ρ being connected at the height of the electrolyte). However, this method requires a bothersome and complicated shaping of the cell bottoms at each approximation and presents serious difficulties in the vicinity of the emitting electrode.

The solution of Poisson's equation by means of a resistive network can proceed in two manners: direct treatment of the expression $\Delta V + \rho/\epsilon_0 = 0$ by modifying, at each approximation, the resistance values in order to take the space charge into consideration (which compares to a modification of the height of the electrolyte in a tank), or else thorough study of the equation $\Delta V = -\rho/\epsilon_0$, in which the first term is represented (once and for all) by fixed resistances while the second term is simulated by an injection of current into each node inside of the electron beam. We have adopted this latter solution.

In a first phase, an approximation of the "Poissonian" is obtained by neglecting the space charge ($\rho = 0$); in a second phase, the voltage readings, made on the network are used for calculating, on a digital computer, the corresponding trajectories and space charge.

The obtained results permit defining a new approximation of the Poissonian and approaching the second iteration, and so forth until convergence is reached.

The computation method described in the present paper is then applied to

ionic propulsion. This (Bibl.29), based on the electrostatic acceleration of electrically charged particles, requires the following:

- power generators;
- ion sources, each represented by a feed of propergol and an ionizing device;
- systems of driving electrodes, generally comprising focusing, accelerating, and decelerating electrodes;
- electron guns for obtaining a neutralization of the beams.

The investigation made on the electrical network specifically requires a perfection of the ionization. This perfection must be obtained in practical work (Bibl.3,4,30,31) since otherwise the presence of nonionized atoms may result in collisions with ions and, consequently in a breakdown of the motor.

On striking the accelerating electrode, the ions produce there an erosion which must be minimized as much as possible. Consequently, the focusing of the beam must be extremely accurate so that the operating time of the motor will be at least several days if not several months.

If the beam of particles ejected by the astronave is not electrically neutral, the propulsor becomes negatively charged (since it yields positive particles) until its potential prevents the departure of new ions. To neutralize the beam it is sufficient to inject electrons downstream of the accelerating electrode, in which case the field of the space charge attracts the electrons to inside the ion beam. To prevent a return of the electrons toward the source of positive particles, it is sufficient to insert an electrode known as the decelerating type. In first approximation, we will neglect the influence of this neutralization, assuming that it has practically no influence on the shape of the trajectories in the vicinity of the emitter.

In the first Part of this report, the equations treating the physical problem are compiled before describing the method of analog solution. The differential equation of the trajectories is solved on digital computers of the Gamma AET type, by the Runge-Kutta method of fourth-order integration. The transformation of the triple integral $\int_V \text{div}(\rho \vec{U}) = 0$ is a surface integral which permits a step-by-step calculation of the space charge, taking the elementary current tubes formed by the beam trajectories into consideration.

The second Chapter discusses the electric and kinematic limit conditions and their representation on the electrical network and on digital computers.

The third Part is devoted to analog realization. The network is composed of several insulating panels which are readily interconnected, each consisting of ten rows of twenty nodes each. The domain under study comprises about 700 nodes. The electric resistance, installed in the pin of an electric plug, is placed between two successive nodes. The electric feed of the network is done by direct current, since practical experience has shown that the high resistances, used for application of electric currents that simulate the space charge, result in considerable dephasing when alternating current is used.

Before considering, in Chapter IV, application of the method to the three-dimensional case of axial symmetry, the problem of the plane diode is first treated in order to check on the rapidity of convergence of the iteration process. Several methods are developed so as to obtain a voltage distribution corresponding to a saturated emission, together with the value of the resultant emission density.

An estimation of the errors in the last Chapter indicates that, although some of these errors can be classified, it is quite difficult to make an evaluation in the case of others.

CHAPTER I

LOCAL EQUATIONS OF STATIONARY FIELDS
AND THEIR APPLICATION1.1 Local Equations of Stationary Fields

For a continuous distribution of electric charges, having a volume density ρ , the classical continuity equation is written as follows:

$$\frac{\partial \rho}{\partial t} + \operatorname{div}(\rho \vec{U}) = 0 \quad (1)$$

where \vec{U} denotes the velocity vector of the particles contained per volume element $d\tau$.

Since the electric field is stationary, eq.(1) reduces to

$$\boxed{\operatorname{div}(\rho \vec{U}) = 0} \quad (2)$$

assuming that $M(\xi, \eta, \zeta)$ represents a point of the volume (V) . Since the charge of the volume $d\tau$ is $\rho d\tau$, the electric field \vec{E} at a point $N(x, y, z)$ will be

$$\vec{E} = \frac{1}{4\pi\epsilon_0} \int_{(V)} \rho \frac{\vec{r}}{r^3} d\tau = -\frac{1}{4\pi\epsilon_0} \int_{(V)} \rho \operatorname{grad}_N \left(\frac{1}{r} \right) d\tau \quad (3)$$

if $\vec{r} = \vec{MN}$.

The electric field is derived from a potential, like any field of central forces:

$$\vec{E} = - \overrightarrow{\text{grad}} V = - \vec{\nabla} V \quad (4)$$

The electric voltage is expressed by the integral

$$V = \frac{1}{4\pi\epsilon_0} \int \frac{\rho}{r} d\tau \quad (5)$$

On introducing the electrostatic induction vector $\vec{D} = \epsilon_0 \vec{E}$ and taking eq.(3) into consideration, we obtain

$$\text{div } \vec{D} = \rho \quad (6)$$

A transformation of eq. (6), taking eq.(4) into consideration, leads to the Poisson equation:

p.11

$$\Delta V = - \frac{\rho}{\epsilon_0} \quad (7)$$

Since the electrostatic drive revolves about the axis OZ, the cylindrical coordinates (r, θ , z) are adopted in all computations in order to make use of the symmetry.

The space charge exerts a double action:

1. The charge creates a radial centrifugal electric field E'_r which increases the angle of aperture of the beam (Fig.1).

In order to overcome this divergence, a third electrode known as a "focusing" electrode must be used, whose input diaphragm must be sufficiently large to permit passage of the beam.

2. The space charge creates an axial field E'_z , opposed to the accelerating field and resulting in a limitation of the current density that the beam is able to carry.

These two effects combine to give rise to a voltage $V_P - V_L$ due to the space charge and also satisfying the Poisson equation because $\Delta V_L = 0$.

1.2 Differential Equation for the Trajectories

The basic equation of dynamics, applied to electric particles of mass m , charge q , and subjected to the accelerating field \vec{E} , is written as follows:

$$m \vec{\gamma} = q \vec{E} = - q \vec{\text{grad}} V \quad (8)$$

neglecting the mass forces.

Assuming that u, v, w are the components of the velocity \vec{U} in cylindrical coordinates, we have p.12

$$\gamma_r = \frac{\partial u}{\partial t} + \vec{U} \cdot \vec{\text{grad}} u$$

Since the field \vec{E} is stationary and taking into consideration the axial symmetry, considerable simplifications are obtained:

$$\frac{\partial \vec{U}}{\partial t} = 0 \quad ; \quad v = 0$$

Consequently,

$$\begin{cases} m \left(u \frac{\partial u}{\partial r} + w \frac{\partial u}{\partial z} \right) = -q \frac{\partial V}{\partial r} \\ 0 = \frac{\partial V}{\partial \theta} \\ m \left(u \frac{\partial w}{\partial r} + w \frac{\partial w}{\partial z} \right) = -q \frac{\partial V}{\partial z} \end{cases} \quad (9)$$

Let us assume that

$$r' = \frac{dr}{dz}$$

$$\left[r'' = \frac{d^2 r}{dz^2} \right]$$

Since

$$u = \frac{dr}{dt} = \frac{dr}{dz} \cdot \frac{dz}{dt} = r' w$$

It follows that

$$\begin{cases} m \left(r'^2 w \frac{\partial w}{\partial r} + w^2 r'' + w r' \frac{\partial w}{\partial z} \right) = -q \frac{\partial V}{\partial r} \\ m \left(w r' \frac{\partial w}{\partial r} + w \frac{\partial w}{\partial z} \right) = -q \frac{\partial V}{\partial z} \end{cases}$$

Let

$$m w^2 r'' = -q \left(\frac{\partial V}{\partial r} - r' \frac{\partial V}{\partial z} \right)$$

The theorem of living forces permits to write

$$\frac{1}{2} m U^2 = -q V + \text{constant.} \quad (10)$$

This latter equation can be obtained also from eqs.(9) and (6).

(10)'

Consequently,
$$m (1 + r'^2) w^2 = -2q V + 2\lambda q$$

p.13

where $2\lambda q$ denote a constant.

Finally, the differential equation for the trajectories is expressed by

$$r'' = \frac{(1 + r'^2) \left(\frac{\partial V}{\partial r} - r' \frac{\partial V}{\partial z} \right)}{2 (V - \lambda)} \quad (11)$$

Since the wanted result is a solution of Poisson's equation for the most general case, the present paper will furnish a method of analog computation, taking all characteristics of the entire unit into consideration (external shape of the electrodes, geometry of the propulsor, initial conditions on the emitted particles, voltages applied to the electrodes).

1.3 Analog Solution of Poisson's Equation

Equation (7) can be written by means of cylindrical coordinates:

$$\frac{\partial^2 V}{\partial r^2} + \frac{1}{r} \frac{\partial V}{\partial r} + \frac{\partial^2 V}{\partial z^2} = -\frac{\rho}{\epsilon_0} \quad (7)'$$

in which the term $\frac{1}{r^2} \frac{\partial^2 V}{\partial \theta^2}$ vanishes because of the symmetry.

Before discussing the analog representation of this equation with partial derivatives by a network of resistances, it is necessary to replace the equation by a relation with finite differences.

1.3.1. Relations with Finite Differences

Let us assume, in the meridian plane, the presence of any grid or lattice (Fig.2) whose sides are parallel to the r axis and to the z axis. To any point of intersection of the two straight lines, forming the lattice, a lattice point or "node" corresponds.

Let us consider a node 0, to which the subscript zero is given, and the "cross" which it forms with the four surrounding nodes (1, 2, 3, 4). Let V_0 , V_1 , V_2 , V_3 , V_4 be the respective values of the function $V(r, z)$ at each of these points and let Δz_1 , Δr_2 , Δz_3 , Δr_4 , be the distances separating the central node from its immediate neighbors (distances which are very short with respect to

p.14

unit length).

From the Taylor formula are derived the following relations, known as "finite-difference relations":

$$\left. \begin{aligned} V_1 - V_0 &= \left(\frac{\partial V}{\partial z} \right)_0 \Delta z_1 + \frac{1}{2} \left(\frac{\partial^2 V}{\partial z^2} \right)_0 \Delta z_1^2 + \frac{1}{6} \left(\frac{\partial^3 V}{\partial z^3} \right)_0 \Delta z_1^3 + \frac{1}{24} \left(\frac{\partial^4 V}{\partial z^4} \right)_0 \Delta z_1^4 + \dots \\ V_2 - V_0 &= \left(\frac{\partial V}{\partial r} \right)_0 \Delta r_2 + \frac{1}{2} \left(\frac{\partial^2 V}{\partial r^2} \right)_0 \Delta r_2^2 + \frac{1}{6} \left(\frac{\partial^3 V}{\partial r^3} \right)_0 \Delta r_2^3 + \frac{1}{24} \left(\frac{\partial^4 V}{\partial r^4} \right)_0 \Delta r_2^4 + \dots \\ V_3 - V_0 &= - \left(\frac{\partial V}{\partial z} \right)_0 \Delta z_3 + \frac{1}{2} \left(\frac{\partial^2 V}{\partial z^2} \right)_0 \Delta z_3^2 - \frac{1}{6} \left(\frac{\partial^3 V}{\partial z^3} \right)_0 \Delta z_3^3 + \frac{1}{24} \left(\frac{\partial^4 V}{\partial z^4} \right)_0 \Delta z_3^4 + \dots \\ V_4 - V_0 &= - \left(\frac{\partial V}{\partial r} \right)_0 \Delta r_4 + \frac{1}{2} \left(\frac{\partial^2 V}{\partial r^2} \right)_0 \Delta r_4^2 - \frac{1}{6} \left(\frac{\partial^3 V}{\partial r^3} \right)_0 \Delta r_4^3 + \frac{1}{24} \left(\frac{\partial^4 V}{\partial r^4} \right)_0 \Delta r_4^4 + \dots \end{aligned} \right\} \quad (12)$$

From which it follows that

$$r \Delta r^2 (\Delta V)_0 = r \frac{\Delta r^2}{\Delta z^2} \left\{ (V_1 - V_0) + (V_3 - V_0) \right\} + \left(r + \frac{\Delta r}{2} \right) (V_2 - V_0) + \left(r - \frac{\Delta r}{2} \right) (V_4 - V_0) \quad (12)'$$

by limiting the calculation to the terms of second order and by adopting a regular meshing with steps Δr and Δz .

Consequently, it seems that the second term of eq.(12)' can be represented by a network of pure resistances.

1.3.2. Electrical Networks

Let us consider an electrical network formed by the conductances C_1 , C_2 , C_3 , and C_4 , arranged in accordance with the preceding lattice (Fig.3).

Kirchhoff's law of networks

$$\sum_{j=0}^{j=4} i_j = 0 \quad (13)$$

(where the current intensity i_0 is applied to the network at the node 0) can be transformed as follows:

$$\sum_{j=1}^{j=4} C_j (\phi_j - \phi_0) + i_0 = 0$$

where ϕ denotes the analog potential function, treated at the network. Expansion in a Taylor series and limitation of the calculation to terms of the second order will yield

$$\begin{aligned} & i_0 + \left(\frac{\partial \phi}{\partial z} \right)_0 (C_1 \Delta z_1 - C_3 \Delta z_3) + \left(\frac{\partial \phi}{\partial r} \right)_0 (C_2 \Delta r_2 - C_4 \Delta r_4) \\ & + \left(\frac{\partial^2 \phi}{\partial z^2} \right)_0 \left(\frac{C_1 \Delta z_1^2 + C_3 \Delta z_3^2}{2} \right) + \left(\frac{\partial^2 \phi}{\partial r^2} \right)_0 \left(\frac{C_2 \Delta r_2^2 + C_4 \Delta r_4^2}{2} \right) = 0 \end{aligned} \quad (14)$$

Let us adopt a regular meshing, following the two axes:

$$\Delta z_1 = \Delta z_3 = \Delta z$$

$$\Delta r_2 = \Delta r_4 = \Delta r$$

The identity of eqs.(7) and (14) requires that

$$\begin{aligned} & C_1 = C_3 \quad \phi = kV \\ & \frac{\Delta r^2}{2} (C_2 + C_4) = r \Delta r (C_2 - C_4) = \frac{\Delta z^2}{2} (C_1 + C_3) = \frac{i_0 \epsilon_0}{k \rho} \end{aligned} \quad (15)$$

Let

$$C_1 = C_3 = C_z$$

$$C_4 = C_r - \frac{\Delta C_r}{2}$$

$$C_2 = C_r + \frac{\Delta C_r}{2}$$

A solution of the system of equations (15) leads to the following results:

$$\frac{\Delta C_r}{C_r} = \frac{\Delta r}{r} \rightarrow \boxed{C_r = \beta r} \quad (16)$$

$$C_z = C_r \frac{\Delta r^2}{\Delta z^2} \rightarrow \boxed{C_z = \beta r \frac{\Delta r^2}{\Delta z^2}} \quad (17)$$

$$\boxed{i_0 = \frac{k \rho C_z \Delta z^2}{\epsilon_0}} \quad (18)$$

The finite-difference method, applied to the electric network, leads to the following conclusions:

The conductances C_r vary linearly with the distance r .

The conductances C_z are constant along a parallel to the axis of the electrostatic drive.

The intensity i_0 is proportional to the space charge over a line $r = \text{const.}$

The direct electric analogy between the voltage V of the physical field and the potential ϕ obtained at the network is expressed by

p.16

$$\phi = kV \quad (19)$$

where the constant k depends in a general manner on the voltages applied to the

electrodes and on the experimental scale. The electric intensities, applied to the network, are therefore equal to

$$\frac{k \rho C_z \Delta z^2}{\epsilon_0}$$

An investigation of formulas (16) and (17) shows that the resistances become infinite near the axis. This leads to a particular difficulty; to overcome this difficulty, certain authors recommend the method of a diagonal network (Bibl.7). We preferred to use the method of "true resistances" combined with the method of "hollow cylinders" (Appendix I).

The current intensity, applied to the network at each node is a function of the local charge density ρ . A computation of this (see Section 1.5) requires knowledge of the trajectories of the electric particles.

1.4 Solution of the Differential Equation of Trajectories on Digital Computers

The differential equation, written in the form of

$$r'' = \frac{(1+r'^2) \left(\frac{\partial \phi}{\partial r} - r' \frac{\partial \phi}{\partial z} \right)}{2(\phi + \nu)} \quad (20)$$

can be solved on digital computers by the Runge-Kutta method of fourth-order integration (Bibl.9,10).

Before this, on the basis of the voltage card ϕ obtained at the electric network, the partial derivatives $\frac{\partial \phi}{\partial r}$ and $\frac{\partial \phi}{\partial z}$ must be calculated. This computation is made by a method of parabolic interpolation, of which a brief discussion is given here for better understanding of the remainder of the present discussion.

Let X_{i-1} , X_i , X_{i+1} be three abscissa points where a function Y assumes, respectively, the values Y_{i-1} , Y_i , Y_{i+1} . The values y_i of the function, at a point of the abscissa x_i located in the interval AB , with A and B being the respective centers of $X_{i-1}X_i$ and X_iX_{i+1} (Fig.4), as well as its derivative $\left(\frac{\partial Y}{\partial X}\right)_{x_i}$ are obtained by the equations of parabolic interpolation:

$$y_i = \frac{(x_i - X_i)(x_i - X_{i+1})}{(X_{i-1} - X_i)(X_{i-1} - X_{i+1})} Y_{i-1} + \frac{(x_i - X_{i+1})(x_i - X_{i-1})}{(X_i - X_{i+1})(X_i - X_{i-1})} Y_i + \frac{(x_i - X_{i-1})(x_i - X_i)}{(X_{i+1} - X_{i-1})(X_{i+1} - X_i)} Y_{i+1} \quad (21)$$

and, deriving with respect to x_i ,

$$\left(\frac{\partial Y}{\partial X}\right)_{x_i} = \frac{\partial y_i}{\partial x_i} = \frac{2x_i - (X_i + X_{i+1})}{(X_{i-1} - X_i)(X_{i-1} - X_{i+1})} Y_{i-1} + \frac{2x_i - (X_{i+1} + X_{i-1})}{(X_i - X_{i+1})(X_i - X_{i-1})} Y_i + \frac{2x_i - (X_{i-1} + X_i)}{(X_{i+1} - X_{i-1})(X_{i+1} - X_i)} Y_{i+1} \quad (22)$$

Formula (21) represents the equation of a parabola passing through the three points (X_{i-1}, Y_{i-1}) , (X_i, Y_i) , (X_{i+1}, Y_{i+1}) . It should also be noted that the parabolic interpolation gives an erroneous result in the case in which the vertex of the cone (21) is located exactly in the interval $X_{i-1} X_i$ to which x_i belongs (Fig.4); this unfavorable conjuncture is the less likely to occur the smaller the intervals.

Let us consider, in the meridian plane (Z, R) , a lattice forming four rectangles at whose vertices the function ϕ , representing the analog electric potential, takes the nine values $\phi_1, \phi_2, \dots, \phi_9$ (Fig.5). The centers of these rec-

tangles define another quadrilateral ABCD.

Let us assume a point of coordinates (z_i, r_j) located inside the rectangle ABCD and let us determine the following at this point:

$$\Phi(z_i, r_j)$$

$$\frac{\partial \Phi}{\partial R}(z_i, r_j)$$

derived in direction of the R-axis

$$\frac{\partial \Phi}{\partial Z}(z_i, r_j)$$

derived in direction of the Z-axis

By directly applying the parabolic interpolation formulas the procedure is as follows:

- Calculation of $\Phi(H), \Phi(I), \Phi(J), \Phi(E), \Phi(F), \Phi(G)$

by means of eq. (21), based on the values of the field at three points located, respectively, on the axes

$$R_{j-1}, R_j, R_{j+1}, Z_{i-1}, Z_i \text{ et } Z_{i+1}$$

- Calculation of $\Phi(z_i, r_j)$ by application of the same formula to the three values $\Phi(H), \Phi(I), \Phi(J)$. This selection of the points H, I, J is completely arbitrary: the points E, F, and G would furnish just as acceptable a value for $\Phi(z_i, r_j)$.

- Calculation of $\frac{\partial \Phi}{\partial R}(z_i, r_j)$ and of $\frac{\partial \Phi}{\partial Z}(z_i, r_j)$ by means of eq.(22) and, respectively, of the values $\Phi(H), \Phi(I), \Phi(J)$ and $\Phi(E), \Phi(F), \Phi(G)$.

Since the initial conditions of a trajectory, i.e., the r_0' and the coor- /19

ordinates z_0, r_0 of the point of departure M_0 are known, it is possible to calculate r''_0 from eq.(20), taking into consideration the results obtained by the parabolic interpolation of the values of the field Φ obtained at nine points surrounding M_0 . The Runge-Kutta integration method thus permits obtaining the quantities r' and r'' in steps;

- at the point $z_0 + \Delta z$, if the values at point z_0 are known;
- at the point $z_0 + 2\Delta z$, if the values at point $z_0 + \Delta z$ are known.

1.5 Calculation of the Space Charge

The research on trajectories (electronic or ionic) on the basis of the configuration of the electric field having been completed, the density of the local charge ρ must satisfy, at all points of the field, the equation of continuity (2). (Outside of the particle beam, we consequently will have $\rho = 0$.)

Let us assume three closely-spaced trajectories 1, 2, 3, (Fig.6).

Let us then consider the annular volume (γ), delimited by the extreme trajectories 1 and 3 and by the planes $z = z_i$ and $z = z_{i+1}$.

For a current tube, Green's formula will be written as

$$\iiint_{\gamma} \operatorname{div}(\rho \vec{U}) d\tau = \iint_{\Sigma} \rho \vec{U} \cdot \vec{n} d\sigma$$

where \vec{n} denotes the normal, outside of the surface (Σ), limiting the domain (γ).

Taking eq.(2) into consideration, we obtain

$$\iint_{\Sigma} \rho \vec{U} \cdot \vec{n} d\sigma = 0 \quad (23)$$

On the lateral surface of the current tube, the velocity vector \vec{U} is nor-

mal to \vec{n} . Consequently, the contribution of this boundary is zero.

Let P_j and P_l be two points appearing on the extreme surfaces (planes) Σ_i and Σ_{i+1} . Then, eq.(23) is transformed in accordance with

/20

$$\iint_{\Sigma_i} \rho(P_j) \vec{U}(P_j) \vec{n}_j d\sigma_j + \iint_{\Sigma_{i+1}} \rho(P_l) \vec{U}(P_l) \vec{n}_l d\sigma_l = 0 \quad (23)'$$

where M_i and M_{i+1} denote the points located on the intermediate trajectory 2;

we assume, in first approximation, that:

- the fields of the velocity vectors $\vec{U}(P_j)$ and $\vec{U}(P_l)$, at each point of the sections Σ_i and Σ_{i+1} , are represented by the uniform fields $\vec{U}(M_i)$ and $\vec{U}(M_{i+1})$.

- the fields of local space charge $\rho(P_j)$ and $\rho(P_l)$ are also replaced by the uniform fields $\rho(M_i)$ and $\rho(M_{i+1})$.

Then, eq.(23)' is simplified into

$$\rho(M_i) \iint_{\Sigma_i} \vec{U}(M_i) \vec{n}_i d\sigma_j + \rho(M_{i+1}) \iint_{\Sigma_{i+1}} \vec{U}(M_{i+1}) \vec{n}_{i+1} d\sigma_l = 0$$

Let

$$\rho(M_i) U(M_i) \cos \varepsilon_i \iint_{\Sigma_i} d\sigma_j = \rho(M_{i+1}) U(M_{i+1}) \cos \varepsilon_{i+1} \iint_{\Sigma_{i+1}} d\sigma_l$$

where

$$\cos \varepsilon_i = \frac{1}{\sqrt{1 + tg^2 \varepsilon_i}} \text{ and } \tan \varepsilon_i = - \left(\frac{dr}{dz} \right)_{M_i}$$

Let us assign the subscripts i and $i+1$ to various quantities attached to the points M_i and M_{i+1} .

Finally:

$$\rho_i U_i \frac{1}{\sqrt{1 + r_i'^2}} \iint_{\Sigma_i} d\sigma_j = \rho_{i+1} U_{i+1} \frac{1}{\sqrt{1 + r_{i+1}'^2}} \iint_{\Sigma_{i+1}} d\sigma_l$$

where

$$\iint_{\Sigma_i} d\sigma_j = \pi (r_3^2 - r_1^2)_i$$

denoting by r_1 and r_3 the radii which correspond to the trajectories 1 and 3 which define the boundary of the plane sections (Fig.6).

From which it follows that

$$\rho_i U_i \frac{(r_3^2 - r_1^2)_i}{\sqrt{1 + r_i'^2}} = \rho_{i+1} U_{i+1} \frac{(r_3^2 - r_1^2)_{i+1}}{\sqrt{1 + r_{i+1}'^2}} \quad (24)$$

Equation (24) permits a step-by-step calculation of the space charge ρ (see Chapter II), taking into consideration the form of the emitter and the initial slope of the trajectories. The computation, programmed on the IBM 610 computer, reduces, on the one hand, the time required for solution and, on the other hand, the risk of manual errors.

1.6 Iterative Solution Method

Solution of the Poisson equation obeys the following law:

Since the emitting electrode is rigidly given, an arbitrary form can be given to the other two electrodes (focusing and accelerating) which, a priori, are unknown. The approximation, of the so-called "zero order", consists in determining, at the electric network, the Laplacian field which satisfies

$$\Delta V_L = 0 \quad (25)$$

On the basis of the beam of trajectories, corresponding to this Laplacian field, the computation furnishes a local space charge ρ_0 which, when applied to the network in the form of electric intensity over the intermediary of high resistances, will result in a first-approximation Poissonian field, such that

$$\Delta V_{P_1} = - \frac{\rho_0}{\epsilon_0} \quad (26)$$

An exploitation by digital computers of this second field leads to a new network of trajectories, from which a space charge ρ_1 is determined. The successive approximations satisfy the following equations:

$$\Delta V_{P_2} = - \frac{\rho_1}{\epsilon_0} \quad (27)$$

$$\Delta V_{P_3} = - \frac{\rho_2}{\epsilon_0} \quad (28)$$

In general, each cycle of approximations takes place at constant emission density j_0 (in this respect, two methods will later be proposed, in order to determine the electric potential corresponding to the case of a saturated emission).

A third, more interesting method, permits a definition of the emission density at saturation, by adjusting the value of the parameter j_0 at each approximation, in such a manner that the electric field is canceled at the surface of the emitter.

Convergence of this iteration method is ensured after the third or fourth approximation.

In view of the fact that the final goal is to obtain an optically correct configuration, it is necessary to repeat the cycle of computations with new dimensions of the accelerating and focusing electrodes, wherever the selection of electrode shapes had not furnished a satisfactory result.

CHAPTER II

LIMIT CONDITIONS

The electric potential which, at any point of the domain of definition, satisfies Poisson's equation (7) must, along the boundary, also satisfy the limit conditions of the physical problem.

2.1 Physical Limit Conditions2.1.1 On the Electric Potential

The electric field \vec{E} , produced by keeping the emitting and accelerating electrodes at two different voltages, must accelerate the particles of charge q .

The direct analogy between the physical potential V and the analog potential Φ , tapped at the network, is expressed by the linear relation

$$\Phi = kV \quad (19)$$

The electrical network has the advantage that it is just as easy to treat either of the two problems which may occur in practical use: the electronic problem and the ionic problem. In the first case, in order to obtain extraction and acceleration toward the propulsor exit, it is necessary - according to eq.(8) - that the vector $\overrightarrow{\text{grad}} V$ and thus also the vector $\overrightarrow{\text{grad}} \Phi$ be directed along the perpendicular exterior to the emitting electrode (the charge q being equal to $-e$, where e denotes the elementary charge of an electron) whereas, in

the second case, $\vec{\text{grad}} V$ must follow the interior perpendicular (the charge q of an ion being equal to $+e$).

The limit condition, obeying the direction of $\vec{\text{grad}} V$ thus will be as follows:

Ionic Problem:

$$V_e = V_a \text{ on the emitting electrode}$$

$$V_a = 0 \text{ on the accelerating electrode}$$

where V_a designates the accelerating potential.

Electronic Problem:

It is sufficient to inverse the preceding potentials on the two electrodes.

The focalizing electrode whose role it is to concentrate the particle beam toward the axis of the propulsor, is brought to a certain voltage V_f . In our experiments, we always adopted $V_e = V_f$ so that it would be definitely possible to use the Runge-Kutta integration method. In fact, this method can be used only if the second derivative $\frac{d^2 r}{dz^2}$ does not become infinite, since otherwise this impossibility can be presented in the two cases (11):

$$\frac{dr}{dz} \longrightarrow \text{infinite}$$

$$V - \lambda = 0$$

In order that the ions are sufficiently repulsed, it would actually be sufficient to bring the focalizing electrode to a voltage higher than that of the emitter. However, there is a certain risk involved since it is definite that an equipotential line exists in the field so that $V - \lambda = 0$. If the ion particle encounters this line or approaches it sufficiently, the integration method will become inoperative. To avoid this risk, it is suggested to adopt equal voltages on both emitting and focalizing electrodes.

2.1.2 On the Initial Velocity of Electric Particles

Let U_0 be the initial velocity of the corpuscles which we will, hereafter, assume to be ions. The influence U_0 on the shape of the trajectories in the vicinity of the emitter is expressed in the following results:

/26

2.1.2.1 Zero Velocity U_0

The limit conditions to be satisfied for the electric potential are as follows:

$$\begin{aligned} V_e &= V_f = V_s \\ V_a &= 0 \end{aligned}$$

Equation (10) yields $\lambda = V_s$.

Consequently, the differential equation for the ion trajectories is written as follows:

$$r'' = \frac{(1+r'^2) \left(\frac{\partial V}{\partial r} - r' \frac{\partial V}{\partial z} \right)}{2(V - V_s)} \quad (29)$$

At each point M_0 of the emitting electrode we have exactly $V - V_s = 0$, so that $\frac{d^2 r}{dz^2}$ becomes infinite there. Thus, application of the Runge-Kutta integration method on digital computers is possible only beyond the point M_0 . However, as will be discussed below, integration can be made by using a point M_1 , located, exterior to M_0 on the normal to the emission surface, as the initial point. In fact, let \vec{r} and \vec{n} be the vectors tangent and normal to the electrode (E) at the point M_0 (Fig.7) and let M_1 be a point of the trajectory issuing

from M_0 , very close to this latter.

A function $f(M, t)$ can be developed by limiting the calculation to terms of the second order, in accordance with

$$f(M_1) - f(M_0) = (t_1 - t_0) f'(M_0) + \frac{(t_1 - t_0)^2}{2!} f''(M_0)$$

where f' and f'' denote the successive derivatives with respect to time.

Consequently,

$$\overrightarrow{M_0 M_1} = \Delta t \quad \vec{U}_0 + \frac{\Delta t^2}{2} \quad \vec{\gamma}_0 \quad (30)$$

$\Delta t = t_1 - t_0;$

by assuming that

where \vec{U}_0 and $\vec{\gamma}_0$ represent, respectively, the velocity and acceleration vectors of the ion particles at the point M_0 .

Thus, by definition: $\vec{U}_0 = 0$

On scalar multiplication of the two terms of eq.(30) by \vec{r} , we obtain

$$\vec{r} \cdot \overrightarrow{M_0 M_1} = \frac{\Delta t^2}{2} \cdot \vec{r} \cdot \vec{\gamma}_0 \quad (31)$$

The fundamental equation of dynamics (eq.8) will yield

$$m \vec{\gamma} = - q \overrightarrow{\text{grad } V}$$

Let

$$\vec{\gamma}_0 = - \frac{q}{m} (\overrightarrow{\text{grad } V})_{M_0} \quad (32)$$

from which it follows that

$$\vec{r} \cdot \overrightarrow{M_0 M_1} = - \frac{q \Delta t^2}{2m} \cdot \vec{r} \cdot (\overrightarrow{\text{grad } V})_{M_0} \quad (33)$$

The emitting surface is an equipotential line; the vectors \vec{n} and $(\text{grad } V)_{M_0}$ are colinear. Consequently,

$$\vec{r} \cdot \vec{M_0 M_1} = 0 \quad (34)$$

The point M_1 , therefore, is located on the normal \vec{n} .

Conclusion: The ion trajectories are orthogonal to the emitting surface if the initial velocity of the electric corpuscles is zero.

This statement makes it possible to apply the Runge-Kutta integration method, starting from the initial points M_1 located on different normals to the emitter. The distance $M_0 M_1 = \Delta n$ may vary in a noticeable fashion. The shorter this distance becomes the more will the trajectories approach their real position, but at the same time, the risk of errors due to a poor parabolic extrapolation (see Section 2.2.1) will increase and the integration step will decrease, leading to a much longer total integration time. Consequently, a compromise must be taken into consideration. The check tests made with the ratios $\frac{\Delta n}{\Delta r}$ are equal to 1; 0.5; 0.25; 0.15; 0.10; 0.05, and the different angular coefficients r'_0 show, in a precise case (Laplacien field), that the trajectories, issuing from one and the same point, constitute a sort of "horse tail" whose thickness varies in the same proportion as the quantity $\frac{\Delta n}{\Delta r}$. If we use δ for denoting the distance (Fig.8), for a given abscissa z , between a trajectory with any angular coefficient and the real trajectory of the ion particle, the curves of Charts II₁ and II₂ will give the evolution of this thickness as a function of the ratio $\frac{\Delta n}{\Delta r}$; when extrapolated to the origin, these curves show that δ actually tends toward zero, which would prove that, if it were possible to apply the integration method up to the emitting electrode - and this no matter what the adopted initial slope may be - the resultant trajectories would all coalesce into one,

namely that corresponding to the angular coefficient of the normal to the point M_0 under consideration.

2.1.2.2. Nonzero Velocity U_0

Let a grid G, charged to a potential V_g , create a "preacceleration" of the emitted particles. The geometry of this grid is homothetic to that of the emitting electrode for the case of a spherical segment and translated in the case of a plane emitter (Fig.9). The electric particles are extracted from the emitting electrode at zero velocity. After being accelerated in the space between emitter and grid, the particles reach the grid with a uniform velocity U_0 . Thus, it is sufficient to treat the problem at the network by means of three electrodes: grid, focusing electrode, and accelerating electrode, where the grid plays the role of a source of ions having an initial velocity U_0 .

The physical limit conditions are

$$V_e = V_s ; V_a = 0 ; V_f = V_g ; \text{ with } 0 < V_g < V_s$$

where $U = U_0$ on the grid.

2.1.3 Influence of the Emitter Shape on Calculation of the Space Charge

The equation

$$\frac{\rho_i U_i (r_3^2 - r_i^2)_i}{\sqrt{1 + r_i'^2}} = \frac{\rho_{i+1} U_{i+1} (r_3^2 - r_i^2)_{i+1}}{\sqrt{1 + r_{i+1}'^2}} \quad (24)$$

derived in the first Chapter (see Section 1.5) permits a step-by-step calcula-

tion of the space charge on a given trajectory, taking into consideration the shape of the emitting electrode and the position of two neighboring trajectories (Fig.6).

2.1.3.1 Spherical Emitter

For an emitter having the shape of a spherical segment and assuming that the ion emission density is constant and corresponds to a uniform current density j_0 on the emitter ($j_0 = \chi e$, denoting by χ the surface density of emission, number of particles emitted per second and per square meter), we will have /30

$$\frac{\rho_i U_i \pi (r_3^2 - r_1^2)_i}{\sqrt{1 + r_i'^2}} = j_0 \int_E 2\pi r ds \quad (35)$$

in which case the ions are emitted orthogonally to the boundary (E) (see Section 2.1.2.1).

The integral $\int_E 2\pi r ds$ represents a surface of revolution. In the case of a spherical segment, we have

$$\int_E 2\pi r ds = 2\pi R h_0 \quad (36)$$

with: R = radius of the sphere

$$h_0 = (z_3 - z_1)_0 \quad (37)$$

where z_1 and z_3 denote the initial abscissas of the trajectories 1 and 3.

From this it follows that

$$\rho_i = \frac{2 R h_0 j_0 \sqrt{1 + r_i'^2}}{(r_3^2 - r_1^2)_i U_i} \quad (38)$$

2.1.3.1.1 Zero Initial Velocity

Equation (10) is written as:

$$\frac{1}{2} m U_i^2 = -e (V_i - V_s)$$

where V_s is the potential of the emitter.

Then, eq.(38) becomes

$$\rho_i = \frac{2Rh_o j_o \sqrt{1+r_i'^2}}{(r_3^2 - r_1^2)_i \sqrt{\frac{2e}{m} (V_s - V_i)}} \quad (39)$$

Let us assume that

$$\alpha = \sqrt{\frac{2e}{m} V_s} \quad (40)$$

The dimensionless quantity $\frac{\alpha \rho_i}{j_o}$ is finally expressed by

$$\frac{\alpha \rho_i}{j_o} = \frac{2Rh_o \sqrt{\frac{1+r_i'^2}{1-\frac{V_i}{V_s}}}}{(r_3^2 - r_1^2)_i} \quad (41)$$

Consequently, the evolution of the quantity $\frac{\alpha \rho_i}{j_o}$, reduced space charge (proportional to the space charge), along a trajectory depends on the slope of this trajectory, on the position of adjacent trajectories, on the parameter $2Rh_o$

linked to the geometric form of the emitter and to the cutting adopted on this emitter (total number of annular current tubes used for the calculation of ρ_i in the entire domain), and on the ratio $\frac{V_i}{V_s}$ between the local electric potential V_i and the accelerating potential V_s .

The parameter j_0 remains arbitrary; it is defined without ambiguity in the case in which the emission is saturated and in which the electrostatic field is canceled at the surface of the emitting electrode.

2.1.3.1.2 Nonzero Initial Velocity

In the same manner, the following is obtained

$$\frac{\rho_i}{j_0} = \frac{2Rh_0 \sqrt{\frac{(1+r_i'^2)}{U_0^2 + \frac{2e}{m}(V_g - V_i)}}}{(r_3^2 - r_1^2)_i} \quad (42)$$

2.1.3.2 Plane Emitter

Identical reasoning leads to the following:

$$\frac{\rho_i U_i \pi (r_3^2 - r_1^2)_i}{\sqrt{1+r_i'^2}} = j_0 \int_E 2\pi r dr$$

by assuming the emitter to be similar to a disk of diameter E (Fig.9).

The preceding expression then becomes:

$$\rho_i = \frac{j_0 h_i \sqrt{1 + r_i'^2}}{(r_3^2 - r_i^2)_i U_i} \quad (43)$$

with

$$h_i = \left| r_3^2 - r_i^2 \right|_{z=0} \quad (44)$$

The formulas expressing the quantity $\frac{\alpha \rho_i}{j_0}$, taking into consideration the values of the initial velocity U_0 of the ions, are just as readily obtained.

2.2 Analog Representation of the Limit Conditions

The analog potential Φ which, at all points of the network, satisfies the equation

$$\Delta \Phi = -k \rho / \epsilon_0 \quad (45)$$

must express, on the contour, the limit conditions of the physical problem.

Let (Γ) be a boundary of the domain (for example, contour of an electrode).

Within the framework of ionic propulsion, two cases may occur:

2.2.1 Dirichlet Problem

Let the potential Φ on an electrode (Γ) be known. This limit condition which is particularly simple is obtained in all cases, no matter what the value of the initial velocity U_0 of the electric particles might be.

Let us assume $U_0 = 0$. Except in the case in which the "saturation" (see Section 2.2.2) is treated directly at the network, it thus is sufficient to attach the potentials Φ_e , Φ_f , and Φ_a to the emitting, focusing, and acceler-

ating electrodes.

In general, the contour (Γ) intersects the meshes (Fig.10). Equations (16) and (17) are no longer valid for the resistances joining a node such as 0 to the boundary. Nevertheless, on applying the finite-difference method (with a possible correction due to the proximity of the axis) to this node, the conductances which terminate in 0 are expressed by

$$C_1 \Delta z_1 - C_3 \Delta z_3 = 0 \quad (17)$$

$$C_3 = C_1 \frac{\Delta z_1}{\Delta z_3} \quad \text{with} \quad C_1 = \beta r \frac{\Delta r^2}{\Delta z^2}$$

where r denotes the distance of the node 0 from the axis of the propulsor.

Since $\Delta r_1 = \Delta r$ and $\Delta z_1 = \Delta z$

it follows that

$$C_3 = \beta r \frac{\Delta r^2}{\Delta z \Delta z_3} \quad (46)$$

In addition, since the values of the conductances C_i have been taken at the center of the meshes, we have

$$\begin{cases} C_4 = \beta \left(r - \frac{\Delta r}{2} \right) \\ C_2 = \beta \left(r + \frac{\Delta r_2}{2} \right) \end{cases} \quad (47)$$

One Dirichlet condition which is rather easy to satisfy nevertheless requires accuracy in the calculation of resistances adjacent to the boundary.

This results in continuity of the field ϕ and of the partial derivatives $\frac{\partial \phi}{\partial r}$ and $\frac{\partial \phi}{\partial z}$ in this portion of the domain and thus also gives the shape of the trajectories.

Because of this continuity, the principle itself of the parabolic interpolation method, applied on the digital computer Gamma AET, leads to serious difficulties. In fact, a calculation of the second derivative $\frac{d^2 r}{dz^2}$ at a point M_1 located on a normal to the emitter and adjacent to this latter, requires knowledge of the values of the field ϕ at nine nodes surrounding the point M_1 (see Section 1.4). Some of these, in the general case, are located at the interior of the electrode (this difficulty may occur in all cases in which an ion trajectory passes near an electrode, no matter which one). The analog potential ϕ , which represents the physical potential V at the network, is constant at the interior of each electrode. Figure 11, for example, shows the evolution of ϕ in the vicinity of the emitter boundary, in a section $r = r_1$. It seems that, for $0 < z < z_0$, the potential ϕ is equal to ϕ_0 . Beyond $z = z_0$, the potential function changes abruptly since the partial derivative $\frac{\partial \phi}{\partial z}$ generally is discontinuous for $z = z_0$. The Runge-Kutta integration method, based on continuous functions, yields erroneous results under these conditions.

The solution adopted to avoid such discontinuities on the partial derivatives of the field consists in replacing the curve ϕ by a series of parabolic arcs and to prolong these in the domain $0 < z < z_0$, corresponding to the interior of the electrode.

This method of parabolic extrapolation, made on the IBM 610 computer, makes it possible to rigorously apply the value ϕ_0 to the point z_0 , and thus to obey the Dirichlet condition, satisfied at the electric network.

Consequently, the principle of parabolic extrapolation is identical with that described in Section 1.4. The analog field is given, at the nodes of the meshes, by the coordinates of the nodes and by the value ϕ of the potential. A discrete series of points, fixed by their coordinates (r_j, z_j) , schematizes

the boundary (Γ) of the electrode. At the interior of this electrode, the analog potential retains a constant value Φ_Γ . Wanted are the values of Φ for the points located at the interior of the electrode, in such a manner that $\Phi = \Phi_\Gamma$ on (Γ).

In reality, the coordinates are r and z . The search for the potential can be effected either at $r = \text{const}$ or at $z = \text{const}$. (In order not to particularize in the program, the coordinates are denoted by x and y , where y is constant and x is variable.)

The extrapolation at the interior of the electrode is done from the boundary point and from the two nearest points, by representing the field variation by a parabola passing through these three points (Fig.12):

$$\Phi(x) = \Phi_r \frac{(x-x_1)(x-x_2)}{(x_r-x_1)(x_r-x_2)} + \Phi_1 \frac{(x-x_2)(x-x_r)}{(x_1-x_2)(x_1-x_r)} + \Phi_2 \frac{(x-x_r)(x-x_1)}{(x_2-x_r)(x_2-x_1)} \quad (48)$$

The mode of extrapolation selected (r constant or z constant) depends on the external shape of the electrodes. Figure 13 shows the various modes used in the case of the problem of revolution (see Section 4.2).

In any case, for a given geometry of the electrode system, the important point is the position of the trajectories with respect to the various boundaries. This problem of neighborhood is of prime importance and determines the extrapolation methods to be adopted. Only the experimental results can yield dependable data. Therefore, it is important to refer constantly to such results in all cases.

Consequently, the physical field, which is discontinuous at the boundary of each electrode, is replaced by a continuous field. It is a question whether

the analog trajectories, obtained by this process, can be considered as being identical to real trajectories. The theory of distribution developed by L. Schwartz (Bibl.12) - see also Appendix II - gives a satisfactory answer to this question.

2.2.2 Neumann Problem

The normal derivative $\frac{d\phi}{dn}$ at the boundary (Γ) is known. This limit condition is obtained whenever it is desired to realize "saturation", i.e., to cancel the electric field at the emitter surface.

Let us examine the representation of the following condition at the network: $\frac{d\phi}{dn} = 0$

2.2.2.1 Case of the One-Dimensional Problem

As discussed below (see Section 4.1.2), the plane diode can be schematized at the network along a line of resistances which can be assumed to be mutually equal (regular meshing). The intensities applied to each node are, respectively, i_1, i_2, \dots, i_n (Fig.14).

To satisfy the condition $\frac{d\phi}{dn} = 0$ on the emitting electrode, it is simply sufficient to have the node 0, which is the image of the ion source, assume a certain potential while imposing $\phi = 0$ on the node $(n + 1)$ representing the accelerating electrode. The potential of the node 0 then is rigorously determined, taking into consideration the values of the resistances R^* and of the injected intensities.

Since the node 0 does not discharge, the current intensity which passes through the resistance linking this node to the following node will thus be zero.

Consequently,

$$\begin{aligned}
 (49) \quad & \Phi_1 = \Phi_0 \\
 & \Phi_1 - \Phi_2 = RI_1^* \\
 & \Phi_2 - \Phi_3 = RI_2^* \\
 & \dots \\
 & \Phi_n - \Phi_{n+1} = RI_n^* \\
 & \Phi_{n+1} = 0
 \end{aligned}
 \quad \text{and}$$

$$\begin{aligned}
 (50) \quad & i_1 = I_1 \\
 & I_1 + i_2 = I_2 \\
 & I_2 + i_3 = I_3 \\
 & \dots \\
 & I_{n-1} + i_n = I_n \\
 & \downarrow \\
 & I_n = \sum_{k=1}^{k=n} i_k
 \end{aligned}$$

2.2.2.2 Case of the Problem of Revolution

The problem is considerably complicated for two reasons, which are due to:

- representation of the emitter shape on the network by a series of discrete points, which makes it impossible to impose the condition $\frac{d\Phi}{dn} = 0$ on the entire electrode;
- presence of a focusing electrode which must discharge while remaining at the same potential as the emitting electrode.

Experimentally, it is sufficient to adjust the intensity I , applied to the focusing electrode across a variable resistance R , in such a manner as to equalize the potentials of this electrode and of the emitter (Fig.15).

If, at each point of the ion source, we are to have $\frac{d\Phi}{dn} = 0$ it will follow that the total intensity $\int \frac{d\Phi}{dn} ds$ must also be zero. In the case of prime interest here, the shape of the emitting electrode (spherical segment) does not permit - in the adopted experimental process - to impose the condition $\frac{d\Phi}{dn} = 0$ at each of the points which schematize this shape at the network. In this manner, /38

we will have (Fig.16) at points such as A and B, the following:

$$\frac{\partial \Phi}{\partial r} = 0 \quad \text{at A}$$

$$\frac{\partial \Phi}{\partial z} = 0 \quad \text{at B}$$

in view of the fact that the intensities, circulating in the electric resistances which link these points A and B to the node M, are zero.

When the adjustment of the intensity I is terminated, the emitting electrode discharges no current, while remaining at the same potential as the focusing electrode. Although not satisfying the condition $\frac{d\Phi}{dn} = 0$ at each point of the boundary from which the ions emerge, it is obvious that the experimental process obeys the condition of zero discharge on this electrode which, finally, must satisfy - in an approximate but sufficient manner - the limit conditions of the physical problem.

ANALOG REALIZATION

3.1 Electrical Network

The network is composed of several insulating panels, manufactured at the ONERA Center. These panels are composed of 20 nodes and are readily interconnectable. The arrangement selected for the nodes forms a regular grid on the panels, which permits to obtain a network with rectangular, equal or unequal meshes.

Each node is presented in the form of a brass socket, located at the rear face of the network and permitting the introduction of a banana plug to tap the voltage or to apply current.

Between two successive nodes there is an electric resistance, installed into the pin of a current plug (Fig. 17).

Each wall plug, of standard distance of 19 mm, thus permits a two-to-two connection of the nodes on the panel. The realization of a given conductance value is obtained simply by branching several resistances to each other which connects them in parallel (Fig. 17).

A front view of the electrical network which permits treatment of Poisson's equation, for the three-dimensional case of axial symmetry, is given in Fig. 18.

3.2 Cutting of the Domain

The cutting step, i.e., the lengths of one mesh, is generally a function of a certain number of parameters generally known at the beginning of the tests: high potential gradient in a given zone, shapes difficult to represent, specific points where measurements are to be made.

Within the framework of ionic propulsion, the local charge density ρ assumes very high values near the emitting boundary (see Fig. 19). p.41

Consequently, the meshing must be sufficiently fine so that such values are effectively represented in the form of electric currents injected into the network. Consequently, it is desirable to tighten the meshing in the portion of the field under consideration. Figure 18a gives a front view of the electrical network after modification of the meshing in the vicinity of the emitting boundary.

Let us consider a cross extracted from the domain under study (D) of the potential function Φ (Fig. 20).

The identity of eqs. (7') and (14) requires that

$$C_1 \Delta z_1 - C_3 \Delta z_3 = 0 \quad (51)$$

$$r \Delta r (C_2 - C_4) = \frac{C_1 \Delta z_1^2 + C_3 \Delta z_3^2}{2} = \frac{\Delta r^2 (C_2 + C_4)}{2} = \frac{i_0 \epsilon_0}{k \rho} \quad (52)$$

The solution of such a system leads to the following formulas:

$$\begin{cases} C_1 = \frac{C_0 \Delta r}{\Delta z_1} r \end{cases}$$

$$\left\{ \begin{array}{l} C_2 = \frac{C_0 (\Delta z_1 + \Delta z_3)}{2 \Delta r} \left(r + \frac{\Delta r}{2} \right) \\ C_3 = \frac{C_0 \Delta r}{\Delta z_3} r \\ C_4 = \frac{C_0 (\Delta z_1 + \Delta z_3)}{2 \Delta r} \left(r - \frac{\Delta r}{2} \right) \end{array} \right. \quad (53)$$

where r denotes the distance of the node 0 to the axis of the propulsor and C_0 is a constant equal to $\beta \frac{\Delta r}{\Delta z}$.

These formulas can also be obtained by the method developed by Karplus p.42 (Bibl. 13) in which the electric resistance, in a given direction, of one volume element cut within one notch is calculated. Figure 21 shows the cutting used near the emitting electrode. Let C , C' , and C'' be the conductances ending at a node M located outside of the demeshed domain. It then is found that division by a number n of the length Δz of all meshes oriented toward the z axes, while conserving a constant step Δr in the direction of the r axes, results in a modification of the resistance values. Thus, those that are located along the axis of z are divided by n and the others, located in a perpendicular direction, are multiplied by the same numbers except at the boundary of two distinct cutting domains.

The electric intensity applied to the network at a node such as 0 (Fig. 20) satisfies eqs. (52).

From this it follows that

$$i_0 = \frac{k\rho}{\epsilon_0} \frac{C_1 \Delta z_1^2 + C_3 \Delta z_3^2}{2} \quad (54)$$

3.3 Electric Feed of the Network

Various means exist for providing the electric feed of the networks:

- Feeding with direct current supplied by either a set of storage batteries or by any rectifier system.
 - Sinusoidal current feed of 800 - 1000 cycles, supplied by a low-frequency generator combined with a power amplifier (Bibl. 14);
 - Alternating current feed of 50 cycles, supplied by the circuit and stepped up to the desired voltage across a transformer.
- p.43

The measurements are made by means of a null method, with a cathode-ray oscillograph arranged in Lissajous figures serving as a null indicator when the network is fed with alternating current. This method, which in most cases satisfies analog experiments made in the laboratory on problems derived from equations of Laplace of heat or of waves, becomes experimentally impossible within the framework of the present study. In fact, the assembly comprises large resistances used for application of the current i_0 representing the space charge at each node. These large resistances are not rigorously pure; effects of inductance and capacitance introduce considerable dephasings (of the order of 6° , i.e., ten times more than the maximums derived in the electric cell) which render accurate measurement of the potentials practically impossible.

Consequently, we preferred to use direct current. To avoid long and complex measurements when using galvanometers (which are, of course, extremely sensitive but whose fragility and slowness in stabilizing are in no proportion with the importance of the experiments made), a digital millivoltmeter, connected as a quotient meter, is used. The instrument selected, a "digital voltmeter" V-34 A made by Nonlinear Systems makes it possible to obtain voltage data to 1/10,000, either automatically or manually, with the maximum time required for one measurement being of the order of two seconds (Fig. 22).

3.4 Application of Current: Method of High Resistances

The classical method known as the method of "High Resistances" (Bibl. 15) consists in feeding each node (of the network) located in the domain traversed by the ion beam, across a resistance of high magnitude, connected to one of the terminals of the current generator (by convention, ± 100 of the analog potentials).

p.44

The high resistances are installed in the drawers (Fig. 23) which each contain 4×11 commutators graduated in conductance, i.e., proportional to the desired current intensities. The available scale ranges from $100 \text{ K}\Omega$ to $10 \text{ M}\Omega$. This scale can be further extended by connecting standardized conductances in parallel.

At each node, the value of the current intensity i_0 is furnished by the expression

$$i_0 = \frac{k \rho C_z \Delta z^2}{\epsilon_0} \quad (55)$$

To this value of i_0 corresponds a conductance C_0 , read from the commutator, so that

$$i_0 = 100 C_0 \quad (56)$$

The real intensity which flows across the high resistance and penetrates

into the network actually is

$$i_r = \frac{100 - \Phi_o}{R_o} = (100 - \Phi_o) C_o \quad (57)$$

where Φ_o denotes the potential of the node under consideration.

Consequently, the error made in labeling the intensities is $\Phi_o\%$. Taking the values of the resistances used within the framework of the present study into consideration, the analog potentials reach very high values (8 to 10 in the case of the first method described in Section 4.1.3.1 and even 40 if the "saturation" is treated directly at the network). Therefore, the real current intensity, entering the network, must be corrected. This operation is done as follows:

A first approximation consists in adopting a conductance equal to C_o at a node 0 of the network. This furnishes a potential Φ_o . After this, it is sufficient to replace C_o by a conductance C_1 so that

$$C_1 = \frac{100 C_o}{100 - \Phi_o} \quad (58)$$

in order to obtain a new value Φ_1 of the potential.

The current intensity fed to the network will then become

$$i_{r1} = i_o \frac{100 - \Phi_1}{100 - \Phi_o} \quad (59)$$

In order that the real intensity, entering the network, becomes i_0 , it is necessary to continue the corrections up to the n^{th} approximation, in such a manner that the fields $\bar{\phi}_{n-1}$ and $\bar{\phi}_n$ are the same.

Experiments made for the readily computable case of a plane diode have shown that a single correction of the large resistances is entirely sufficient to obtain satisfactory results.

Figure 24 shows the electric assembly corresponding to one of the methods described in Section 4.1.3. A stabilized power source furnishes the direct reference voltage ^+V_r , comprised in the interval of 0-30 v. Since all measurements of the voltage are positive, only the index + is of interest here. The V-34 voltmeter, connected as a quotient meter, therefore permits a recording of the experimental results on an analog scale of 0 - 100. The electric intensities i_0 , representing the space charge, are applied to the network across high resistances connected between the reference + 100 and the node under consideration.

Figure 25 gives an overall view of the experimental assembly, permitting a representation of the Poisson equation at the electrical network.

CHAPTER IV

p.47

APPLICATION TO THE THREE-DIMENSIONAL PROBLEM OF AXIAL SYMMETRY

In order to check on the rapidity of convergence of the iteration process and in order to evaluate the accuracy of the calculation method, it is useful to discuss first the problem of a plane diode.

p.48

4.1 - Verification of the Method on the Theoretical Case of a Plane Diode

4.1.1 - Theoretical Investigation

When considering a metal placed in a void at a temperature T , it is found that a certain portion of "free electrons" has a tendency to leave the solid. In the absence of external action, this leads to the formation of an electric field known as "space charge" which opposes the departure of new electrons and thus leads to equilibrium.

If the emitted electrons are entrained by means of an applied electric field, the phenomenon continues and leads to a dynamic equilibrium characterized by a certain electron flux (current density). This density increases with the applied field; however, it cannot exceed the value corresponding to the "saturation current" j_s , which corresponds, in turn, to the thermionic emission at the temperature under consideration. The value of j_s is given by the Dushman formula:

$$j_s = AT^2 \exp\left(-\frac{\psi}{k'T}\right) \quad (60)$$

where k' represents the Boltzmann constant.

The application of an accelerating electric field to the surface of a solid has the tendency to increase the electric emission there, in accordance with two distinct processes: Schottky effect and cold emission (Bibl. 16).. These two effects are not represented at the electrical network.

Let us assume a plane diode whose two electrodes, spaced at a distance of d (Fig. 26), are brought, respectively, to the potentials V_s and 0.

Solution of the Poisson equation $\frac{d^2 V}{dz^2} = - \frac{\rho}{\epsilon_0}$ yields the classical result (eq. 61):

$$1 - \frac{V}{V_s} = \left(\frac{z}{d}\right)^{4/3} \quad (61)$$

if the density of the ionic current takes the following value of saturation (eq. 62):

$$j_s = \frac{4}{9} \epsilon_0 \sqrt{\frac{2e}{m}} \frac{V_s^{3/2}}{d^2} \quad (62)$$

4.1.2 - Solution of Poisson's Equation at the Electrical Network

Figure 27 gives a schematic view of the characteristics of one node 0.

We have

$$C_1 (\phi_1 - \phi_0) + C_3 (\phi_3 - \phi_0) + i_0 = 0$$

By limiting the calculation to terms of the second order, we obtain

$$\left(\frac{\partial \phi}{\partial z}\right)_0 (C_1 \Delta z_1 - C_3 \Delta z_3) + \frac{1}{2} \left(\frac{\partial^2 \phi}{\partial z^2}\right)_0 (C_1 \Delta z_1^2 + C_3 \Delta z_3^2) + i_0 = 0$$

In the case of a regular meshing, we have

$$\Delta z_1 = \Delta z_3 = \Delta z ; \quad C_1 = C_3 = C_z ;$$

Using $\phi = kV$ in such a manner that $k = \frac{100}{V_s}$, the expression for the current intensity i_0 applied to the network, at the node under consideration, will still be

$$i_0 = \frac{k\rho}{\epsilon_0} C_z \Delta z^2 \quad (55)$$

The velocity of one ion is expressed by

p.50

$$U = \sqrt{\frac{2e}{m} (V_s - V)} \quad (63)$$

(in the case in which the positive particles are emitted without initial velocity), while the space charge is expressed by

$$\rho = \frac{j_0}{U} \quad (64)$$

where V_s denotes the accelerating potential, always assuming that

$$\alpha = \sqrt{\frac{2e}{m} V_s} \quad (40)$$

The intensity i_0 is transformed in accordance with

$$i_0 = \frac{k c_z \Delta z^2}{\epsilon_0 \alpha} \frac{j_0}{\sqrt{1 - \frac{\Phi}{100}}} \quad (65)$$

The analog potential must prove the equation

$$\frac{\Phi}{100} = 1 - \left(\frac{z}{d} \right)^{4/3} \quad (66)$$

if the density of the current j_0 assumes the value at saturation j_s , which then yields, as the intensity:

$$i_0 = \frac{400}{9} c_z \frac{\Delta z^2}{d^2} \frac{1}{\sqrt{1 - \frac{\Phi}{100}}} \quad (67)$$

Practical tests made on the problem of a plane diode have demonstrated that it is useful to open the meshes of the network in the vicinity of the emitting cathode, in order to increase the accuracy. Thereafter, in the expression (65) for the intensity i_0 it is sufficient to replace the product $C_z \Delta z^2$ by $\frac{Cz_1 \Delta z_1^2 + Cz_3 \Delta z_3^2}{2}$, where the subscripts 1 and 3 designate the nodes surrounding the central node 0. The network which actually is limited to one line, is divided into twenty-five meshes, where the nodes are designated, respectively, by the following values of z/d : 0; 0.005; 0.010; ... 0.025; 0.0375; 0.05; 0.10; ... 0.95 and 1. The electric resistances used are also selected equal to 50 Ω ; 125 Ω ; and 500 Ω .

p.51

4.1.3 - Solution Methods

Since it is desired to obtain the configuration of the potential corresponding to the law of Child (eq. 66), it is necessary, in the solution by successive approximations, to supply the network with electric intensities corresponding to the saturation density j_s and specifically to the cancelation of the gradient $\frac{d\phi}{dn}$ on the emitting surface.

The Poissonian field ϕ_p satisfies the equation

$$\Delta \phi_p = -k\rho/\epsilon_0 \quad (68) \text{ with } k = \frac{100}{V_s}$$

whereas the Laplacian field ϕ_L obeys the classical equation: $\Delta \phi_L = 0$

Let us assume that

$$\varphi = \phi_p - \phi_L \quad (69)$$

The analog potential φ , defined in this manner, also satisfies the Poisson equation

$$\Delta \varphi = -k\rho/\epsilon_0 \quad (70)$$

An investigation of the function φ has the advantage of increasing the accuracy in the Poissonian field. The limit conditions are reduced to an application of zero potential to the two electrodes (in the case in which the initial velocity of the particles is zero). In each approximation, the current intensities applied across high resistances (these latter are subjected

to the correction introduced in Section 3.4) obey the law (67). The curves giving the evolution of the potential Φ_p in each approximation (Charts IV₁ and IV_{1a}) represent the numerical results of Table IV.

Consequently, the method yields an excellent convergence since the mean deviation, with respect to the theoretical solution, is -0.28% at the fourth approximation, this mean deviation being defined by

$$\varepsilon \% = \frac{1}{25} \sum_{i=1}^{i=25} \left(\frac{\Phi_i - \Phi_{Ti}}{\Phi_{Ti}} \right) \% \quad (71)$$

where Φ_i and Φ_{Ti} denote, respectively, the experimental and theoretical values of the Poissonian potential at the node i .

Unfortunately, this method is not applicable to the case of the problem of revolution with electrodes of any shape, since it would be necessary to know the value of the saturation current density j_s . Since this latter is an unknown of the problem, it becomes necessary to find an experimental process which will, in a satisfactory manner, impose the conditions $\frac{d\phi}{dn} = 0$ on the emitter, test this process on the theoretical case of a plane diode in order to define its practical interest, and evaluate its accuracy.

4.1.3.1 - First Method

This method is based on solution of the equation:

$$\Delta \varphi = - k e / \varepsilon_0 \quad (70)$$

where the applied current intensities obey the law (65), which latter is subjected to the above-mentioned modification at the boundary of two different meshes.

In view of the fact that the parameter j_0 is assumed as being variable, the determination of the saturation value j_s of the emission density is done experimentally. The principle of the method, based on measuring the intensity discharged by the emitting electrode, is as follows:

Assume that, to the Laplacian field, there corresponds an intensity i_L positive by convention, with the analog currents directed toward increasing z for the case of ionic propulsion.

Assume that, to the field $\phi = \phi_p - \phi_L$ there corresponds a negative intensity i_p which is sufficiently well measured by a null method. From this, the analog intensity i_p is readily derived.

Since the cycle of approximations proceeds at a given j_0 , it is sufficient to calculate the ratio i_p/i_L in % for each of the approximations and to plot the curve which gives the evolution of this ratio (see Charts IV₂, IV₃, IV₄). To each value of the emission density there corresponds a convergence (denoted by its mean deviation $\epsilon\%$) after the fourth approximation. The plotting of the various results in the form of the curve $(i_{p3}/i_L - i_{p4}/i_L) \%$ as a function of $\epsilon_4\%$ (Fig. 28), calculated to the fourth approximation, yields the deviation with respect to the theoretical solution, corresponding to a given gradient of the ratio $i_p/i_L\%$ (gradient determined after the two last approximations). Tables V shows the results referring to a series of experiments made at j_0 constant. Consequently, the curve plotted in Fig. 28 can be used as a test for the case of the three-dimensional problem of axial symmetry, by taking notice of the fact that a gradient $(i_{p3}/i_L - i_{p4}/i_L)$, varying between

1.95% and 7.80%, corresponds to a convergence located between -1% and +1% of the ideal convergence.

This method, when applied to the theoretical case of the plane diode, thus permits establishing the experimental value of j_0 leading to perfect convergence. The obtained value, $j_0 = 48.20 \text{ amp/m}^2$, consequently differs by 1.7% from the theoretical value of $j_0 = 47.38 \text{ amp/m}^2$, obtained from the tube characteristics. These are:

$$\begin{aligned}\epsilon_0 &= 8,85374 \cdot 10^{-12} \text{ F/m} \\ d &= 10^{-2} \text{ m} \\ V_s &= 10^4 \text{ V} \\ \alpha &= 1,20406 \cdot 10^5 \text{ m/s}\end{aligned}$$

in which case the electric particles selected are cesium ions whose charge and mass are

$$\begin{aligned}e &= 1,602 \cdot 10^{-19} \text{ C} \\ m &= 2,21 \cdot 10^{-25} \text{ kg}\end{aligned}$$

This deviation of 1.7% from the value of the emission density, due largely to the ^{of application} mode of currents simulating the space charge (because, in practical use, only a single correction has been made on the high resistances; see Section 3.4), nevertheless produces only a minimal error (- 0.28%) for the potential distribution obtained after convergence of the iterative process.

4.1.3.2 - Second Method

This second method is based on a direct solution of the following equation

$$\Delta \Phi_P = -k \rho / \epsilon_0 \quad (68)$$

In Section 2.2.2.1, we showed that, to impose the conditions $\frac{d\Phi}{dn} = 0$ on the emitter (which is transformed into $\frac{d\Phi}{dz} = 0$), it is sufficient to allow the node 0, which is an image of the ion source, to assume a potential which is perfectly defined from the characteristics of the network and from the intensities applied to each of the other nodes. After terminating the experiment, the numerical results must be translated to the scale 0 - 100.

Since, however, the node 1, being the closest to the emitter, is at the same potential as the emitter, it becomes impossible to calculate the intensity simulating the space charge at this node, because of the fact that - according to eq. (65) - its value is infinite. To reduce this inconvenience somewhat, it seems logical to correct the potential at this node 1 by "smoothing" the curve which gives the electric potential distribution in the vicinity of the ion source. The smoothing adopted consists either in application of a parabolic interpolation method, based on the known numerical results on the nodes 0, 2, and 3 whenever possible (most frequent case) or based on application of a graphical method. Solution of eq. (68) by such a process, tested for various values of the current density j_0 , has proved highly satisfactory.

The advantage of this second analog method resides primarily in the selection of the parameter j_0 ; no matter what the value of this parameter, "saturation" is obtained at the electrical network by imposing the condition $\frac{d\phi}{dn} = 0$. Consequently, a value of j_0 , different from that at saturation, can be adopted, yielding an excellent agreement with the (66) after the fourth approximation.

However, in order to reduce the analog potentials and thus also to reduce the extent of possible corrections made on the large resistances in the simulation of space charge by electric currents, it is of interest to keep the value j_0 smaller than j_s . For example (Charts IV₅ and IV_{5a} and Table VI), the convergence obtained at an emission density equal to 10 amp/m² is excellent: +0.16% mean deviation between the experimental potential distribution and the theoretical law (66).

4.1.3.3 - Third Method

The saturation also can be rigorously obtained in the case of the one-dimensional problem, by reasoning on eq. (70):

$$\Delta\psi = -k\rho/\epsilon_0 \quad (70)$$

with

$$\psi = \phi_p - \phi_L \quad (69)$$

Consequently,

$$\frac{d\psi}{dn} = \frac{d\phi_p}{dn} - \frac{d\phi_L}{dn} \quad (72)$$

The experimental solution of the Laplace equation leads to an intensity i_1 (discharge of the emitting electrode) which is positive by convention (see Section 4.1.3.1).

Consequently,

$$i_L = \frac{d\phi_L}{dn} = \frac{d\phi_L}{dz}$$

Thereafter, it is sufficient to adjust the value of the parameter j_0 at each approximation, in such a manner that the electric intensities applied to the network and satisfying eq. (65), lead to a discharge of the emitting electrode in such a manner that

$$i_\psi = \frac{d\psi}{dn} = - i_L \quad (73)$$

Then, in accordance with eq. (72), we have

$$i_p = \frac{d\phi_p}{dn} = 0$$

Probably, this third method is best. In fact, the method permits a determination of the potential distribution satisfying Child's law (66) and the value of the ion emission density at saturation.

In each approximation, the first step is to obtain approximately the saturation in such a manner that the corrections made on the large resistances, used for application of the electric currents, will yield a verification of the condition

The experimental solution of the Laplace equation leads to an intensity i_1 (discharge of the emitting electrode) which is positive by convention (see Section 4.1.3.1).

Consequently,

$$i_L = \frac{d\phi_L}{dn} = \frac{d\phi_L}{dz}$$

Thereafter, it is sufficient to adjust the value of the parameter j_0 at each approximation, in such a manner that the electric intensities applied to the network and satisfying eq. (65), lead to a discharge of the emitting electrode in such a manner that

$$i_\psi = \frac{d\psi}{dn} = - i_L \quad (73)$$

Then, in accordance with eq. (72), we have

$$i_p = \frac{d\phi_p}{dn} = 0$$

Probably, this third method is best. In fact, the method permits a determination of the potential distribution satisfying Child's law (66) and the value of the ion emission density at saturation.

In each approximation, the first step is to obtain approximately the saturation in such a manner that the corrections made on the large resistances, used for application of the electric currents, will yield a verification of the condition

$$\frac{d\Phi_p}{dn} = 0 \quad \text{at} \quad \pm 0,25 \%$$

This method, tested on the problem of a plane diode, made it possible to define the value of the emission density j_e (47.38 amp/m²) and to obtain a voltage distribution which closely approaches the law (66), the mean deviation being equal to -0.10%.

Table VII shows the evolution of the quantities j_e and $\epsilon\%$. It seems that, after the second approximation, the function Φ satisfies in an acceptable manner ($\epsilon\% = -1.32$) eq. (66).

The experimental results shown in Table VIII and Charts IV_e and IV_e_a, prove that convergence is rapidly obtained, with the parameter j_e and the theoretical law (66) being excellently verified.

4.2 - Application of the Various Methods to the Revolution Problem

In this study, the electric particles are assumed to have no initial velocity. The fact that the emitter has a spherical shape, permits giving a satisfactory orientation to the ion trajectories by having them converge toward the axis of the propulsor in the case in which the space charge is neglected. The configuration of the two other electrodes, reproduced in Fig. 29, is sufficiently close to that given in the literature (Bibl. 4).

The electrical resistances of the network, measured to within 0.5%, have values ranging between 30 ohm and 300 KΩ. The method of true values, combined with that of hollow cylinders (see Appendix I), is applied to the vicinity of the propulsor axis. Conversely, beyond the limiting radius r_1 , the

finite-difference method is entirely sufficient (Table I).

The geometric characteristics of the ion gun (Fig. 29) are readily obtained at the network, taking the adopted cutting into consideration:

$$25 \Delta r = 10^{-2} \text{ m}$$

The other data (mass and charge of the ions, absolute permittivity in vacuo, accelerating potential) are identical to those given in Section 4.1.3.

4.2.1 - Laplace's Field

159

The limit conditions of the Dirichlet type are as follows for the three electrodes:

$$\begin{cases} \Phi_e = \Phi_f = 100 \\ \Phi_a = 0 \end{cases}$$

As soon as the Laplacian field Φ_L (Field I) is obtained, solution of $\Delta\Phi = 0$ is immediate. Figure 30 gives the distribution of equipotentials in a meridian semi-plane. The exploitation of this field by the computation center leads to the network of trajectories shown in Fig. 31, after a parabolic extrapolation (see Section 2.2.1) made with extreme care so that the partial derivatives $\frac{\partial\Phi}{\partial r}$ and $\frac{\partial\Phi}{\partial z}$ are continuous in the vicinity of the three electrodes (and, specifically, near the emitter). These trajectories converge quite strongly toward the axis of the propulsor.

Some of these even intersect near the exit from the gun. The calculation

of the space charge, in accordance with the method described in the first Chapter, obviously is no longer valid after intersection of the trajectories.

4.2.2 - Poisson's Field

Equation (41) of the dimensionless quantity $\alpha \rho_i / j_0$ becomes

$$\alpha \rho_i / j_0 = \frac{2Rh_0 \sqrt{\frac{100(1+r_i'^2)}{100-\Phi_i}}}{(r_3^2 - r_1^2)_i} \quad (41)'$$

The number of trajectories used for calculating the space charge, in the entire domain occupied by the ions, is equal to twenty for a meridian-plane.

The values of the parameter h_0 (Fig. 6) are reproduced in Table IX for each trajectory.

4.2.2.1 - First Method

The limit conditions satisfy the equality $\varphi_0 = \varphi_r = \varphi_a = 0$ since the derived equation has the following form:

$$\Delta \varphi = -k\rho / \epsilon_0 \quad (70) \quad \text{with} \quad k = \frac{100}{V_s}$$

The wiring diagram in Fig. 32 gives the principle of the method, based on measuring the current density discharged by the emitting electrode.

Two stabilized feeder lines, connected in series, furnish the reference voltages of +100 and -100. The center point of the Wheatstone bridge is connected to one of the terminals of the commutator J. The variable resistance R ,

which permits measuring the intensity i_0 penetrating into the emitting electrode, is connected between this latter and the analog reference -100. A derivation makes it possible to approach the second terminal of the commutator J. The current intensities i_0 , simulating the space charge, are applied by the method of high resistances, with the focalizing and accelerating electrodes being charged to the potentials $\varphi_1 = \varphi_2 = 0$. The operation is done in the following manner: The galvanometer G is connected between ground and commutator, with the latter being placed in position (1); the power feed control is rectified in such a manner that the pointer of the galvanometer no longer deviates, which permits application of the potential 0 at the center point of the Wheatstone bridge; the commutator is placed in position (2) and provides the junction between the output terminal of the galvanometer and the emitting electrode. It then is sufficient to trigger the resistance R in such a fashion as to apply the potential 0 to this electrode, which results in zero current in the galvanometer.

A repetition of the above-described manipulation permits a verification of the control and a check on the satisfactory value of the resistance R .

In addition, it should be mentioned that the quotient meter V $\frac{3}{4}$ A, used for obtaining the potential readings, is highly suitable for replacing the above-mentioned Wheatstone bridge and galvanometer (Fig. 33). The measurements show perfect agreement between the intensities obtained by means of the two processes.

The results of each approximation are given in Table X. The Chart IV, shows the evolution of the ratio $i_p/i_1\%$ for an emission density equal to 15 amp/m². The corresponding gradient $(i_p/i_1 - i_p/i_1)/i_1\%$ yields a convergence at +0.21% of the distribution at saturation, in accordance with the curve in

/61

Fig. 28 which is taken as reference point. The cycle of approximations, repeated for several values of j_0 , made it possible to emphasize the lower and upper limits of this parameter that are able to yield a satisfactory convergence. The interval of 14 amp/m^2 to 17 amp/m^2 which is much shorter than in the one-dimensional case, obviously is a function of the resistances of the network. However, it is understood that the numerical values given to the emission density j_0 depend on the geometric and electric characteristics of the gun. If, for technical reasons (maximum electric field not to be exceeded, different nature of the ions), the values of the accelerating potential V , or of the mass of electric corpuscles have undergone a change, it would be sufficient to multiply the value of j_0 by a readily determinable coefficient, in such a manner as to obtain, at the network, the same configuration of the Poissonian field. Figures 34 and 35, respectively, give the distribution of the equipotential lines and trajectories, corresponding to the fourth approximation, for a density j_0 equal to 15 amp/m^2 . A comparison of these trajectories with those in Fig. 31 readily demonstrates the effect of the space charge mentioned (see Section 1.1). The beam, obtained on the basis of the focalizing and accelerating electrode dimensions in Fig. 29, consequently has the desired qualities (see Introduction).

4.2.2.2 - Second Method

The working procedure described in Section 2.2.2.2 involves a difficulty which had already been encountered in the case of the plane diode. However, instead of a mesh (the first) traversed by a zero current (the emitting electrode does not discharge), it is now a question of several successive nodes which have the same potential. Everything proceeds as though the surface of

the emitter had undergone a "translation" toward increasing z . The extent of this "translation" varies in the same sense as the cutting step, in the vicinity of the electrode. The decrease in the length of the meshes, in this portion of the field, thus has a favorable effect despite the fact that it results in an increase in the number of nodes charged to the same potential.

In practical application, the field, in the domain under consideration, is modified in accordance with a parabolic extrapolation method described above (see Section 2.2.1). This transformation, which is rather difficult to realize because of the number of nodes involved, requires special care in order to ensure the continuity of the quantities ϕ , $\frac{\partial \phi}{\partial r}$, and $\frac{\partial \phi}{\partial z}$.

The calculations made at constant ion emission density, equal to 15 amp/m^2 , yields a rather satisfactory convergence. However, it is quite possible that a fifth approximation would be desirable in order to perfect the convergence of the iterative process.

Charts IV_8 , IV_9 , IV_{10} and IV_{11} give the distribution of the analog potential ϕ at the first, second, third, and fourth approximations. Figure 36 furnishes a good illustration of the modifications suffered by certain equipotential lines during the various approximations.

The Charts IV_{12} and IV_{15} give plottings of the trajectory beams, with respect to the first and fourth approximation.

4.2.2.3 - Third Method

A generalization to the problem of revolution of the method described in Section 4.1.3.3 involves a difficulty, produced by the representation of the emitting boundary.

The condition of cancellation of the electric field on the electrode Γ ,

from which the ions are emitted, is written as follows:

$$\int_{\Gamma} \frac{d\Phi_P}{dn} ds = 0$$

where s denotes the curvilinear abscissa along the contour Γ .

In this case, eq. (72) becomes

$$\int_{\Gamma} \frac{d\varphi}{dn} ds = \int_{\Gamma} \frac{d\Phi_P}{dn} ds - \int_{\Gamma} \frac{d\Phi_L}{dn} ds \quad (72)'$$

In practical work, the discharge of the emitting electrode is measured during solution of the equation $\Delta\Phi_L = 0$ at the electric network. Let us denote this discharge by i_L .

Then, the value of the parameter J_0 is so adjusted that the discharge i_φ of the emitter satisfies the condition

$$i_\varphi = -i_L \quad (73)$$

when deriving eq. (70):

$$\Delta\varphi = -k\rho/\epsilon_0 \quad (70)$$

From this it follows that

$$i_p = 0$$

Thus, eq. (72)' is satisfied in an approximate but sufficient manner.

The discharges measured at the electrical network are given in Table XI.

Since the saturation results in a rather severe limit condition, the partial derivatives $\frac{\partial \phi}{\partial r}$ and $\frac{\partial \phi}{\partial z}$ are weak in the vicinity of the emitting electrode. To obtain continuous quantities ϕ , $\frac{\partial \phi}{\partial r}$, and $\frac{\partial \phi}{\partial z}$ in this domain, a parabolic extrapolation is made from the values obtained at the electrical network.

On Charts IV₁₃ and IV₁₄ are plotted the trajectory networks relative to the second and third approximations.

Charts IV₁₅, IV₁₇, IV₁₈, and IV₁₉ give the potential distribution ϕ , created by the space charge, over various approximations.

Figures 37 and 38 contain the equipotential curves ϕ and the trajectories corresponding to the fourth approximation. The ion emission density, obtained by this iterative process ($j_0 = 15.25 \text{ amp/m}^2$) is close to that obtained by the method No. 1. It is quite possible also, that in this case, a supplementary approximation would have yielded a further perfection of the convergence.

Figures 39 and 40 emphasize the influence of the space charge on the distribution of equipotential lines and on the shape of the trajectories. The two effects of the space charge, showing in an increase of the aperture angle of the beam (Fig. 40) and the creation of an axial electric field E'_z , opposed to the accelerating field (Fig. 39) are clearly visible.

The values of the potential ϕ , satisfying Poisson's equation and corresponding to the fourth approximation, are given in a Table (Field II).

CHAPTER V

/66

ESTIMATION OF ERRORS

The analogies are divided into two large categories: functional analogies and topological analogies. Certain types of errors are common to all: notation, reading, auxiliary calculations. The topological analogies, with which the present study is concerned, may also lead to certain errors of representation of the domain: material limitation for the case that this domain is theoretically infinite; cutting errors which concern the entire useful space in the case of networks and uniquely the limit conditions in the case of rheoelectric analogies. Let us successively investigate the various error sources.

/67

5.1 Errors Linked to the Network

5.1.1 Cutting Errors

The Poisson equation

$$\Delta \Phi = -k\rho/\epsilon_0 \quad (68)$$

in which the partial derivatives are replaced by finite differences, will yield, at each node of the network,

$$\sum_{j=1}^{j=4} C_j (\Phi_j - \Phi_0) + i_0 + \mathcal{R}_0 = 0 \quad (74)$$

where R_0^* denotes the error due to the introduction of finite differences and expressed in form of a series of terms which are functions of the derivatives of Φ , of a more or less elevated order. Thus, in the case of a regular meshing having a step Δz and Δr , eq.(74) will be written as follows:

$$\beta r \Delta r^2 \Delta \Phi_0 + i_0 + \frac{\beta}{6} \Delta r^2 \left\{ \Delta r^2 \left(\frac{\partial^3 \Phi}{\partial r^3} \right)_0 + \frac{1}{2} \Delta r^2 r \left(\frac{\partial^4 \Phi}{\partial r^4} \right)_0 + \frac{1}{2} \Delta z^2 r \left(\frac{\partial^4 \Phi}{\partial z^4} \right)_0 \right\} + \dots = 0 \quad (75)$$

since

$$C_r = \beta r \quad (16)$$

and

$$C_z = \beta r \frac{\Delta r^2}{\Delta z^2} \quad (17)$$

68

Let us also assume that

$$\Delta \Phi_0 + \frac{i_0}{\beta r \Delta r^2} + \frac{\Delta r^2}{6} \frac{1}{r} \left(\frac{\partial^3 \Phi}{\partial r^3} \right)_0 + \frac{1}{12} \left\{ \Delta r^2 \left(\frac{\partial^4 \Phi}{\partial r^4} \right)_0 + \Delta z^2 \left(\frac{\partial^4 \Phi}{\partial z^4} \right)_0 \right\} + \dots = 0 \quad (76)$$

Consequently, the error R_0^* is expressed in the form of

$$R_0^* = \frac{\Delta r^2}{6} \frac{1}{r} \left(\frac{\partial^3 \Phi}{\partial r^3} \right)_0 + \frac{1}{12} \left\{ \Delta r^2 \left(\frac{\partial^4 \Phi}{\partial r^4} \right)_0 + \Delta z^2 \left(\frac{\partial^4 \Phi}{\partial z^4} \right)_0 \right\} + \dots \quad (77)$$

Similarly, in the case of a cutting (Fig.41), in such a manner that

$$\begin{aligned} \Delta r_2 &= \Delta r_4 = \Delta r \\ \Delta z_3 &= \frac{\Delta z_1}{2} = \frac{\Delta z}{2} \end{aligned} \quad (78)$$

the formulas (53) become

$$\begin{cases} C_1 = C_0 \frac{\Delta r}{\Delta z} r \\ C_2 = \frac{3 C_0 \Delta z}{4 \Delta r} \left(r + \frac{\Delta r}{2} \right) \\ C_3 = \frac{2 C_0 \Delta r}{\Delta z} r \\ C_4 = \frac{3 C_0 \Delta z}{4 \Delta r} \left(r - \frac{\Delta r}{2} \right) \end{cases} \quad (79)$$

Equation (74) is transformed in accordance with

$$\begin{aligned} & \frac{3}{4} C_0 r \Delta r \Delta z \Delta \Phi_0 + i_0 + \frac{C_0 r}{8} \Delta r \Delta z \left\{ \Delta z \left(\frac{\partial^3 \Phi}{\partial z^3} \right)_0 + \frac{\Delta r^2}{r} \left(\frac{\partial^3 \Phi}{\partial r^3} \right)_0 \right\} \\ & + \frac{C_0 r \Delta r \Delta z}{16} \left\{ \frac{3}{4} \Delta z^2 \left(\frac{\partial^4 \Phi}{\partial z^4} \right)_0 + \Delta r^2 \left(\frac{\partial^4 \Phi}{\partial r^4} \right)_0 \right\} + \dots = 0 \end{aligned} \quad (80)$$

A comparison with Poisson's equation (68) yields

$$i_0 = \frac{3 C_0 r \Delta r \Delta z k \rho}{4 \epsilon_0} \quad \text{with} \quad C_0 = \frac{\beta \Delta r}{\Delta z}$$

a result which agrees with eq. (54).

And

$$\mathcal{R}_0 = \frac{1}{6} \left\{ \frac{\Delta r^2}{r} \left(\frac{\partial^3 \Phi}{\partial r^3} \right)_0 + \Delta z \left(\frac{\partial^3 \Phi}{\partial z^3} \right)_0 \right\} + \frac{1}{12} \left\{ \frac{3}{4} \Delta z^2 \left(\frac{\partial^4 \Phi}{\partial z^4} \right)_0 + \Delta r^2 \left(\frac{\partial^4 \Phi}{\partial r^4} \right)_0 \right\} + \dots = 0 \quad (81)$$

In this investigation, the error R_0^* always is of the third order. The use of very small meshes permits a reduction of this error to very low proportions. The test, which consists in studying - in the portion of the network which has no electrodes - the potential distribution in a cylindrical coaxial capacitor, has made it possible to detect errors of less than 0.1% at each node (in which case the method of true resistances replaces the method of finite differences in the vicinity of the axis) despite the fact that the resistances of the network are posted at 0.5%.

On solving the system of N equations (74) where $R_0^* = 0$ has been set (N being the total number of nodes), by means of a network of conductances, the solutions Φ_0 appear in the form of electric voltages. In fact, the accuracy

on Φ which is of the order of several thousandths is limited not so much by the number of necessary nodes or by the accuracy of the resistances used than by the difficulties which may occur in application of the limit conditions. Whereas, in an electrolytic tank or on a paper conductor, the contours where these conditions must be satisfied at each point can be represented in a continuous fashion, the reproduction of a boundary at the network can be done only approximately by means of a finite series of points, which in itself already reduces the accuracy. In addition, the Poisson equation (eq.68), expressed in the form of finite differences, is satisfied in the vicinity of an electrode only with a certain error R_0 (Fig.42):

$$\mathcal{R}_0 = a_1 \frac{\partial \Phi}{\partial r} + a_2 \left(\frac{1}{r} \frac{\partial \Phi}{\partial r} + \frac{\partial^2 \Phi}{\partial r^2} \right) + a_1 b_1 \frac{\partial^2 \Phi}{\partial r^2} + \dots \quad (82)$$

where

$$\left\{ \begin{array}{l} a_1 = \frac{\Delta r_2 - \Delta r}{\Delta r^2} \\ a_2 = \frac{\Delta r_2^2 - \Delta r^2}{2 \Delta r^2} \\ b_1 = \frac{\Delta r_2^2 + \Delta r_2 \Delta r + \Delta r^2}{4 r} \end{array} \right. \quad (83)$$

and where the conductances ending at the node 0, are expressed as follows:

$$\left\{ \begin{array}{l} c_1 = c_0 \frac{\Delta r}{\Delta z_1} r \\ c_2 = c_0 \frac{(\Delta z_1 + \Delta z_3)}{2 \Delta r} \left(r + \frac{\Delta r_2}{2} \right) \\ c_3 = c_0 \frac{\Delta r}{\Delta z_3} r \end{array} \right. \quad (84)$$

$$C_4 = C_0 \frac{(\Delta z_1 + \Delta z_3)}{2 \Delta r} \left(r - \frac{\Delta r}{2} \right)$$

The error R_0^* , which is of the first order, has only a minor influence on the distribution of equipotential lines in the entire domain. In fact, to verify this, it is sufficient to treat the problem without space charge in the revolution tank (Bibl.15). The tank, having a plane and sloping bottom, represents a sector comprised between two meridian planes of which one corresponds to the bottom of the cell and the other to the free surface. The edge of the liquid dihedron thus forms the image of the axis of revolution oz.

Since the sloping of the bottom is relatively slight (20%), the electrode models are cylindrical and have vertical generatrices; the contour of the right section of the cylinder reproduces the form of the meridian contour of the electrode (Fig.43). The reading of the potential, made at the free surface of the electrolyte (city water) by immersing the probe only slightly, is rapidly obtained by means of an automatic tracer of equipotential lines (Fig.44), developed by J.Besson (Bibl.17) and M.Langlois (Bibl.18). The agreement between the Laplacien fields (one and the other being, respectively, simulated at the network and in the revolution tank is very good in the vicinity of the electrodes.

5.1.2 Errors of Material Limitation

The presence of walls introduces an error which is extremely difficult to evaluate. An electric cut will lead to a limitation of the domain and, in addition, play the role of a mirror with respect to the equipotential lines. On this subject, the revolution tank yields valuable data. A careful selection of the dimensions of the models, taking the dimensions of the inclined tank into

consideration ($1.50 \text{ m} \times 1.50 \text{ m}$), permits an enlargement of the domain under study and, consequently, an experimental definition of the error produced by the limitation of the electric network. The considerable distance of the cell wall with respect to the exit of the ion gun (Fig.44) almost completely eliminates all possible trouble in this zone. The four experiments made (Fig.45) a-b-c-d lead to the following results:

a) The configuration studied in the tank exactly simulates the domain defined at the network (Fig.45). The agreement between the two Laplacien fields is excellent.

b) Elimination of the insulator B leads to only a minor change in the slope of the equipotential lines at the exit from the gun. This important result makes it possible to define the error committed by the limitation in this region.

c) After re-introducing the insulator B, the insulator A is removed (Fig.43 and 44). This operation introduces no noticeable trouble into the field. This is most likely due to the parallelism of the equipotential lines with the two focusing and accelerating electrodes in the domain of interest.

d) Elimination of the two insulators A and B results in a noticeable disturbance of the field at the exit from the electrostatic propulsor (see the network of curves on the graph of Fig.44). This case, which is of a purely instructive nature, corresponds to no physical reality in view of the fact that the real domain is necessarily limited in the region of the insulator A. This perturbation obviously will only occur if the electric currents, flowing in the electrolytes, are allowed to surround the accelerating electrode.

72

5.1.3 Electric Errors

This denomination is reserved exclusively to errors produced by the measuring methods used. Thanks to the quotient meter V-34 A, with which potential readings to within $1/10,000$ are obtained, the error becomes insignificant with respect to the approximation of the principle which entrains the systematic use of large resistances and which has been described in Section 3.4.

5.1.4 Errors of Quantification

Instead of varying in a continuous manner, the large resistances are realized in the form of contactors giving about one hundred different values, ranging from $10^5 \Omega$ to $10^7 \Omega$, which leads to the introduction of a quantification error.

Values lower than $10^5 \Omega$ are posted by connecting the resistances in parallel. If, conversely, certain nodes must be fed by resistances higher than $10^7 \Omega$, these can be neglected without appreciable error in measurements in which the entity of the domain, traversed by the ions, is also traversed by sufficient intensities. /73

All these errors, except for the error of material limitation of the field, are encountered in the investigation of the one-dimensional problem. The convergence obtained by the method described in Section 4.1.3 shows a deviation of -0.28% between the experimental and theoretical fields (the large resistances being corrected in accordance with the process described in Section 3.4). It therefore seems permissible to estimate the overall error, due to the use of an electric network, as being less than 1% .

5.2 Errors Due to Computation on Digital Computers

The Runge-Kutta integration method which requires knowledge, at a given point of the domain under consideration, of the quantities r , z , r' , and r'' , introduces only an insignificant error if the field ϕ as well as its partial derivatives $\frac{\partial \phi}{\partial r}$ and $\frac{\partial \phi}{\partial z}$ are perfectly continuous. For proving this, it is sufficient to assume the particularly simple case of a uniform field created by two plane-parallel electrodes E and E' , spaced at a distance of d and brought to the respective potentials V_s and 0 (Fig.46). The voltage distribution obeys the linear law

$$\frac{V}{V_s} = 1 - \left(\frac{x}{d}\right) \quad (85)$$

where the Cartesian coordinates x and y are assumed, respectively, as being in the direction of the normal and of the tangent to the electrode E .

Let us assume an electron of the characteristics m and $-e$, issuing from the origin O at an initial velocity U_0 .

The fundamental equation of dynamics (eq.8). when applied to this particle, will yield

$$\begin{cases} m \frac{d^2 x}{dt^2} = +e \frac{\partial V}{\partial x} = -e \frac{V_s}{d} \\ m \frac{d^2 y}{dt^2} = 0 \end{cases} \quad (86)$$

An integration of the system of equations (86) will result in

$$\begin{cases} mx = -\frac{eV_s t^2}{2d} + At + B \\ my = Ct + D \end{cases} \quad (87)$$

at $t = 0$

$$\begin{cases} x = y = 0 \rightarrow B = D = 0 \\ x' = \left(\frac{dx}{dt}\right)_0 \text{ et } y' = \left(\frac{dy}{dt}\right)_0 \rightarrow \left(\frac{dy}{dx}\right)_0 = \frac{C}{A} \\ U_o^2 = \left(\frac{dx}{dt}\right)_0^2 + \left(\frac{dy}{dt}\right)_0^2 \rightarrow \frac{A^2 + C^2}{m^2} = U_o^2 \end{cases}$$

From this it follows that

$$\begin{cases} A = \frac{m U_o}{\sqrt{1 + \left(\frac{dy}{dx}\right)_0^2}} \\ C = \frac{m U_o \left(\frac{dy}{dx}\right)_0}{\sqrt{1 + \left(\frac{dy}{dx}\right)_0^2}} \end{cases} \quad (88)$$

An elimination of the time between the equations (87) will yield the Cartesian equation of the trajectory:

$$x = ay^2 + by \quad (89)$$

by assuming that

$$\begin{cases} a = - \frac{e V_s \left[1 + \left(\frac{dy}{dx}\right)_0^2 \right]}{2 m d U_o^2 \left(\frac{dy}{dx}\right)_0^2} \\ b = \frac{1}{\left(\frac{dy}{dx}\right)_0} \end{cases} \quad (90)$$

The variation in the coordinates, defined by

$$\begin{cases} x = - \frac{b^2}{4a} + X \\ y = - \frac{b}{2a} + Y \end{cases} \quad (91)$$

shows that the theoretical trajectory is a parabola:

$$X = a Y^2 \quad (92)$$

Equation (11) which is valid in Cartesian coordinates where y and x replace, respectively, r and z , is written as follows:

$$\frac{d^2 y}{dx^2} = \frac{\left\{ 1 + \left(\frac{dy}{dx} \right)^2 \right\} \left(\frac{\partial V}{\partial y} - \frac{dy}{dx} \frac{\partial V}{\partial x} \right)}{2 \left(V + \frac{m U_0^2}{2e} - V_s \right)} \quad (93)$$

Figure 46 shows various theoretical trajectories merged with their homologs, obtained by an exploitation of the uniform field on the Gamma AET computer. The parabola cuts the y -axis at a certain ordinate point y_1 . Solution by digital computers yields an error defined by $\frac{|\Delta y_1|}{y_1}$. Table XII furnishes a series of results, corresponding to a given value of $\frac{m U_0^2}{2e}$ and to entrance angles to the field, varying from 10° to 10° . It thus seems that the errors due to the mode of calculation on digital computers are negligible.

5.3 Errors Introduced by the Method of Calculating the Space Charge

Let us use the ^{current} tube of Fig. 6. Then, the relation (23), derived in Section 1.5, is valid over the entire surface Σ of elementary volume γ .

$$\iint_{\Sigma} \rho \vec{U} \cdot \vec{n} d\sigma = 0 \quad (23)$$

This equation (23) is then transformed into

$$\iint_{\Sigma_i} \rho(P_j) \vec{U}(P_j) \vec{n}_j d\sigma_j + \iint_{\Sigma_{i+1}} \rho(P_l) \vec{U}(P_l) \vec{n}_l d\sigma_l = 0 \quad (23)$$

Let us denote these two integrals by $J_i(P_j)$ and $J_{i+1}(P_l)$.

Let us assume that V_j is the electric potential at a point P_j of the sector Σ_i (Fig.47).

By hypothesis, the electrode (E) emits ions, having the characteristics m and $+e$, without initial velocity.

Consequently:

$$\frac{1}{2} m U_j^2 = e (V_s - V_j)$$

The integral $J_i(P_j)$ can then be written as follows:

$$J_i(P_j) = \iint_{\Sigma_i} \rho(P_j) \sqrt{\frac{2e}{m} (V_s - V_j)} \frac{1}{\sqrt{1+r_j'^2}} d\sigma_j \quad (94)$$

In the method, discussed in Section 1.5, the calculation of the integral J_i was based on the hypothesis of uniformity of the fields $\vec{U}(P_j)$ and $\rho(P_j)$ in the sector Σ_i .

From this it follows that

$$J_i(M_i) = \rho(M_i) \sqrt{\frac{2e(V_s - V_i)}{m(1+r_i'^2)}} \iint_{\Sigma_i} d\sigma_j \quad (95)$$

Let us assume that

$$\rho(r_j) = \rho(M_i) + \delta r_j \frac{d\rho}{dr}(M_i) + \frac{1}{2} \delta r_j^2 \frac{d^2\rho}{dr^2}(M_i) \quad (96)$$

Since $d\sigma_j = 2\pi r_j dr_j$, it follows that

$$J_i(P_j) = 2\pi \rho(M_i) \sqrt{\frac{2e}{m}} \int_{r_{1(i)}}^{r_{3(i)}} \sqrt{\frac{V_s - V_j}{1 + r_j'^2}} r_j dr_j + 2\pi \frac{d\rho}{dr}(M_i) \sqrt{\frac{2e}{m}} \int_{r_{1(i)}}^{r_{3(i)}} \sqrt{\frac{V_s - V_j}{1 + r_j'^2}} \delta r_j r_j dr_j \quad (97)$$

$$+ \pi \frac{d^2\rho}{dr^2}(M_i) \sqrt{\frac{2e}{m}} \int_{r_{1(i)}}^{r_{3(i)}} \sqrt{\frac{V_s - V_j}{1 + r_j'^2}} \delta r_j^2 r_j dr_j$$

with

$$\delta r_j = r_j - r_{2(i)} \quad (98)$$

However,

$$V_j = \frac{V_s}{100} \Phi_j \quad \text{and} \quad \alpha = \sqrt{\frac{2e}{m} V_s}$$

Consequently,

$$J_i(P_j) = \frac{\pi\alpha}{10} \left\{ 2\rho(M_i) K_1 + 2 \frac{d\rho}{dr}(M_i) K_2 + \frac{d^2\rho}{dr^2}(M_i) K_3 \right\} \quad (99)$$

where the integrals K_1 , K_2 , and K_3 are expressed by

$$K_\ell = \int_{r_{1(i)}}^{r_{3(i)}} \sqrt{\frac{100 - \Phi_j}{(1 + r_j'^2)}} r_j (\delta r_j)^{\ell-1} dr_j \quad (100)$$

where $l = 1, 2, \text{ and } 3$.

Since

$$J_l(M_l) = \frac{\pi \alpha}{10} \rho(M_l) \sqrt{\frac{100 - \Phi_l}{1 + r_l'^2}} (r_3^2 - r_1^2)_l \quad (101)$$

The error committed in calculating the space charge can therefore be written as follows:

$$E\% = \frac{2K_1 - \Theta_l}{\Theta_l} + \frac{2K_2 \frac{d\rho}{dr}(M_l)}{\Theta_l \rho(M_l)} + \frac{K_3 \frac{d^2\rho}{dr^2}(M_l)}{\Theta_l \rho(M_l)} \quad (102)$$

while denoting by Θ_l the coefficient $\sqrt{\frac{100 - \Phi_l}{1 + r_l'^2}} (r_3^2 - r_1^2)_l$

Two examples are given, with the current tube defined by the trajectories 9 and 11 in the case of the Laplacien field (three-dimensional problem of axial symmetry). In the sectors $z = 10Ar$ (Table XIII) and $z = 2Ar$ (Table XIV), several intermediary trajectories are considered for calculating the integrals K_l . The numerical results demonstrate the validity of the approximation made in the determination of the space charge by the method described in Section 1.5, where the quantity $\frac{\alpha\rho}{j_0}$ evolves rather slowly in the sector $z = 10Ar$ (the most frequent case) and much more rapidly in the sector which is closer to the emitter.

In summation, this a priori study of the accuracy, supported by several calculations in specific cases, leads to differentiation of two predominant errors: The first error, due to the principle of high resistances, is readily

reduced to a lower order if the posted intensities are "corrected" (see Section 3.4); the second error, acting on the determination of the trajectories and thus also on the calculation of the space charge, is due to the continuity of the field and of its partial derivatives $\frac{\partial \phi}{\partial r}$ and $\frac{\partial \phi}{\partial z}$. The importance of the parabolic extrapolation, described in Section 2.2.1, is thus proved by its incidence on automatic auxiliary computations (digital computer) and numerical calculations (space charge).

By reducing the three preponderant errors, it seems logical to estimate the overall error as being 1 to 2%.

CONCLUSION

/80

The combination of an electrical network with digital computers, for investigating a configuration of focusing and accelerating electrodes adapted to an ion generator, permits solution of Poisson's equation $\Delta V = -\rho/\epsilon_0$ which links the electric potential to the space charge in an ion propulsor.

The trajectories corresponding to the card of potentials read on the network, at a finite number of points, are determined by means of the Runge-Kutta fourth-order integration method, adapted for digital computers.

The cutting of the ion beam into a certain number of elementary current tubes permits a step-by-step calculation of the space charge. This charge is simulated by injecting current into each node of a network composed of pure resistances.

The solution of Poisson's equation by this iterative method leads to a satisfactory convergence after the fourth approximation.

The potential distribution, satisfying the condition of cancellation of the electric field at the surface of the emitter, is obtained by three methods tested for the theoretical case of a plane diode. The results show that the ion beam has the desired optical qualities.

The potential distribution, satisfying Laplace's equation, is readily obtained in an electrolytic tank, regardless of the shape of the electrodes used or of the voltages applied. Its study in the vicinity of the axis, which can be reduced to a one-dimensional problem, will lead, at the end of a cycle of approximations, to a configuration of the potential quite far from reality.

Actually, experiments were made on an electric network, based on values of the analog potential ϕ_L on the axis of the propulsor (Field I and Fig.49) and

/81

based on the space charge calculated in the elementary tube (D'), as shown in Fig.48a, by assimilating the equipotential surfaces to orthogonal planes at the axis OZ . These experiments are based on the rather rough hypothesis which transforms Fig.48a into Fig.48b. Such an approximation, which replaces the function ρ (variable in the plane $z = z_1$ and canceled outside of the ion beam) by a constant ρ_1 will lead to a potential distribution on the axis, after convergence of the iterative process, which is clearly different from that obtained in the Field II. Consequently, it is rather difficult to draw definite conclusions on the basis of a single distribution of the Laplacian potential Φ_L on the axis of revolution of the system.

However, an investigation of the equipotential lines, of the current lines, and specifically of the trajectories obtained either in the electrolytic tank or by one of the methods discussed in the Introduction, yields useful indications on the form of the final beam. The influence of the space charge, using the shape of the electrodes shown in Fig.29 and the resultant potential distribution on the axis (Fig.49), leads to a widening of the beam (at convergence) to the right of the exit electrode of the ion gun, equal to 2.09 times that corresponding to the Laplacian field; obviously, the maximum broadening of the beam takes place after the first approximation (for the methods No.2 and No.3), characterized by the coefficient 2.58.

Since the space charge results in an increase of the angle of aperture of the beam, it is necessary that the trajectories which had been calculated by neglecting this charge, converge strongly toward the axis of revolution of the vacuum tube, which a priori excludes any emitting surface whose concavity is not directed toward positive z .

The described analog calculation method may be readily generalized no

matter what the geometric and electric characteristics of the propulsor and no matter what the initial conditions imposed on the electric particles might be.

APPENDIX I

METHOD OF TRUE RESISTANCES AND HOLLOW CYLINDER

Using the denotations by J.Miroux (Bibl. 8), Fig. 50 shows a notch cut by two meridian planes in a cylinder, as well as a portion of the network (resistances arranged in accordance with the radius vector).

By definition, the true value R_v of a resistance R_r corresponds to the integration of a corona having a thickness dr :

$$R_{v_n} = \int_{\rho_{n-1}^*}^{\rho_n^*} \frac{dr}{2\pi r} = \frac{1}{2\pi} \text{Log} \frac{\rho_n^*}{\rho_{n-1}^*} \quad (103)$$

For a regular meshing, we have

$$R_{v_n} = \frac{1}{2\pi} \text{Log} \frac{n}{n-1} \quad (104)$$

The resistance R_l is infinite. A priori, it seems that the difficulty actually increases. Nevertheless, it is obvious (eq. 8) that R_v is the only value which, at each node, would give the exact distribution of voltages and currents at permanent regime.

In view of the fact that the investigations require a satisfactory accuracy in the vicinity of the axis, use of the artifice of the hollow cylinder (the cylinder having along its axis a void space of very small radius r_0) permits giving a finite value to the resistances R_l (as in the case of the

finite-difference method) as well as to the resistances located along the pseudo-axis which will then be equal to .

$$R_z = \frac{\Delta z^2}{\Delta r^2} \frac{1}{\beta r_0}$$

We adopted this artifice and therefore had to determine the value of the radius r_0 . This quantity, by using the method of true values, makes it possible to define the values of resistances coinciding with those obtained by the finite-difference method from a certain previously selected radius r_0 .

To do this, let us assume a hollow cylinder of revolution (Fig. 51) of infinite length, composed of two armatures defined by the radii r_0 and r_1 and charged, respectively, to the analog potentials of +100 and 0. If l denotes the length of the cylinder and Q its charge, the potential distribution at a distance r from the axis will obey the law

$$100 - \Phi(r) = \frac{2Q}{\epsilon_0 l} \log \frac{r}{r_0} \quad (105)$$

with

$$\Phi(r_1) = 0$$

Let us assume that

$$r_1 = 10 \Delta r$$

$$r_0 = k_0 \Delta r \quad \text{with} \quad 0 < k_0 < 1$$

from which it follows that

$$100 = \frac{2Q}{\epsilon_0 l} \log \frac{10}{k_0}$$

Equation (105) is transformed in accordance with

$$100 - \Phi(r) = \frac{100}{\log \frac{10}{k_0}} \log \frac{r}{r_0} \quad (105)'$$

Two different methods for calculating r_0 can be applied here.

Numerical Method:

The conductances C_r are obtained by giving to r values equal to multiples of the meshing Δr , except for the first line where $r = k_0 \Delta r$ [for the second line, $r = \Delta r$, ... ; for the n^{th} line, $r = (n-1)\Delta r$]. Conversely, the conductances C_r are calculated by means of the finite-difference method, taking the center (see Fig. 50) of each mesh into consideration (for R_1 , $r = \frac{\Delta r}{2}$; for R_2 , $r = \frac{3}{2} \Delta r$... ; for R_n , $r = \frac{(2n-1)\Delta r}{2}$). /85

Since all conductances are defined to within a factor β , all computations and experiments are made with

$$\beta \Delta r = 10^{-4}$$

When applying the finite-difference method after the axis ($r = 0$), the resistances R_r assume the values shown in Table I.

Let us apply an analog potential equal to +100 to the axis, and equal to zero to the node defined by $r = r_1$; then, the analog intensity circulating within the "line" will be

$$i = \frac{100}{\sum_{n=1}^{n=10} R_n}$$

Using $r_l = 5\Delta r$, we obtain

$$\Phi(r_l) = \frac{100}{\sum_{n=1}^{n=10} R_n} \cdot \sum_{n=6}^{n=10} R_n = 16,217$$

Then, eq. (105)' can be written as follows:

$$83,783 = \frac{100 (\log 5 - \log k_0)}{(1 - \log k_0)}$$

From which it follows that

$$\log k_0 = \bar{1},14374 \quad (106)$$

and

$$k_0 = 0,13923$$

Graphical Method:

Let us now apply the finite-difference method after the pseudo-axis ($r = r_0$). Only the resistance R_1 is modified. Reasoning as before, we obtain:

$$i = \frac{100}{\sum_{n=2}^{n=10} R_n + \frac{2 \cdot 10^4}{1 - k_0}}$$

Similarly,

$$\Phi(r_l) = \frac{100}{\sum_{n=2}^{n=10} R_n + \frac{2 \cdot 10^4}{1 - k_0}} \sum_{n=6}^{n=10} R_n$$

From this it follows that

$$100 - \frac{100 \sum_{n=6}^{n=10} R_n}{\sum_{n=2}^{n=10} R_n + \frac{2 \cdot 10^4}{1 - k_0}} = \frac{100 (\log 5 - \log k_0)}{1 - \log k_0}$$

Let

$$\frac{6919,1(1 - k_0)}{42665 - 22665 k_0} = \frac{1 - \log 5}{1 - \log k_0}$$

Let us assume that

$$\begin{cases} x = k_0 \\ y = \log k_0 \end{cases}$$

from which we obtain

$$y = 1 + \frac{0,98609 x - 1,85623}{1 - x} \quad (107)$$

Equation (107) represents an equilateral hyperbola $y_1(x)$ (see Table II).

It is sufficient to define the intersection of this hyperbola with the curve

$y_2 = \log x$ in order to obtain the desired value of k_0 (see Table III and

Chart I).

This graphical method will finally yield

$$k_0 = 0,109 \quad (108)$$

Conclusion

The two methods thus lead to values of k_0 which are equal to 0.139 and 0.109. In accordance with our experiments, neither of the two methods apparently is preferable. Consequently, their use can be left to the discretion of the experimenter.

APPENDIX II

STUDY OF TRAJECTORIES BY THE DISTRIBUTION THEORY

/88

The analog potential function, in the two sectors r_j and z_e , in the vicinity of the emitter (most critical case) is Φ , so that

/89

$$\Phi = \Phi_1 \quad \text{for} \quad z \geq z_{ej} \quad \text{and} \quad 0 \leq r \leq r_j$$

$$\Phi = \Phi_2 = \Phi_e \quad \text{for} \quad 0 \leq z \leq z_{ej} \quad \text{and} \quad r_j \leq r \leq \frac{D}{2}$$

where

$$\Phi_1(r_j, z_{ej}) = \Phi_2(r_j, z_{ej}) = \Phi_e$$

(Fig. 52)

The parabolic extrapolation leads to a new function Φ^* , which is continuous at the boundary of the electrode, so that

$$\Phi^* = \Phi_1 \quad \text{for} \quad z \geq z_{ej} \quad \text{and} \quad 0 \leq r \leq r_j$$

$$\Phi^* = \Phi_3 \quad \text{for} \quad 0 \leq z \leq z_{ej} \quad \text{and} \quad r_j \leq r \leq \frac{D}{2}$$

$$\text{with} \quad \Phi_1(r_j, z_{ej}) = \Phi_3(r_j, z_{ej}) = \Phi_e$$

and

$$\begin{aligned} \frac{\partial \Phi_1}{\partial z}(r_j, z_{ej}) &= \frac{\partial \Phi_3}{\partial z}(r_j, z_{ej}) \\ \frac{\partial \Phi_1}{\partial r}(r_j, z_{ej}) &= \frac{\partial \Phi_3}{\partial r}(r_j, z_{ej}) \end{aligned}$$

Let us assume that $f(x_1)$ is an indefinitely derivable function in the complementary of a regular hypersurface (S) in such a manner that each partial

derivative has a limit on either side of (S), at each point of (S). The difference between these limits represents the "jump" of the corresponding partial derivative. This jump is determined for a fixed direction of "traversal" of the surface (S) and changes its sign as soon as the direction of this traversal is modified. This jump is a definite function of the surface (S).

Let us denote by $D^P f$ a derivative of f in the direction of the distributions and let $\{D^P, f\}$ be the distribution represented by the conventional derived function, defined for $x \notin (S)$ and undefined for $x \in (S)$. It can be demonstrated that

$$\frac{\partial f}{\partial x_i} = \left\{ \frac{\partial f}{\partial x_i} \right\} + (\sigma_0 \cos \theta_i) \delta_{(S)} \quad (109)$$

and

$$\frac{\partial^2 f}{\partial x_i^2} = \left\{ \frac{\partial^2 f}{\partial x_i^2} \right\} + \frac{\partial}{\partial x_i} \left[(\sigma_0 \cos \theta_i) \delta_{(S)} \right] + \sigma_i \cos \theta_i \delta_{(S)} \quad (110)$$

where:

θ_1 = angle of the x_1 axis with the normal to (S) in the direction of the traversal corresponding to the intersection of x_1 (Fig. 53);

σ_0 = discontinuity of f when traversing (S) in the direction of the x_1 axis;

σ_1 = jump of $\frac{\partial f}{\partial x_1}$ at the traversal of (S);

$(\sigma_0 \cos \theta_1) \delta_{(S)}$ = symbolic notation for the distribution corresponding to masses placed on (S), having a surface density of $\sigma_0 \cos \theta_1$,

The emitting surface plays the role of the surface (S) in the case under consideration.

The discontinuities of Φ , on traversing (S) in the direction of the r and z axes, are zero. Consequently, $\sigma_{or} = \sigma_{oz} = 0$.

Conversely:

$$\sigma_{1r} = \frac{\partial \Phi_1}{\partial r} (r_j, z_{ej})$$

$$\sigma_{1z} = \frac{\partial \Phi_1}{\partial z} (r_j, z_{ej})$$

in view of the fact that

$$\frac{\partial \Phi_2}{\partial r} (r_j, z_{ej}) = \frac{\partial \Phi_2}{\partial z} (r_j, z_{ej}) = 0$$

In the domain, defined by $z \geq z_0$, and $0 \leq r \leq r_1$, and when applying eq. (109), 91
we will have:

$$\frac{\partial \Phi}{\partial r} - r' \frac{\partial \Phi}{\partial z} = \left\{ \frac{\partial \Phi^*}{\partial r} \right\} - r' \left\{ \frac{\partial \Phi^*}{\partial z} \right\}$$

Thereafter, the differential equation (eq. 20) assumes the form

$$r'' = \frac{(1 + r'^2) \left[\left\{ \frac{\partial \Phi^*}{\partial r} \right\} - r' \left\{ \frac{\partial \Phi^*}{\partial z} \right\} \right]}{2 (\Phi^* + V)} \quad (111)$$

From this it follows that the ion trajectories are not at all modified in the vicinity of the emitter by the presence of the discontinuities σ_{1r} and σ_{1z} on the first-order partial derivatives of the field Φ . The parabolic extrapolation, provided that it is done with special care by eliminating these discontinuities and by respecting the field in the domain $z \geq z_0$, and $0 \leq r \leq r_1$, will permit a correct calculation of the functions $\frac{\partial \Phi}{\partial r}$ and $\frac{\partial \Phi}{\partial z}$ and thus also of

the expression (20).

In practical work, a single extrapolation is often sufficient. The selection of this extrapolation is of prime importance and, almost always, results in a perfectly continuous field in the other section.

1. Musson-Genon, R. Application of Rheographic Methods to the Study of Plane Electronic Trajectories, Taking the Space Charge into Consideration (Application des méthodes rhéographiques à l'étude des trajectoires électroniques planes compte tenu de la charge d'espace). Annales des Télécommunications, Vol. 2, Nos. 8, 9, 10, 1947.
2. Lapostolle, Picquendar, and Cahen. The Effects of Space Charge in Electron Guns (Les effets de la charge d'espace dans les canons à électrons). Étude C.N.E.T., No. 432 PDT.
3. Fox, R. Physics of the Ion Thrust System. American Rocket Society, 14th Annual Meeting 1959.
4. Brewer, G.R., Etter, J.E., and Anderson, J.R. Design and Performance of Small Model Ion Engines. A.R.S. May 1960.
5. Marvaud, J. Automatic Trajectory Tracers, Using the Electric Tank (Traceurs automatiques de trajectoires utilisant le bassin électrique). Doctor Thesis, July 1953.
6. Pierce, J.R. Theory and Design of Electron Beams. Second Edition. D. Van Nostrand Company, Inc. 1954.
7. Persico, E. Il novo cimento, Vol. IX, No.1, 1952, P. 1.
8. Miroux, J. On a New Analog Analyzer of Transitory States; Application to the Study of Certain Phenomena of Variable State. (Sur un nouvel analyseur analogique de régimes transitoires - Application à l'étude de certains phénomènes de régime variable). Publication O.N.E.R.A., No. 81, 1955.
9. Hildebrand, F.B. Introduction to Numerical Analysis. McGraw-Hill Book Company, Inc., 1956.
10. Mineur, H. Technique of Numerical Computation. (Techniques de calcul

numerique). Librairie Polytechnique Ch. Béranger, 1952.

11. Huard de la Marre, P. Solution of Problems of Infiltrations at a Free Surface, Using Electric Analog Means (Résolution de problèmes d'infiltrations à surface libre au moyen d'analogies électriques).

Doctor Thesis, June 1956.

12. Schwartz, L. Theory of Distributions, Volumes I and II (Théorie des distributions, Tomes I et II). Act. Scient et Industr. Hermann 1950.

13. Karplus, W.J. Analog Simulation. Solution of Field Problems. McGraw-Hill Book Company, Inc., 1958.

14. Duquenne, R. Study, by Electric Analogy, of Load-Carrying Surfaces in the Nonstationary State (Étude, par analogie électrique, des surfaces portantes en régime instationnaire). Doctor Thesis, May 1960.

15. Malavard, L. The Use of Galvanometric Analogies in Aerodynamics (L'emploi des analogies rhéoélectriques en aerodynamique). Agardograph 18, August 1956.

16. Bayet, M. Electron Physics of Gases and Solids (Physique électronique des gaz et des solides). Masson.

17. Besson, J. Tracer for Galvanometric Tanks (Traceur pour cuves rhéoélectriques). La Recherche Aéronautique, No.82, May-June 1961.

18. Langlois, M. Automatic Tracer of Equipotential Lines. System of Commutation of the Role of Variables (Traceur automatique de lignes équipotentiellles. Système de commutation du rôle des variables). Etude 1514 AP (Interdepartmental Note).

19. Kirchhoff - On the Theory of the Capacitor (Zur Theorie des Condensators). Berlin, Monatsberichte 1878, pp.144-162.

20. Gray, F. Theory of Electrostatic Fields as Lenses for Electron Beams in

/94

Systems where the Fields are Symmetrical about a Central Axis. The Bell System Technical Manual, Vol. 18, January 1939, pp.1-29.

21. Cockroft, J.D. The Effect of Curved Boundaries on the Distribution of Electric Stress Round Boundaries. Journal I.E.E., Vol.66, 1928, pp.385-409.

22. Kucera, J. Distribution of Magnetic Fluxes in Stators and Rotors (Répartition des flux magnétiques dans les stators et rotors). R.G.E., Vol.27, 1930, pp.645-657.

23. Duchon, R. Study of the Potential Created by Two Equal Coaxial Cylinders, Having Equal and Opposite Charges (Etude du potentiel créé par deux cylindres coaxiaux égaux portant des charges égales et opposées). Les Cahiers de Physique, December 1943.

24. Balachowsky - Note on a Plotting of Electric Fields (Note sur un tracé de champs électriques). Bulletin de la Société Française des Electriciens, No.58, April 1946, pp.181-186.

25. Frocht, M. The Numerical Solution of Laplace's Equation in Composite Rectangular Areas. Journal of Applied Physics, Vol.17, September 1946, pp.730-742.

26. Lehmann, T. Graphic Determination of Laplacian and Turbulent Magnetic Fields, with Plane Flux Lines (Détermination graphique des champs magnétiques laplaciens et tourbillonnaires à lignes de flux planes). R.G.E., Vol.14, 1923, pp.347-357, 395-403.

27. Gabor - Mechanical Tracer for Electron Trajectories. Nature, Vol.39, February 1937.

28. Langmuir - Automatic Plotting of Electron Trajectories. Nature, Vol.39, 1937, p.1066.

/95

29. Melin, L. Electric Propulsion (La propulsion electrique). Congress on
Aeronautic Information, May-June 1960 (ENSA).

30. Edwards, R.N. and Kuskevics, G. Research on Cesium and Ion Rockets (Re-
cherches sur les fusées à ions de césium). ASME (59 - AV - 32),
March 1959.

31. Forrester, A.T. and Speiser, R.C. Propulsion by Cesium Ions (Propulsion
par ions de césium). Astronautics, October 1959.

TABLES, GRAPHS, and ILLUSTRATIONS

1
2
3
4
5
6
7
8
9
10
11
12
13
14
15
16
17
18
19
20
21
22
23
24
25
26
27
28
29
30
31
32
33
34
35
36
37
38
39
40
41
42
43
44
45
46
47
48
49
50
51
52

TABLE I

Resistances R_r in Ω		True resistances
R_1	20.000	19.997
R_2	6.666,6	6.931
R_3	4.000	4.054
R_4	2.857,1	2.876
R_5	2.222,2	2.231
R_6	1.818,2	1.818,2
R_7	1.538,5	1.538,5
R_8	1.333,3	1,333,3
R_9	1.176,5	1,176,5
R_{10}	1.052,6	1.052,6
$\sum_{n=1}^{n=10} R_n = 42.665$		

TABLE II

x	-0,50	-0,20	0	0,10	0,20	0,30	0,40	0,50	0,60	0,70	0,80	1
y_1	-0,566	-0,711	-0,856	-0,953	-1,074	-1,229	-1,436	-1,726	-2,161	-2,887	-4,337	$-\infty$

TABLE III

x	0	0,01	0,05	0,10	0,15	0,20	0,30	0,50	0,70	0,85	1
y_2	$-\infty$	-2	-1,301	-1	-0,824	-0,698	-0,523	-0,301	-0,155	-0,071	0

TABLE IV

Diode: Method No.1 $J_0 = 47.98 \text{ amp/m}^2$															
Φ	Z/d	0	0.005	0.010	0.015	0.020	0.025	0.0375	0.05	0.10	0.15	0.20	0.25	0.30	0.35
Approximation 0	100	99.50	99.00	98.50	98.00	97.50	96.245	94.995	89.99	84.995	79.99	74.99	69.99	64.99	59.99
Approximation 1	100	99.78	99.54	99.29	98.03	96.76	94.04	91.29	84.02	76.49	68.99	61.49	53.99	46.49	38.99
Approximation 2	100	99.85	99.68	99.49	98.28	97.06	94.46	91.82	84.84	77.84	70.84	63.84	56.84	49.84	42.84
Approximation 3	100	99.89	99.74	99.57	98.38	97.18	94.62	92.01	85.11	78.11	71.11	64.11	57.11	50.11	43.11
Approximation 4	100	99.90	99.76	99.60	98.42	97.23	94.68	92.08	85.19	78.19	71.19	64.19	57.19	50.19	43.19
Child's Law	100	99.915	99.785	99.63	98.46	97.27	94.745	92.16	85.36	78.36	71.36	64.36	57.36	50.36	43.36

Φ	Z/d	0.40	0.45	0.50	0.55	0.60	0.65	0.70	0.75	0.80	0.85	0.90	0.95	1	$\epsilon\%$
Approximation 0	59.99	54.39	49.99	44.99	39.99	34.995	30.00	25.00	20.00	15.00	10.00	5.00	0	0	-12.49
Approximation 1	68.60	63.67	58.565	53.32	47.92	42.37	36.69	30.88	24.95	18.89	12.69	6.41	0	0	-2.08
Approximation 2	69.88	64.90	59.735	54.40	48.90	43.26	37.47	31.54	25.48	19.29	12.97	6.54	0	0	-0.72
Approximation 3	70.19	65.19	59.995	54.65	49.13	43.46	37.64	31.69	25.60	19.38	13.04	6.58	0	0	-0.38
Approximation 4	70.28	65.27	60.075	54.72	49.19	43.50	37.69	31.73	25.63	19.40	13.05	6.58	0	0	-0.28
Child's Law	70.53	65.52	60.365	54.95	49.395	43.695	37.855	31.86	25.735	19.48	13.11	6.615	0	0	

TABLE V

Emission density J_0 (amp/cm ²)	1 st Approximation					2 nd Approximation					3 rd Approximation					4 th Approximation					
	$\mathcal{R}_p(\alpha)$	i_p	i_p/i_L	$\epsilon\%$	$\mathcal{R}_p(\alpha)$	i_p	i_p/i_L	$\epsilon\%$	$\mathcal{R}_p(\alpha)$	i_p	i_p/i_L	$\epsilon\%$	$\mathcal{R}_p(\alpha)$	i_p	i_p/i_L	$\epsilon\%$	$\mathcal{R}_p(\alpha)$	i_p	i_p/i_L	$\epsilon\%$	$\left(\frac{i_p-i_p^0}{i_L}\right)\%$
35	24.602	-4.010	58.425	-4.75	21.121	-4.735	52.655	-4.075	20.480	-4.591	5.120	51.195	-3.96	20.323	-4.906	5.035	50.945	-3.94			0.25
40	21.607	-4.611	55.035	-3.64	17.940	-5.574	44.265	-2.74	17.165	-5.026	4.175	41.745	-2.55	16.940	-5.303	4.080	40.975	-2.54			0.77
45.5	19.029	-5.255	47.465	-2.45	15.280	-6.5445	34.56	-1.245	14.219	-7.033	2.968	29.68	-0.99	13.820	-7.236	2.765	27.65	-0.903			2.03
47.38	18.344	-5.451	45.485	-2.00	14.459	-6.916	30.85	-0.72	13.270	-7.536	2.465	24.65	-0.30	12.780	-7.825	2.176	21.76	-0.20			2.89
49	17.719	-5.644	43.565	-1.715	13.815	-7.2365	27.62	-0.27	12.549	-7.969	2.032	20.32	+0.065	11.931	-8.305	1.6195	16.195	+0.275			4.125
51	17.037	-5.8655	41.31	-1.30	13.118	-7.623	23.70	+0.30	11.713	-8.535	1.4635	14.635	+0.765	10.774	-9.205	0.7195	7.195	+0.97			7.44

TABLE VII

Diode: Method No.2 $J_0 = 10 \text{ amp/m}^2$

$\frac{z}{d}$	0	0.005	0.010	0.015	0.020	0.025	0.0375	0.05	0.10	0.15	0.20	0.25	0.30	0.35
Approximation 0	100	99.50	99.00	98.50	98.00	97.50	96.245	94.995	89.99	84.995	79.99	74.99	69.99	64.99
Approximation 1	100	99.9985	99.98	99.92	99.86	99.79	99.54	99.21	97.355	94.88	91.905	88.47	84.62	80.425
Approximation 2	100	99.9955	99.83	99.62	99.38	99.13	98.43	97.675	94.19	90.295	86.115	81.705	77.10	72.33
Approximation 3	100	99.98	99.925	99.83	99.715	99.575	99.155	98.68	96.21	93.145	89.645	85.785	81.60	77.11
Approximation 4	100	99.99	99.925	99.885	99.66	99.50	99.02	98.47	95.69	92.355	88.605	84.53	80.16	75.545
Child's Law	100	99.915	99.785	99.63	99.46	99.27	98.745	98.16	95.36	92.03	88.305	84.25	79.92	75.34

$\frac{z}{d}$	0.40	0.45	0.50	0.55	0.60	0.65	0.70	0.75	0.80	0.85	0.90	0.95	1	$\epsilon \%$
Approximation 0	59.99	54.99	49.99	44.99	39.99	34.995	30.00	25.00	20.00	15.00	10.00	5.00	0	-12.49
Approximation 1	75.88	71.01	65.82	60.34	54.59	48.59	42.34	35.84	29.095	22.14	14.97	7.59	0	+6.67
Approximation 2	61.405	62.34	57.16	51.87	46.465	40.96	35.36	29.67	23.895	18.04	12.095	6.09	0	-3.73
Approximation 3	72.375	67.385	62.19	56.775	51.17	45.37	39.375	33.21	26.88	20.38	13.725	6.935	0	+2.32
Approximation 4	70.705	65.665	60.44	55.035	49.465	43.74	37.87	31.865	25.73	19.47	13.09	6.60	0	+0.16
Child's Law	70.53	65.52	60.365	54.95	49.385	43.695	37.855	31.86	25.735	19.48	13.11	6.615	0	

* Values obtained by parabolic interpolation

TABLE VII

	J_0 amp/m ²	$R^2 \Omega$	i_φ	i_p/i_L %	2%	Maximum errors + -
1 st Approximation	87,50	10.019	- 9,981	+ 0,19	+ 6,53	14,59
2 nd Approximation	37,50	10.004	- 9,986	+ 0,04	- 1,32	0,19 3,40
3 rd Approximation	47,00	9.994	- 10,006	- 0,06	- 0,27	0,13 0,69
4 th Approximation	47,38	10.004	- 9,996	+ 0,04	- 0,10	0,13 0,38

TABLE VIII

Diode: Method No. 3

Φ	Z/d	0	0.005	0.010	0.015	0.020	0.025	0.0375	0.05	0.10	0.15	0.20	0.25	0.30	0.35
Approximation 0	100	99.50	99.00	98.50	98.00	97.50	96.245	94.995	89.99	84.995	79.99	74.99	69.99	64.99	
Approximation 1	100	99.989	99.96	99.91	99.85	99.77	99.52	99.18	97.39	94.84	91.82	88.36	84.50	80.27	
Approximation 2	100	99.99	99.91	99.78	99.63	99.45	98.93	98.32	95.30	91.75	87.82	83.58	79.10	74.38	
Approximation 3	100	99.99	99.88	99.74	99.58	99.40	98.87	98.27	95.36	91.94	88.15	84.04	79.67	75.07	
Approximation 4	100	99.99	99.88	99.74	99.58	99.39	98.87	98.28	95.42	92.04	88.28	84.18	79.83	75.23	
Child's Law	100	99.915	99.785	99.63	99.46	99.27	98.745	98.16	95.36	92.03	88.305	84.25	79.92	75.34	

Φ	Z/d	0.40	0.45	0.50	0.55	0.60	0.65	0.70	0.75	0.80	0.85	0.90	0.95	1	$\epsilon\%$
Approximation 0	59.99	54.99	49.99	44.99	39.99	34.995	30.00	25.00	20.00	15.00	10.00	5.00	0	0	-12.49
Approximation 1	75.70	70.83	65.64	60.19	54.47	48.48	42.24	35.76	29.05	22.12	14.94	7.58	0	0	+6.53
Approximation 2	69.48	64.42	59.17	53.79	48.28	42.63	36.86	30.98	24.99	18.89	12.67	6.39	0	0	-1.32
Approximation 3	70.25	65.24	60.03	54.67	49.15	43.47	37.65	31.69	25.60	19.38	13.02	6.57	0	0	-0.27
Approximation 4	70.42	65.41	60.18	54.82	49.29	43.60	37.76	31.79	25.68	19.44	13.06	6.59	0	0	-0.10
Child's Law	70.53	65.52	60.365	54.95	49.395	43.695	37.855	31.86	25.735	19.48	13.11	6.615	0	0	

TABLE IX

$r_0/\Delta r$	$z_0/\Delta r$	r'_0	$h_0/\Delta r$	$2Rh_0/\Delta r^2$
1	0,013608	- 0,0272210		
2	0,054462	- 0,0545025	0,109046	8,014881
3	0,122654	- 0,0819060	0,1638735	12,044702
4	0,2183355	- 0,1094941	0,219071	16,1017185
5	0,341725	- 0,1373314	0,2747685	20,195485
6	0,493104	- 0,1654858	0,331101	24,3359235
7	0,672826	- 0,1940285	0,388212	28,533582
8	0,881316	- 0,2230358	0,4462535	32,799632
9	1,1190795	- 0,2525896	0,505391	37,1462385
10	1,386707	- 0,2827791	0,5658025	41,586484
11	1,684882	- 0,3137021	0,6276845	46,134811
12	2,0143915	- 0,3454668	0,6912545	50,807206
13	2,3761365	- 0,3781943	0,756755	55,6214925
14	2,7711465	- 0,4120210	0,824460	60,597810
15	3,2005965	- 0,4471018	0,8946805	65,759017
16	3,665827	- 0,4836149	0,9677755	71,131499
17	4,168372	- 0,5217664	1,044159	76,7456865
18	4,709986	- 0,5617975	1,1243155	82,637189
19	5,2926875	- 0,6039931	1,2088205	88,848307
20	5,9188065	- 0,6486937		

TABLE X

1 st method $J_0 = 15 \text{ amp/m}^2$					
	R'_Ω	i_L	i_ϕ	i_P	$i_P/i_L \%$
Laplacian Field	5.667	0,017645			
1 st Approximation	11.130		0,008985	0,00866	49,08
2 nd Approximation	8.843		0,01131	0,006335	35,90
3 rd Approximation	8.171		0,01224	0,005405	30,63
4 th Approximation	7.730		0,01294	0,004705	26,665

TABLE XII

θ°	10	20	30	40	45	50	60	70	80
y_{1T}	21,89	41,1385	55,425	63,0276	64	63,0276	55,425	41,1385	21,89
y_{1e}	21,89	41,20	55,435	63,15	64	63,025	55,33	41,17	21,92
$ \Delta y_1 $	0,00	0,0615	0,010	0,1224	0,00	0,0026	0,095	0,0315	0,03
$\frac{ \Delta y_1 }{y_1} \%$	0,00	0,15	0,02	0,19	0,00	0,00	0,17	0,08	0,14

TABLE II

	J_0 amp/m ²	Focusing Electrode		Accelerating Electrode		Emitting Electrode		Emiller i_p	i_p / i_L %
		R_a	i_p	R_a	i_p	R_a	i_p		
1 st Approximation	31,60	14.135	-7,075	9.050	-11,050	5720	-17,4825	0	0
2 nd Approximation	13,35	24.715	-4,046	19.750	-5,063	5714	-17,5009	-0,0184	-0,105
3 rd Approximation	21,00	18.370	-5,444	10.395	-9,620	5723,5	-17,4718	+0,0107	+0,06
4 th Approximation	15,25	19.795	-5,052	13.867	-7,211	5719,5	-17,4840	-0,0015	-0,01
Laplacian Field		593,3	$i_L =$ 168,548	597,6	$i_L =$ -186,012	5720	$i_L =$ 17,4825	$i_L = 17,4825$	

TABLE III

\textcircled{H}_i	$\alpha\rho/j_0$	$\frac{d(\alpha\rho/j_0)}{dr}$	$\frac{d^2(\alpha\rho/j_0)}{dr^2}$	K_1
98,627	4,165	0,024	negligible	49,74
K_2	K_3	$E_1 \%$	$E_2 \%$	$E_3 \%$
1,36	10,63	- 0,15	+ 0,02	negligible
		$E \% = -0,13$		

TABLE IV

\textcircled{H}_i	$\alpha\rho/j_0$	$\frac{d(\alpha\rho/j_0)}{dr}$	$\frac{d^2(\alpha\rho/j_0)}{dr^2}$	K_1
40,098	10,371	1,769	0,401	19,746
K_2	K_3	$E_1 \%$	$E_2 \%$	$E_3 \%$
0,63	4,065	- 1,51	+ 0,54	+ 0,39
		$E \% = -0,58$		

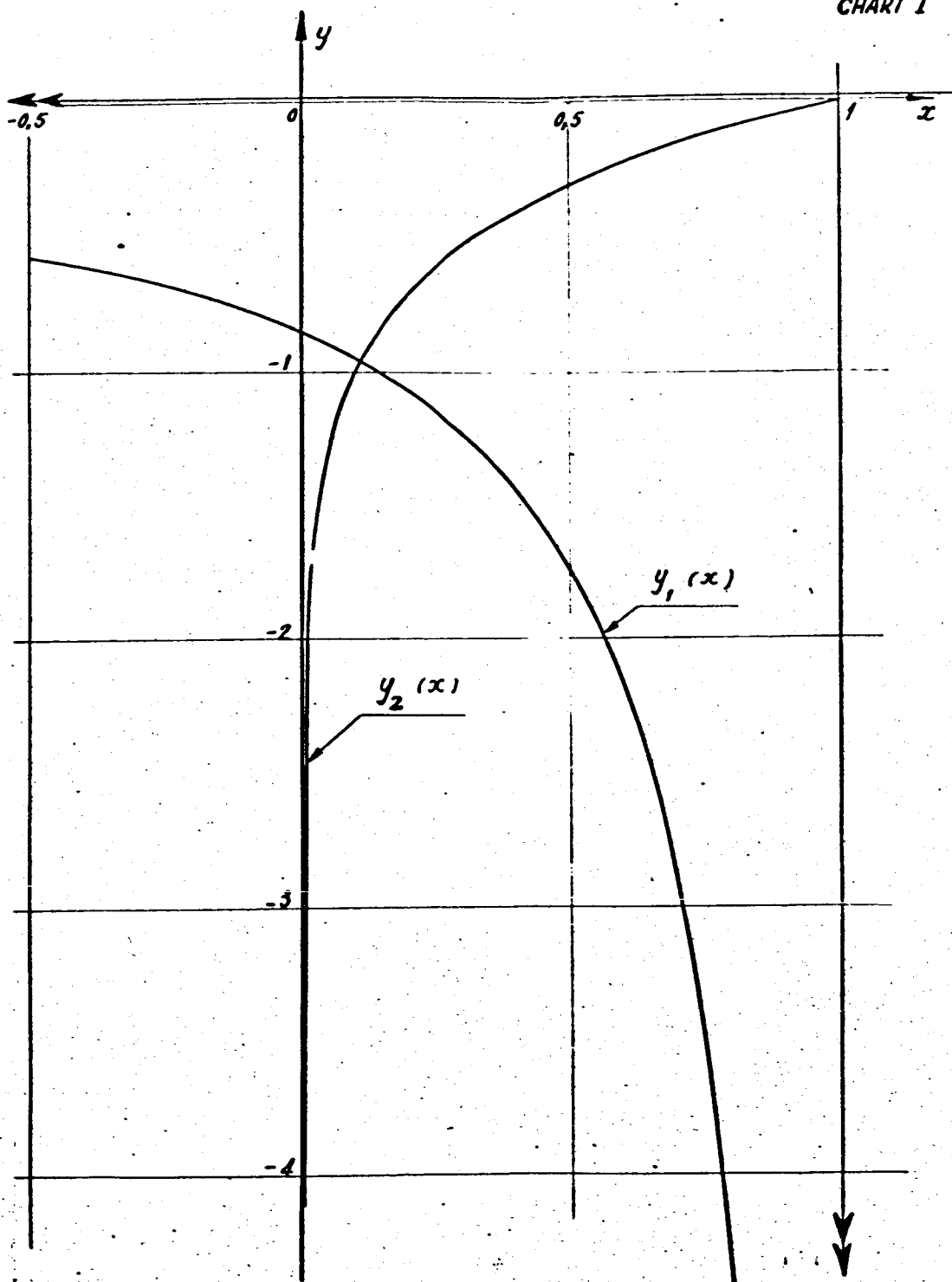
FIELD I

Boundary does not discharge

Potential distribution Φ solution of $\Delta\Phi = -e/\epsilon_0$ Method No.3 - 4th approximation

$\frac{z}{\Delta r}$	$\frac{\rho}{\Delta r}$	0	0.25	0.50	0.75	1	1.5	2	2.5	3	4	5	6	8	10	12	14	16	18	20	22	24	26	28	30	32	34	36	38	40	42	44
0.135		99.99	99.97	99.95	99.93	99.91	99.89	99.87	99.85	99.83	99.81	99.79	99.77	99.75	99.73	99.71	99.69	99.67	99.65	99.63	99.61	99.59	99.57	99.55	99.53	99.51	99.49	99.47	99.45	99.43	99.41	99.39
1		99.99	99.97	99.95	99.93	99.91	99.89	99.87	99.85	99.83	99.81	99.79	99.77	99.75	99.73	99.71	99.69	99.67	99.65	99.63	99.61	99.59	99.57	99.55	99.53	99.51	99.49	99.47	99.45	99.43	99.41	99.39
2		99.99	99.97	99.95	99.93	99.91	99.89	99.87	99.85	99.83	99.81	99.79	99.77	99.75	99.73	99.71	99.69	99.67	99.65	99.63	99.61	99.59	99.57	99.55	99.53	99.51	99.49	99.47	99.45	99.43	99.41	99.39
3		99.99	99.97	99.95	99.93	99.91	99.89	99.87	99.85	99.83	99.81	99.79	99.77	99.75	99.73	99.71	99.69	99.67	99.65	99.63	99.61	99.59	99.57	99.55	99.53	99.51	99.49	99.47	99.45	99.43	99.41	99.39
4		99.99	99.97	99.95	99.93	99.91	99.89	99.87	99.85	99.83	99.81	99.79	99.77	99.75	99.73	99.71	99.69	99.67	99.65	99.63	99.61	99.59	99.57	99.55	99.53	99.51	99.49	99.47	99.45	99.43	99.41	99.39
5		99.99	99.97	99.95	99.93	99.91	99.89	99.87	99.85	99.83	99.81	99.79	99.77	99.75	99.73	99.71	99.69	99.67	99.65	99.63	99.61	99.59	99.57	99.55	99.53	99.51	99.49	99.47	99.45	99.43	99.41	99.39
6		99.99	99.97	99.95	99.93	99.91	99.89	99.87	99.85	99.83	99.81	99.79	99.77	99.75	99.73	99.71	99.69	99.67	99.65	99.63	99.61	99.59	99.57	99.55	99.53	99.51	99.49	99.47	99.45	99.43	99.41	99.39
7		99.99	99.97	99.95	99.93	99.91	99.89	99.87	99.85	99.83	99.81	99.79	99.77	99.75	99.73	99.71	99.69	99.67	99.65	99.63	99.61	99.59	99.57	99.55	99.53	99.51	99.49	99.47	99.45	99.43	99.41	99.39
8		99.99	99.97	99.95	99.93	99.91	99.89	99.87	99.85	99.83	99.81	99.79	99.77	99.75	99.73	99.71	99.69	99.67	99.65	99.63	99.61	99.59	99.57	99.55	99.53	99.51	99.49	99.47	99.45	99.43	99.41	99.39
9		99.99	99.97	99.95	99.93	99.91	99.89	99.87	99.85	99.83	99.81	99.79	99.77	99.75	99.73	99.71	99.69	99.67	99.65	99.63	99.61	99.59	99.57	99.55	99.53	99.51	99.49	99.47	99.45	99.43	99.41	99.39
10		99.99	99.97	99.95	99.93	99.91	99.89	99.87	99.85	99.83	99.81	99.79	99.77	99.75	99.73	99.71	99.69	99.67	99.65	99.63	99.61	99.59	99.57	99.55	99.53	99.51	99.49	99.47	99.45	99.43	99.41	99.39
11		99.99	99.97	99.95	99.93	99.91	99.89	99.87	99.85	99.83	99.81	99.79	99.77	99.75	99.73	99.71	99.69	99.67	99.65	99.63	99.61	99.59	99.57	99.55	99.53	99.51	99.49	99.47	99.45	99.43	99.41	99.39
12		99.99	99.97	99.95	99.93	99.91	99.89	99.87	99.85	99.83	99.81	99.79	99.77	99.75	99.73	99.71	99.69	99.67	99.65	99.63	99.61	99.59	99.57	99.55	99.53	99.51	99.49	99.47	99.45	99.43	99.41	99.39
13		99.99	99.97	99.95	99.93	99.91	99.89	99.87	99.85	99.83	99.81	99.79	99.77	99.75	99.73	99.71	99.69	99.67	99.65	99.63	99.61	99.59	99.57	99.55	99.53	99.51	99.49	99.47	99.45	99.43	99.41	99.39
14		99.99	99.97	99.95	99.93	99.91	99.89	99.87	99.85	99.83	99.81	99.79	99.77	99.75	99.73	99.71	99.69	99.67	99.65	99.63	99.61	99.59	99.57	99.55	99.53	99.51	99.49	99.47	99.45	99.43	99.41	99.39
15		99.99	99.97	99.95	99.93	99.91	99.89	99.87	99.85	99.83	99.81	99.79	99.77	99.75	99.73	99.71	99.69	99.67	99.65	99.63	99.61	99.59	99.57	99.55	99.53	99.51	99.49	99.47	99.45	99.43	99.41	99.39
16		99.99	99.97	99.95	99.93	99.91	99.89	99.87	99.85	99.83	99.81	99.79	99.77	99.75	99.73	99.71	99.69	99.67	99.65	99.63	99.61	99.59	99.57	99.55	99.53	99.51	99.49	99.47	99.45	99.43	99.41	99.39
17		99.99	99.97	99.95	99.93	99.91	99.89	99.87	99.85	99.83	99.81	99.79	99.77	99.75	99.73	99.71	99.69	99.67	99.65	99.63	99.61	99.59	99.57	99.55	99.53	99.51	99.49	99.47	99.45	99.43	99.41	99.39
18		99.99	99.97	99.95	99.93	99.91	99.89	99.87	99.85	99.83	99.81	99.79	99.77	99.75	99.73	99.71	99.69	99.67	99.65	99.63	99.61	99.59	99.57	99.55	99.53	99.51	99.49	99.47	99.45	99.43	99.41	99.39
19		99.99	99.97	99.95	99.93	99.91	99.89	99.87	99.85	99.83	99.81	99.79	99.77	99.75	99.73	99.71	99.69	99.67	99.65	99.63	99.61	99.59	99.57	99.55	99.53	99.51	99.49	99.47	99.45	99.43	99.41	99.39
20		99.99	99.97	99.95	99.93	99.91	99.89	99.87	99.85	99.83	99.81	99.79	99.77	99.75	99.73	99.71	99.69	99.67	99.65	99.63	99.61	99.59	99.57	99.55	99.53	99.51	99.49	99.47	99.45	99.43	99.41	99.39
21		99.99	99.97	99.95	99.93	99.91	99.89	99.87	99.85	99.83	99.81	99.79	99.77	99.75	99.73	99.71	99.69	99.67	99.65	99.63	99.61	99.59	99.57	99.55	99.53	99.51	99.49	99.47	99.45	99.43	99.41	99.39
22		99.99	99.97	99.95	99.93	99.91	99.89	99.87	99.85	99.83	99.81	99.79	99.77	99.75	99.73	99.71	99.69	99.67	99.65	99.63	99.61	99.59	99.57	99.55	99.53	99.51	99.49	99.47	99.45	99.43	99.41	99.39
23		99.99	99.97	99.95	99.93	99.91	99.89	99.87	99.85	99.83	99.81	99.79	99.77	99.75	99.73	99.71	99.69	99.67	99.65	99.63	99.61	99.59	99.57	99.55	99.53	99.51	99.49	99.47	99.45	99.43	99.41	99.39
24		99.99	99.97	99.95	99.93	99.91	99.89	99.87	99.85	99.83	99.81	99.79	99.77	99.75	99.73	99.71	99.69	99.67	99.65	99.63	99.61	99.59	99.57	99.55	99.53	99.51	99.49	99.47	99.45	99.43	99.41	99.39
25		99.99	99.97	99.95	99.93	99.91	99.89	99.87	99.85	99.83	99.81	99.79	99.77	99.75	99.73	99.71	99.69	99.67	99.65	99.63	99.61	99.59	99.57	99.55	99.53	99.51	99.49	99.47	99.45	99.43	99.41	99.39
26		99.99	99.97	99.95	99.93	99.91	99.89	99.87	99.85	99.83	99.81	99.79	99.77	99.75	99.73	99.71	99.69	99.67	99.65	99.63	99.61	99.59	99.57	99.55	99.53	99.51	99.49	99.47	99.45	99.43	99.41	99.39
27		99.99	99.97	99.95	99.93	99.91	99.89	99.87	99.85	99.83	99.81	99.79	99.77	99.75	99.73	99.71	99.69	99.67	99.65	99.63	99.61	99.59	99.57	99.55	99.53	99.51	99.49	99.47	99.45	99.43	99.41	99.39
28		99.99	99.97	99.95	99.93	99.91	99.89	99.87	99.85	99.83	99.81	99.79	99.77	99.75	99.73	99.71	99.69	99.67	99.65	99.63	99.61	99.59	99.57	99.55	99.53	99.51	99.49	99.47	99.45	99.43	99.41	99.39
29		99.99	99.97	99.95	99.93	99.91	99.89	99.87	99.85	99.83	99.81	99.79	99.77	99.75	99.73	99.71	99.69	99.67	99.65	99.63	99.61	99.59	99.57	99.55	99.53	99.51	99.49	99.47	99.45	99.43	99.41	99.39
30		99.99	99.97	99.95	99.93	99.91	99.89	99.87	99.85	99.83	99.81	99.79	99.77	99.75	99.73	99.71	99.69	99.67	99.65	99.63	99.61	99.59	99.57	99.55	99.53	99.51	99.49	99.47	99.45	99.43	99.41	99.39

CHART I



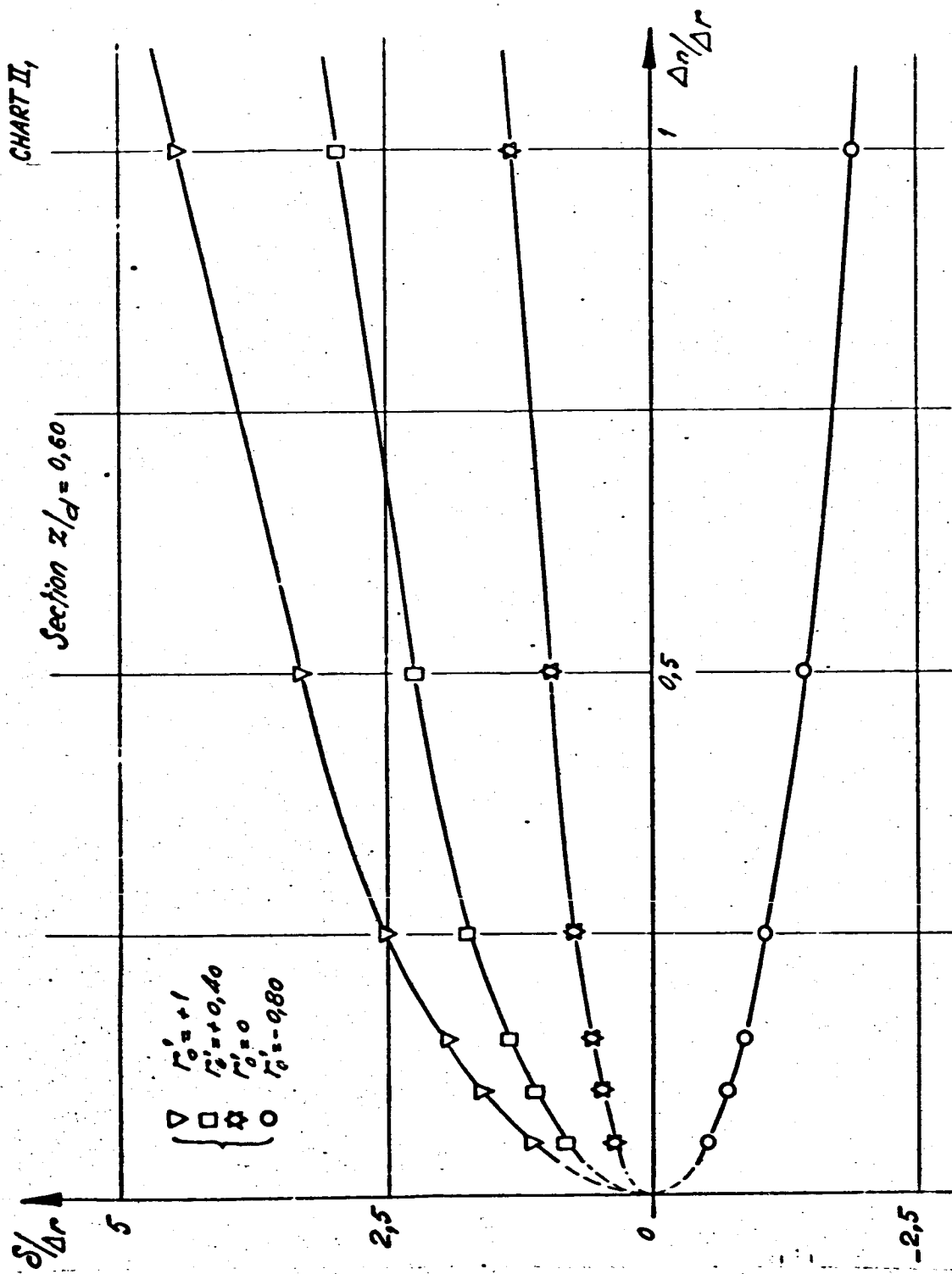


CHART II₂

Section $z/d = 1$

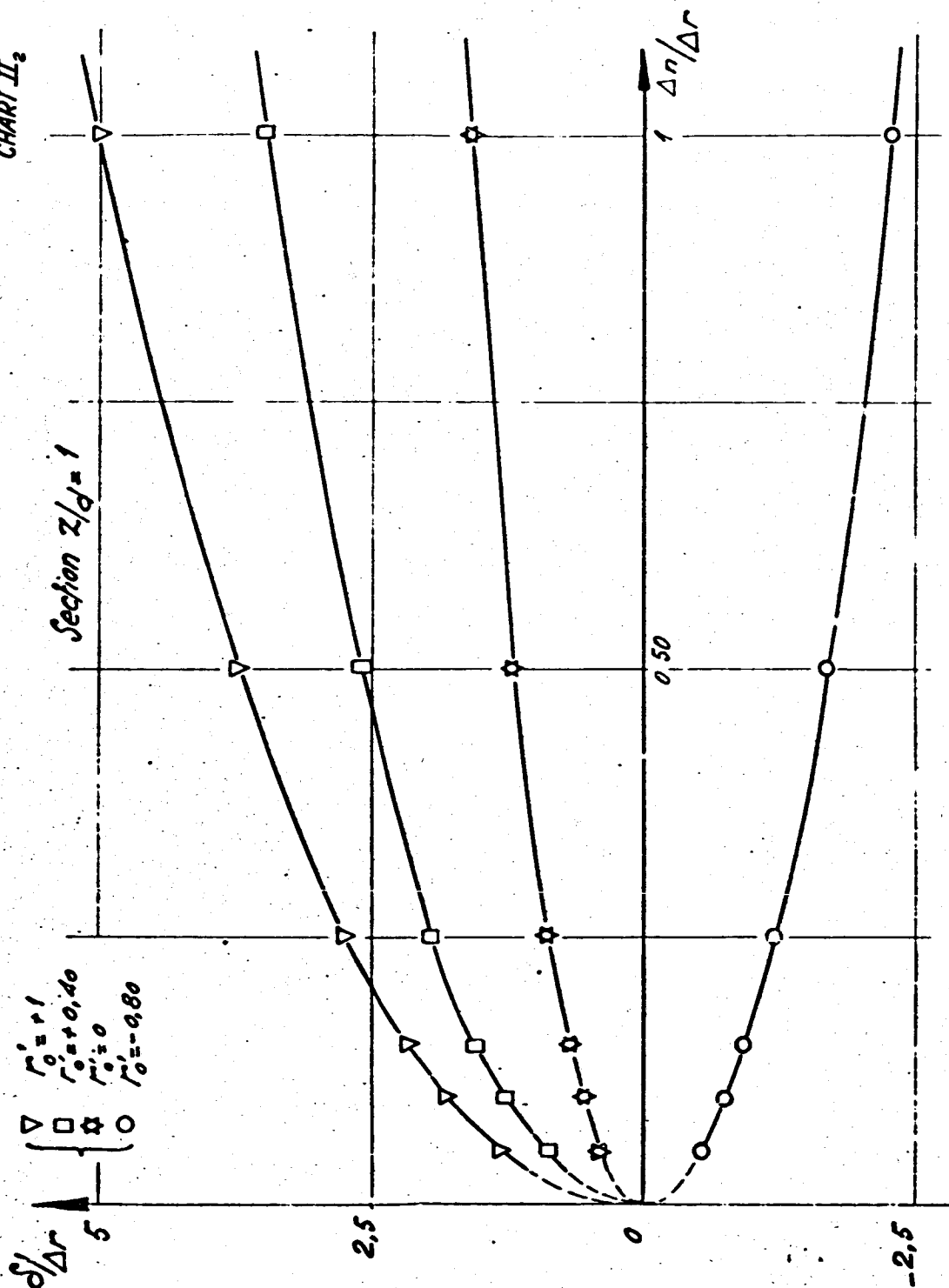


CHART IV,

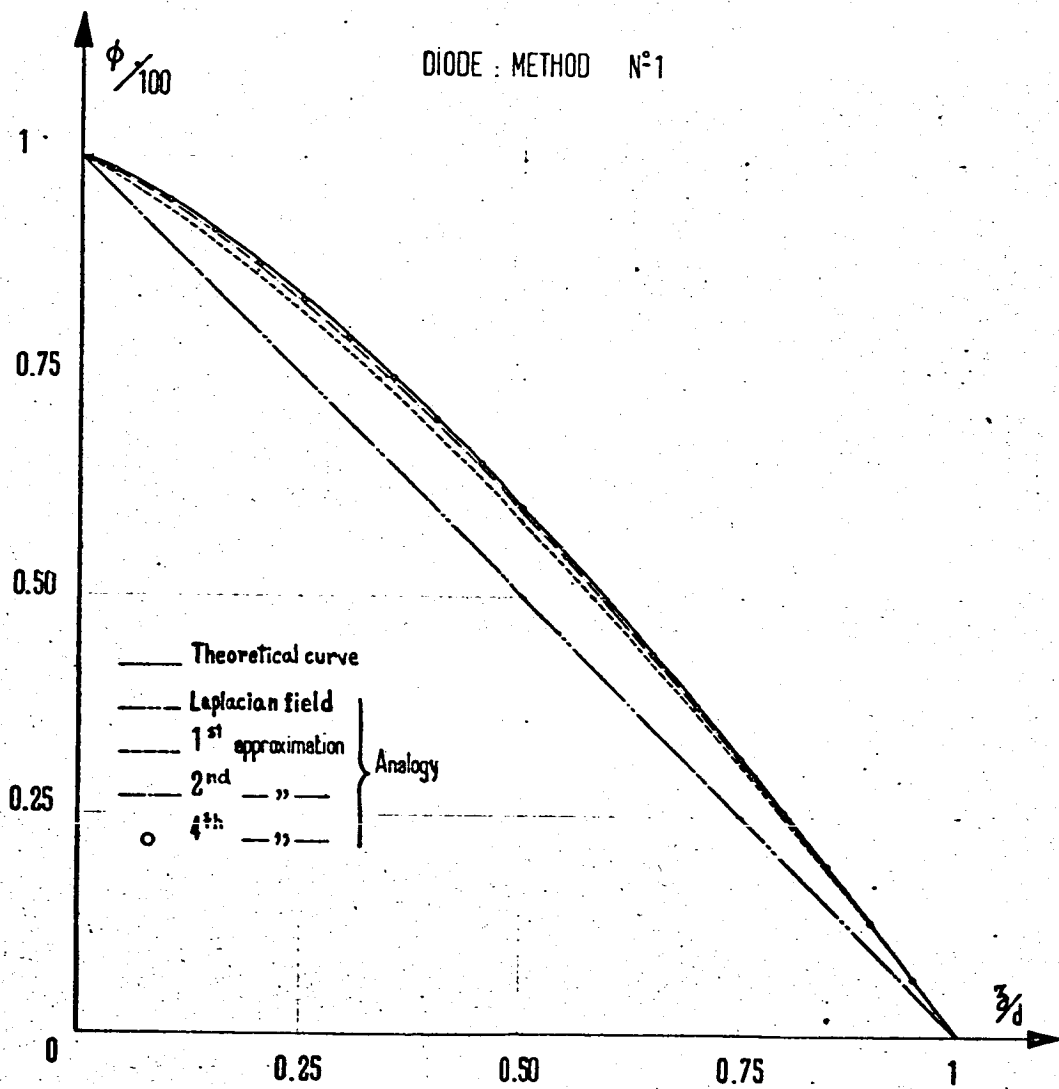


CHART IV_{1a}

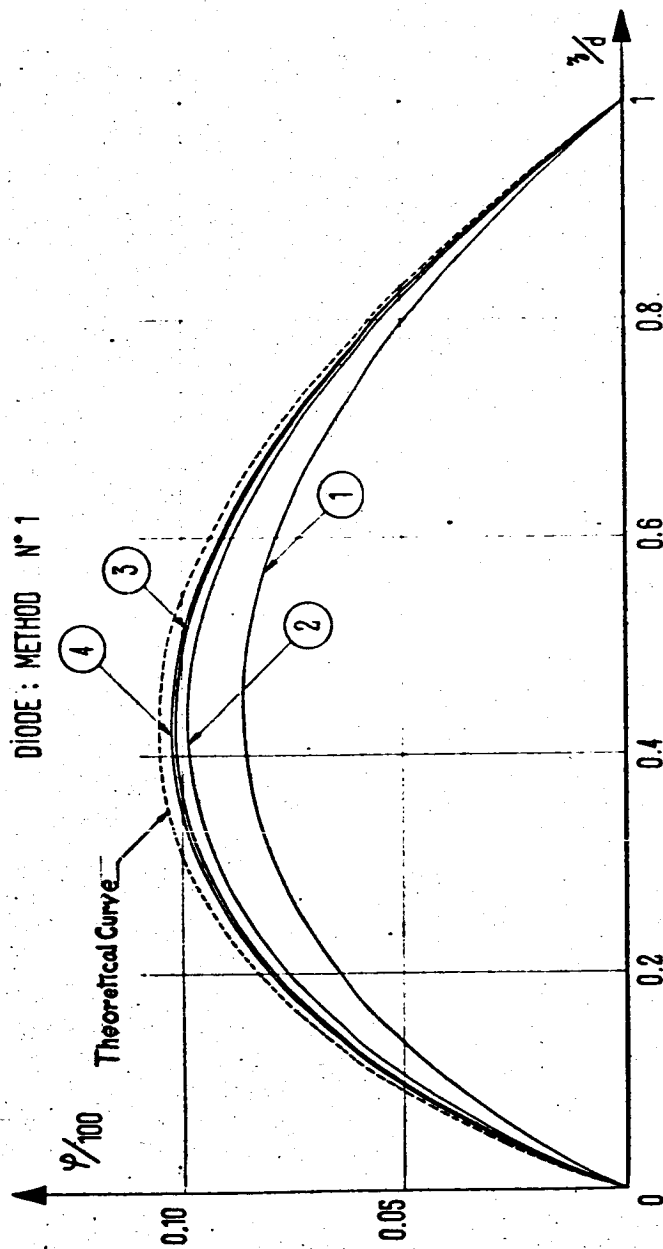


CHART IV₂

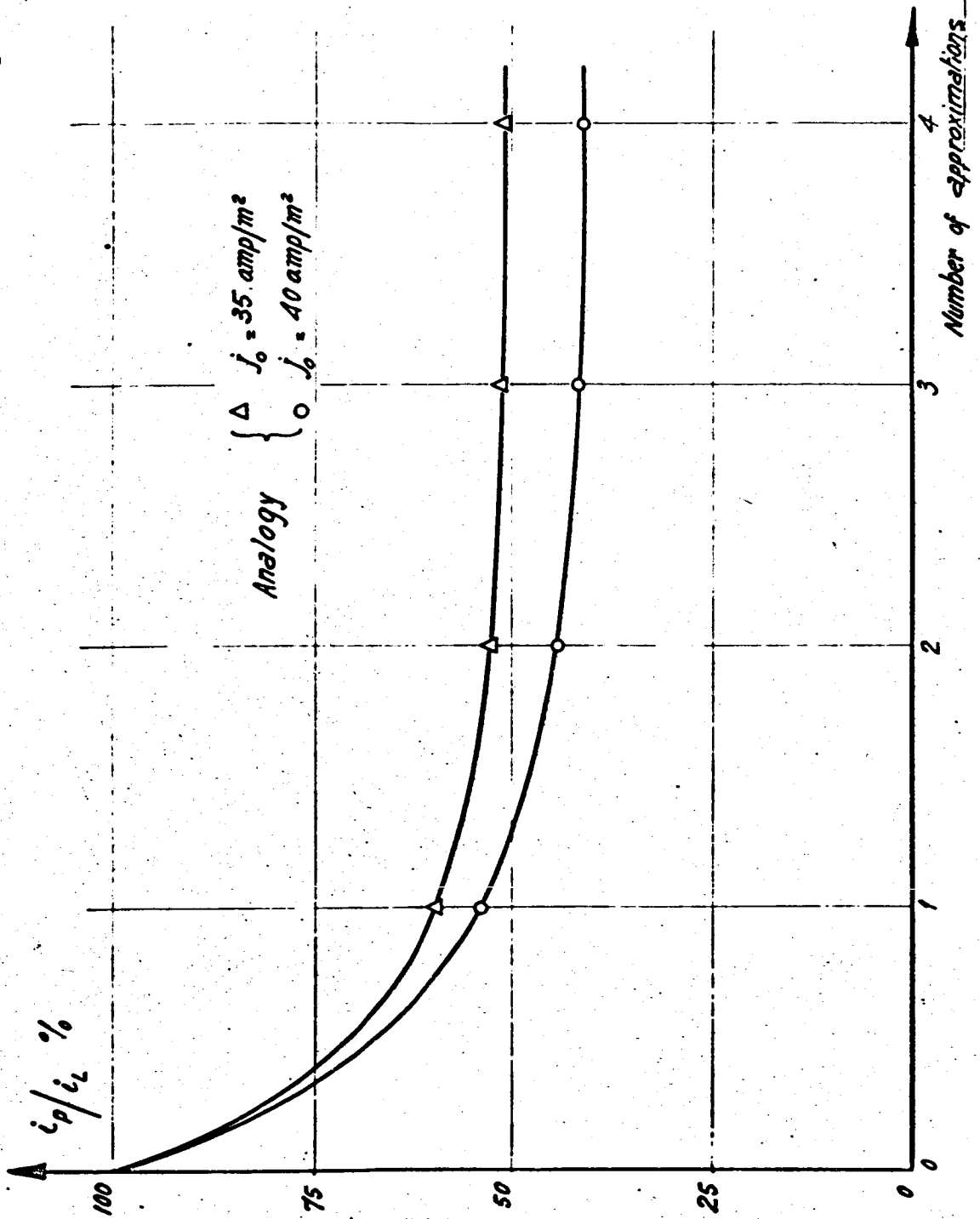


CHART IV₃

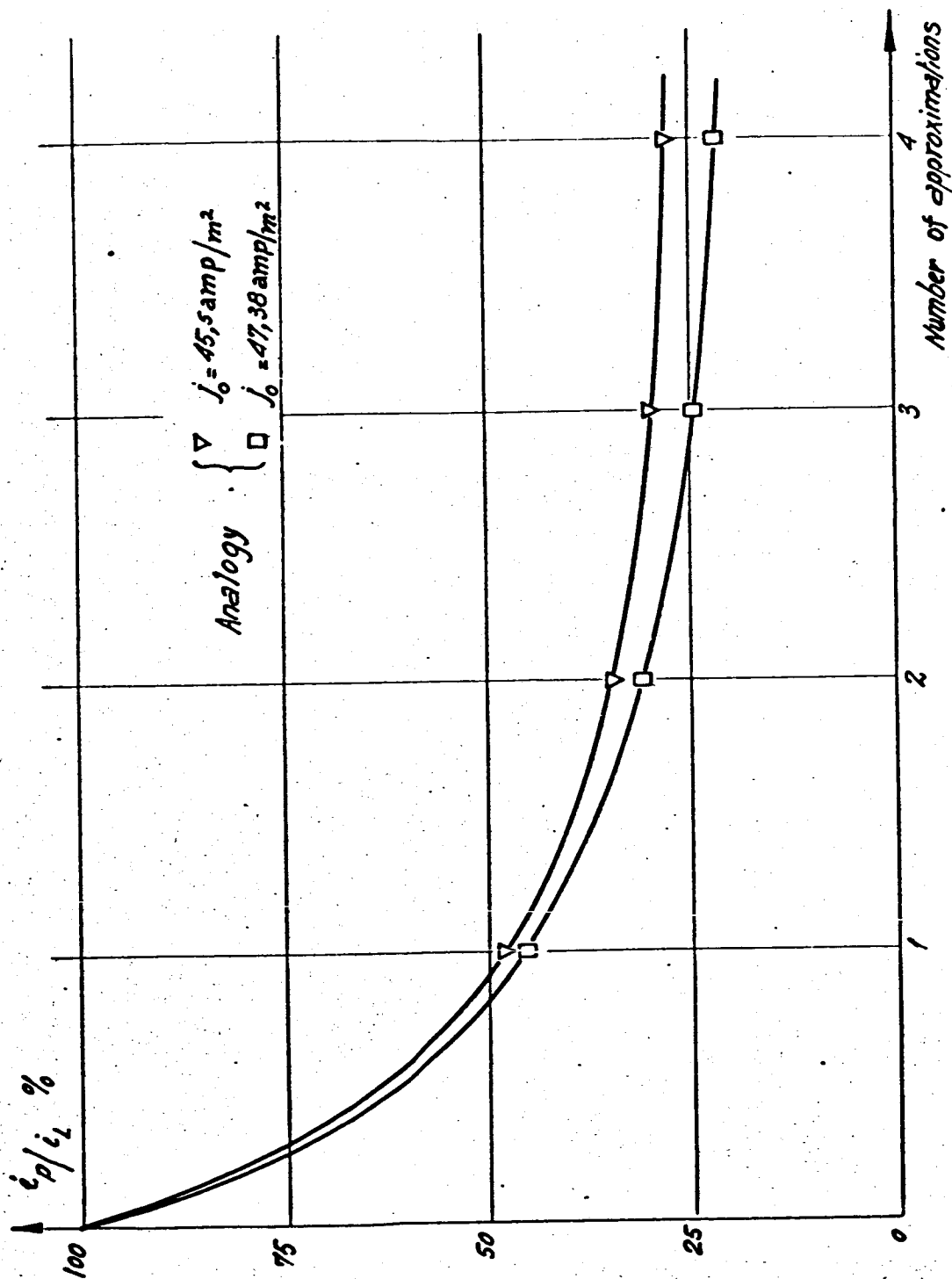


CHART IV₄

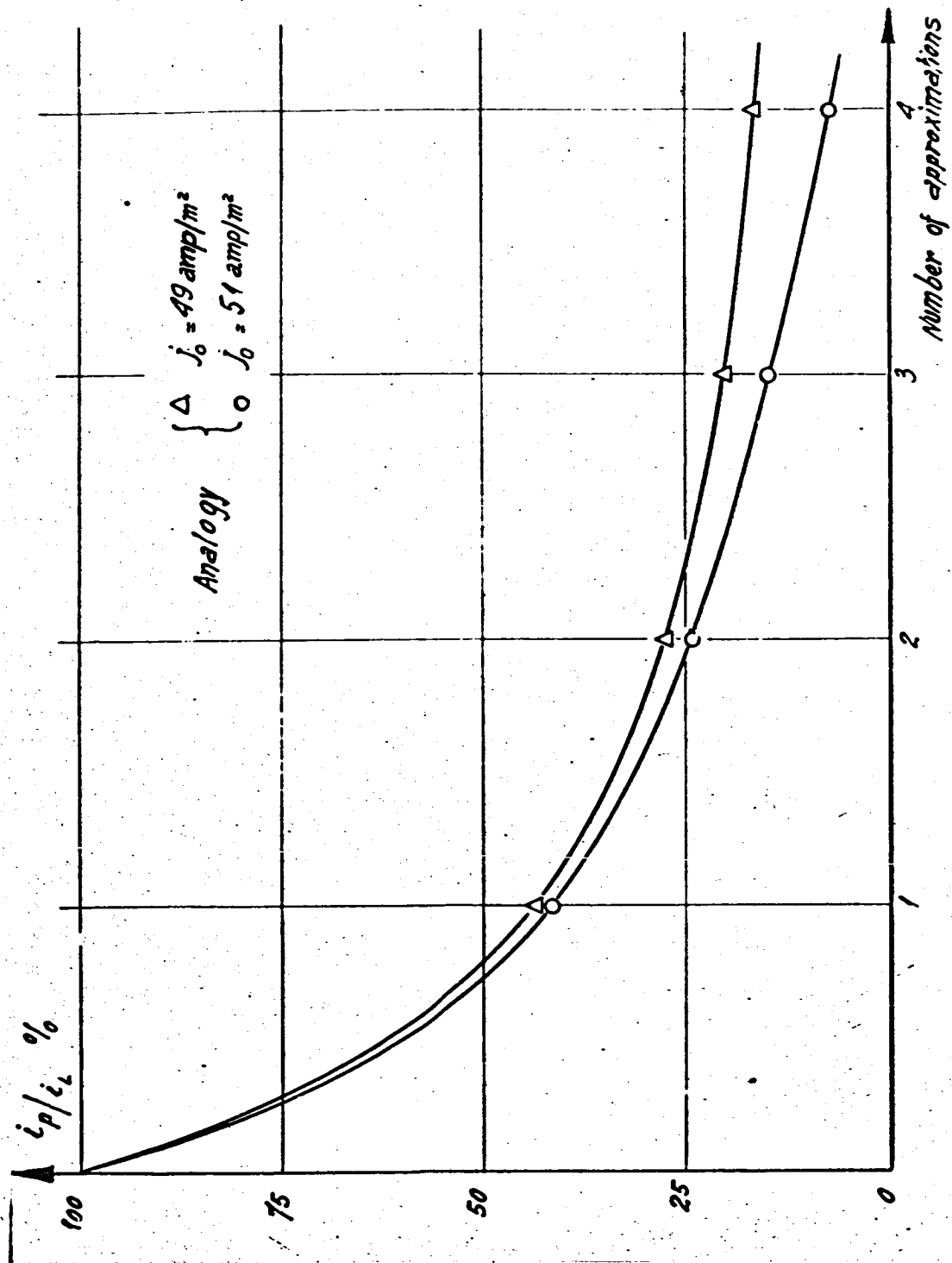


CHART IV₅

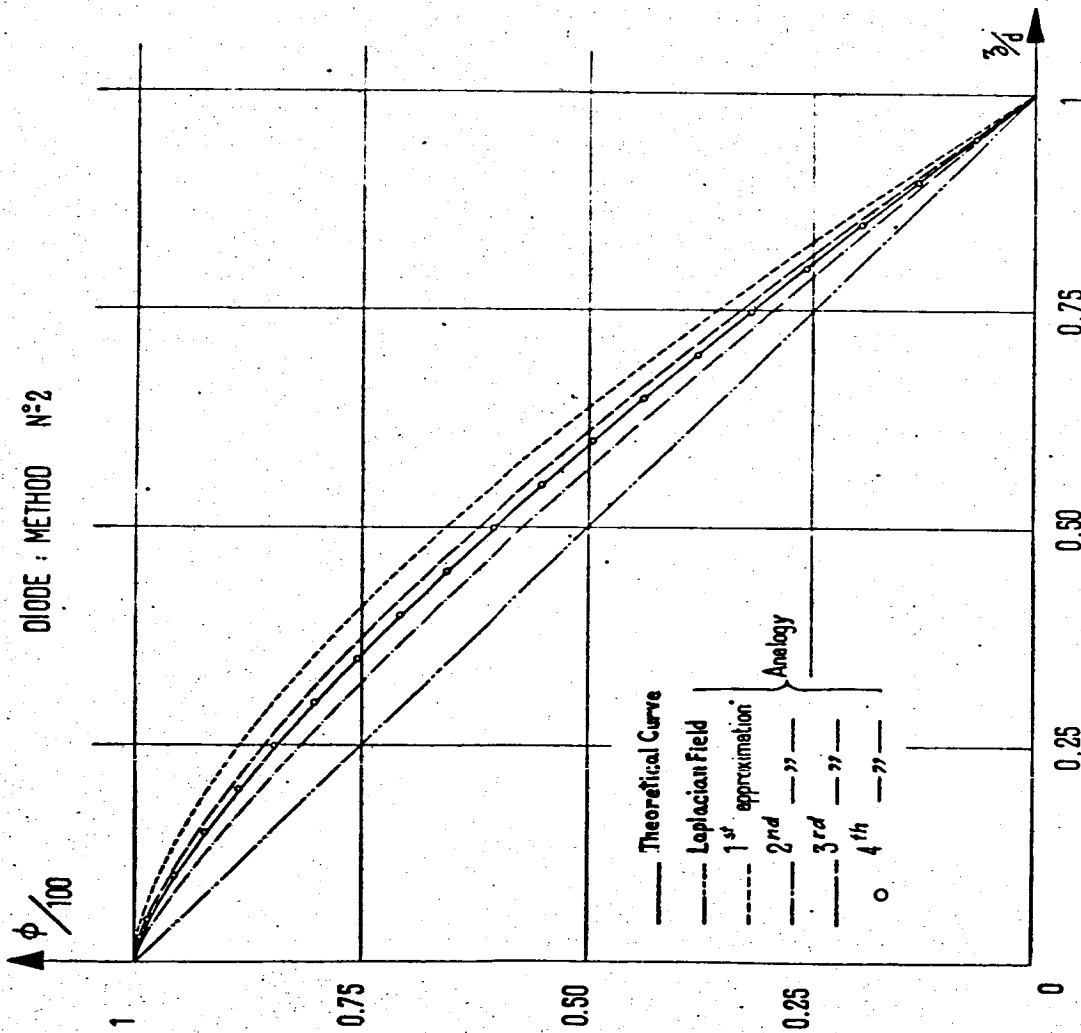


CHART IV_{5a}

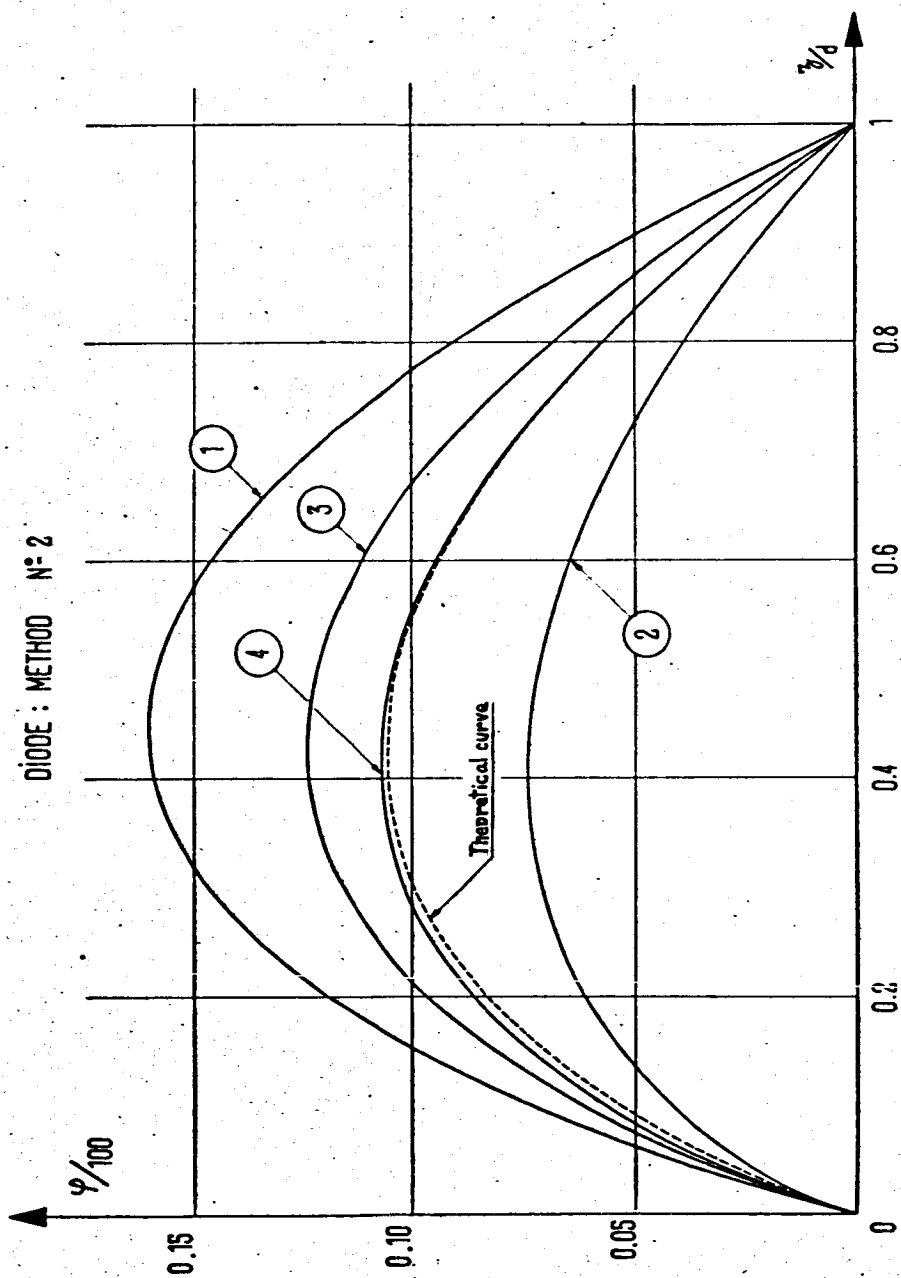


CHART IV₆

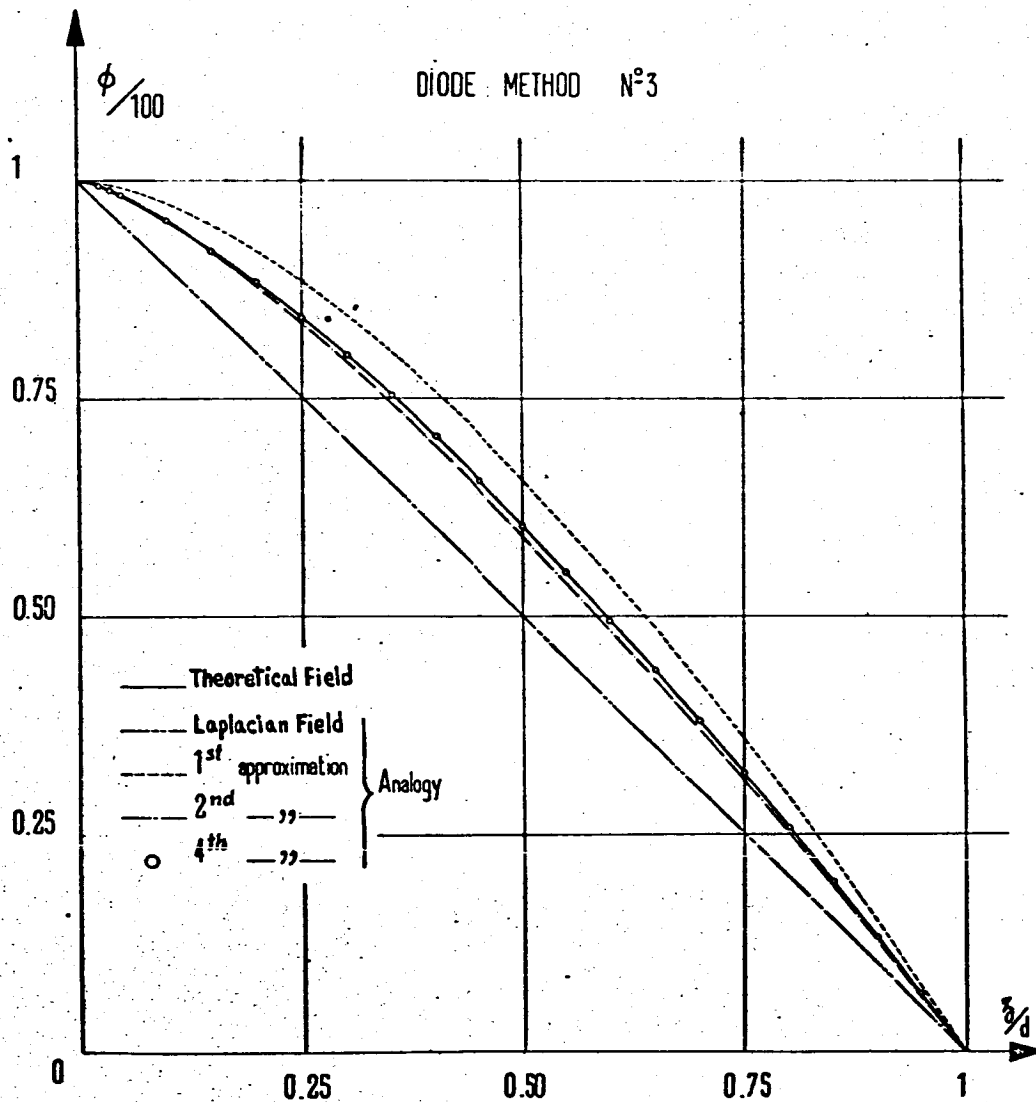


CHART IV_{6a}

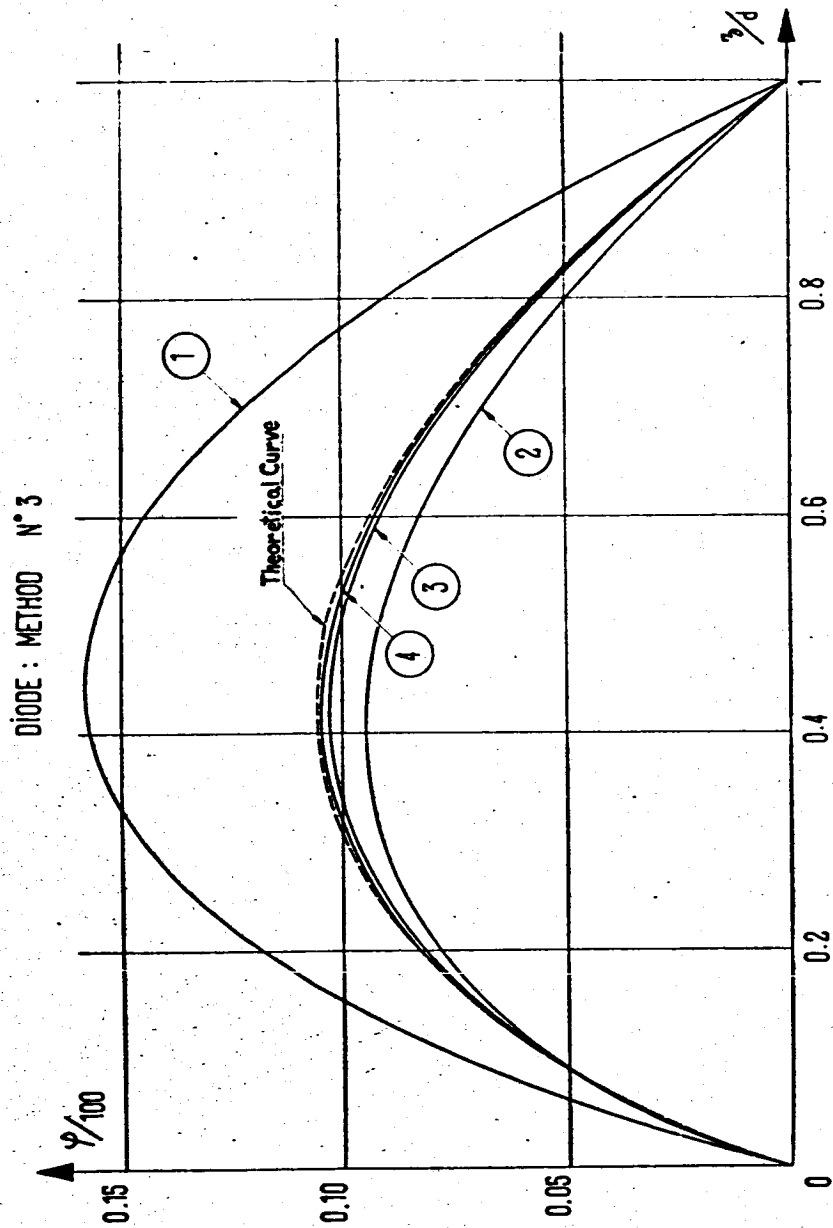


CHART IV,

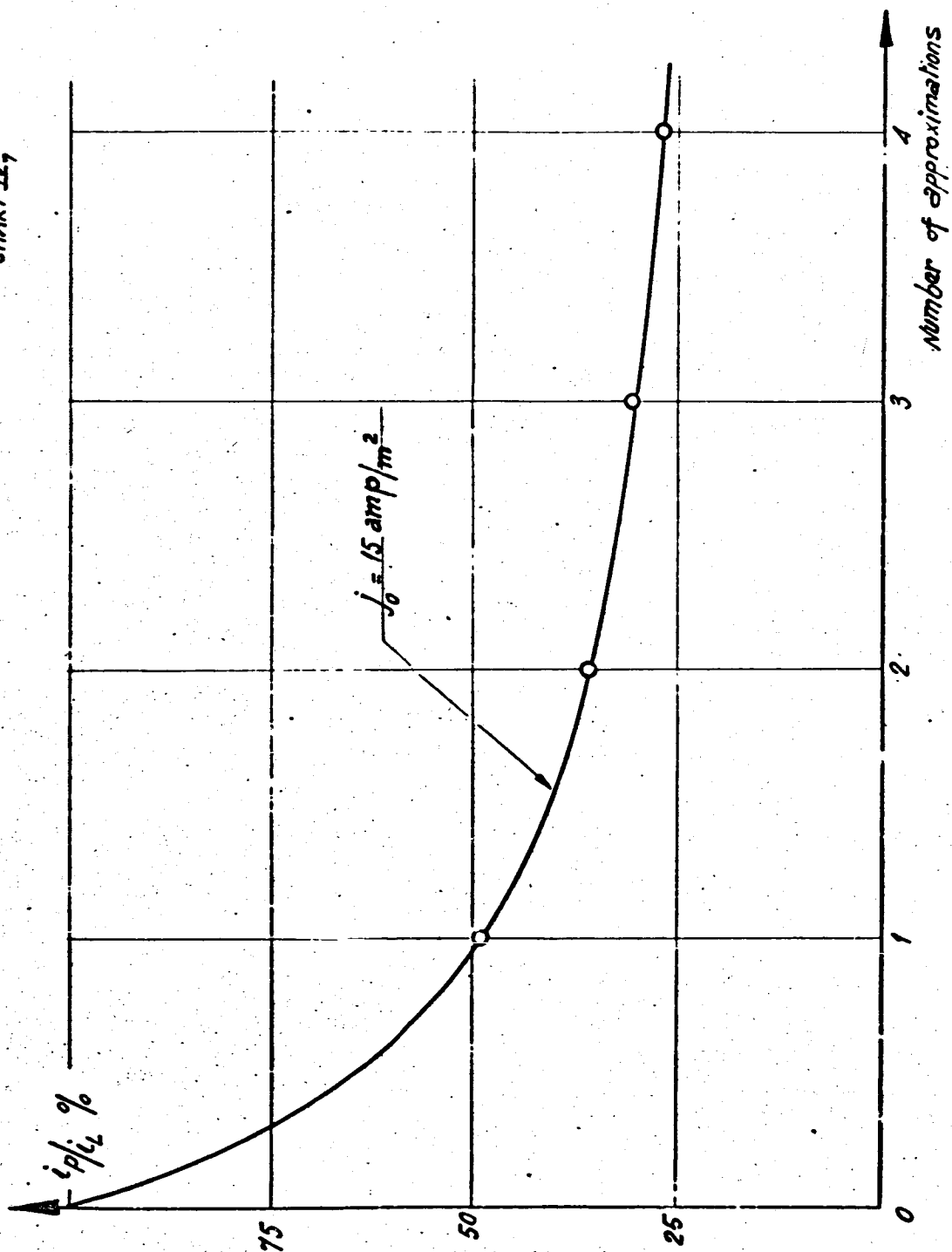
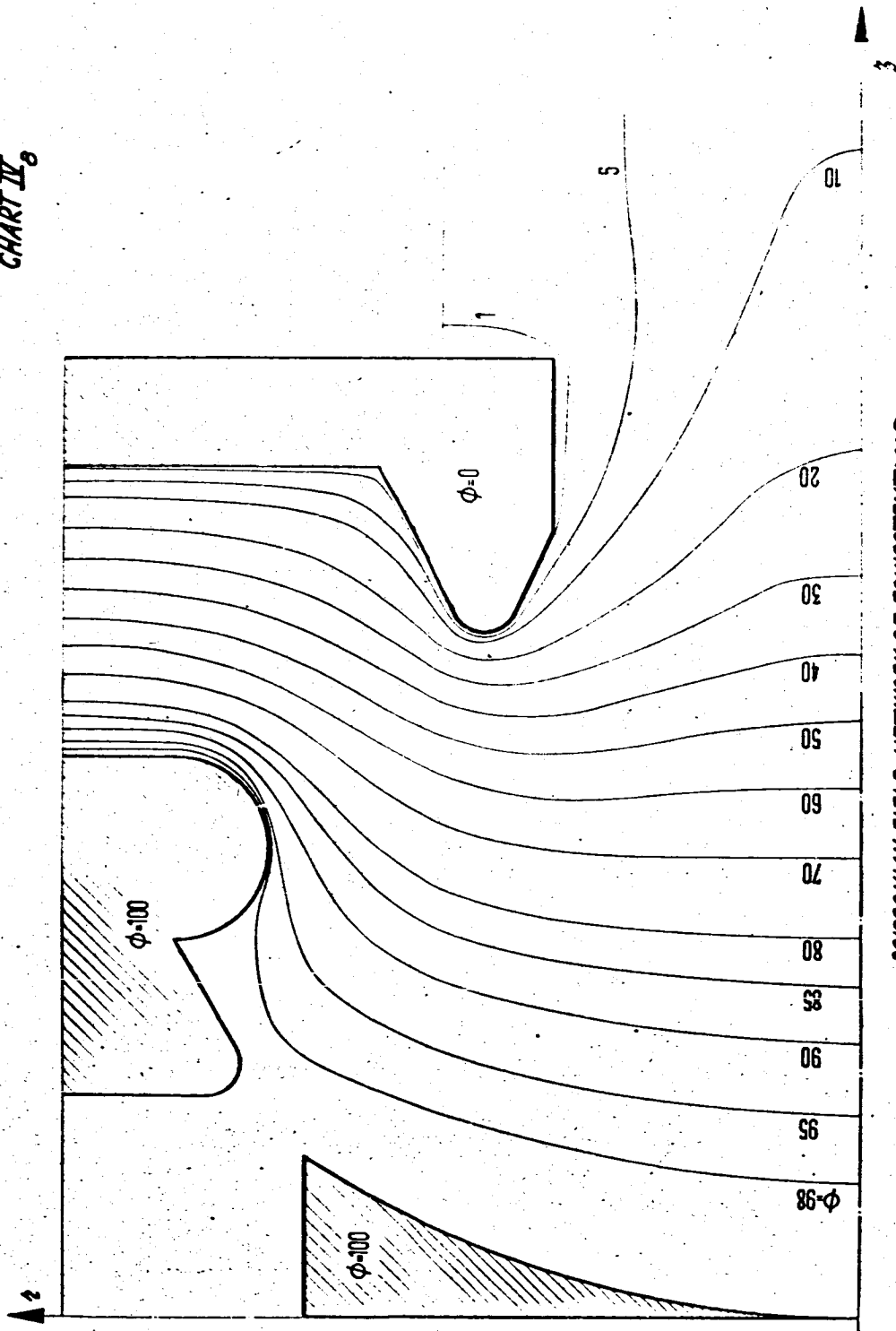


CHART IV₈



POISSONIAN FIELD, NETWORK OF EQUIPOTENTIALS

Method No2 - 1st Approximation - $J_0 = 15 \text{ amp/m}^2$

CHART IV₉

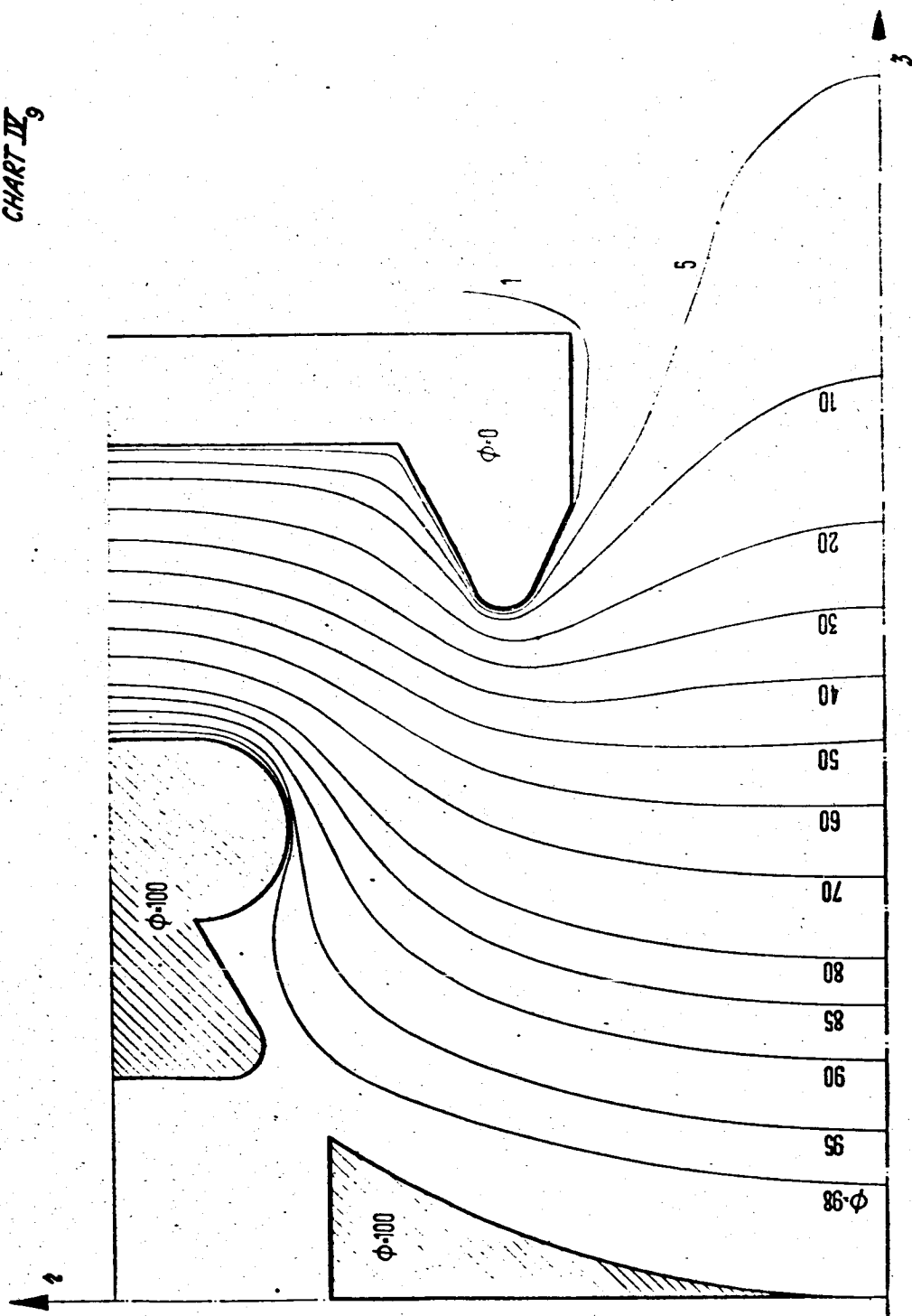
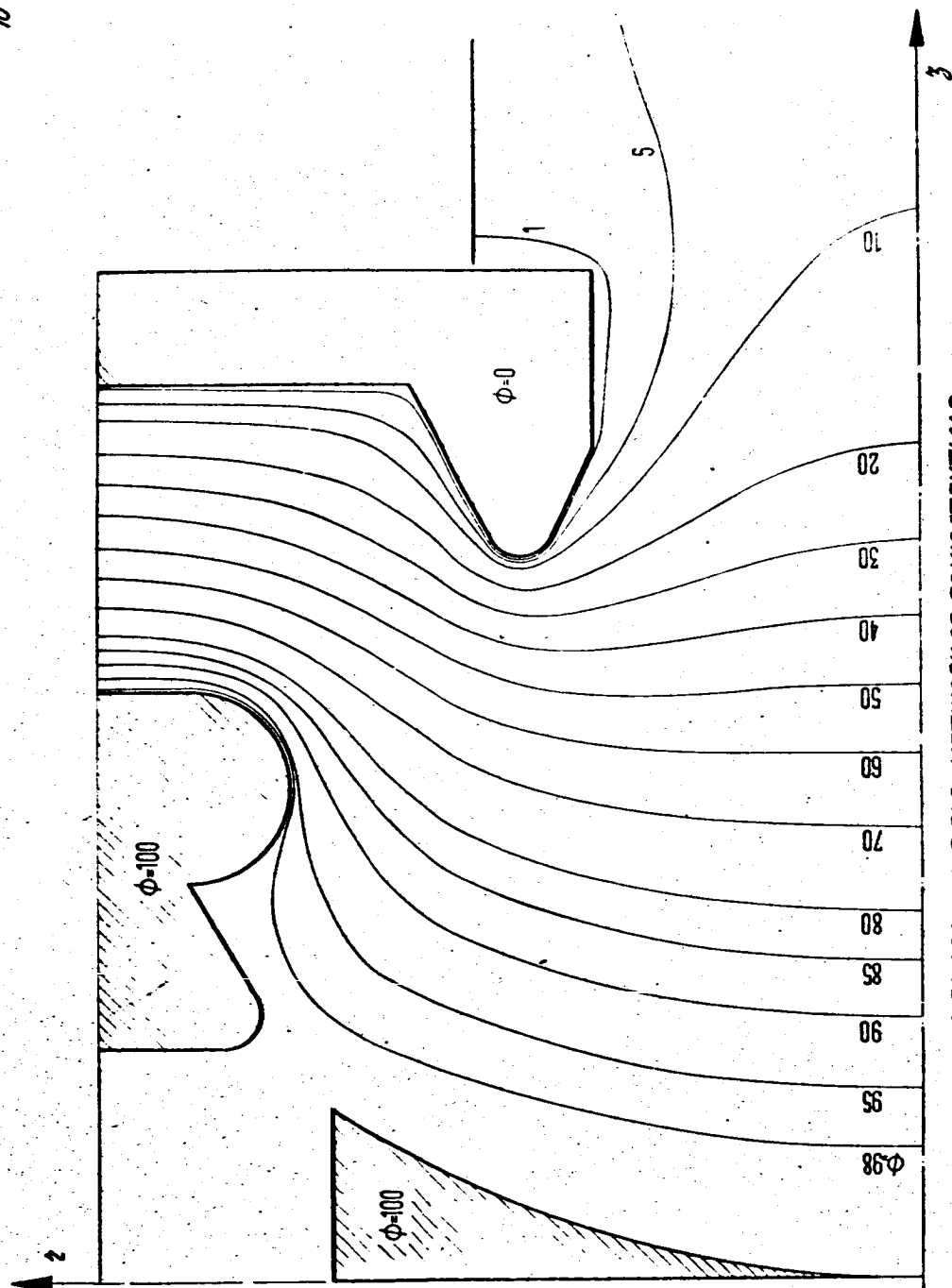


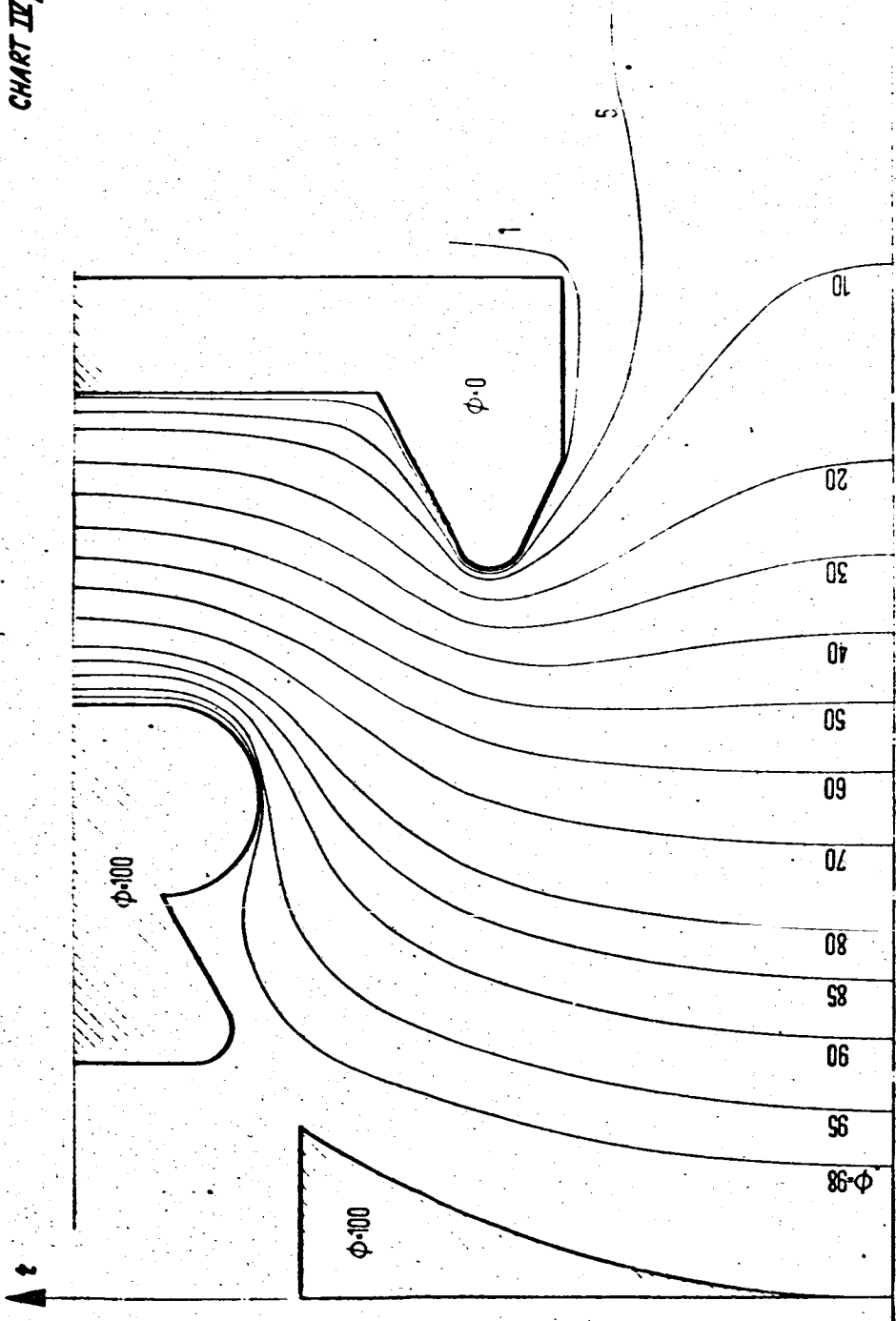
CHART IV₁₀



POISSONIAN FIELD, NETWORK OF EQUIPOTENTIALS

Method №2 3rd Approximation $j_0 = 15 \text{ amp/m}^2$

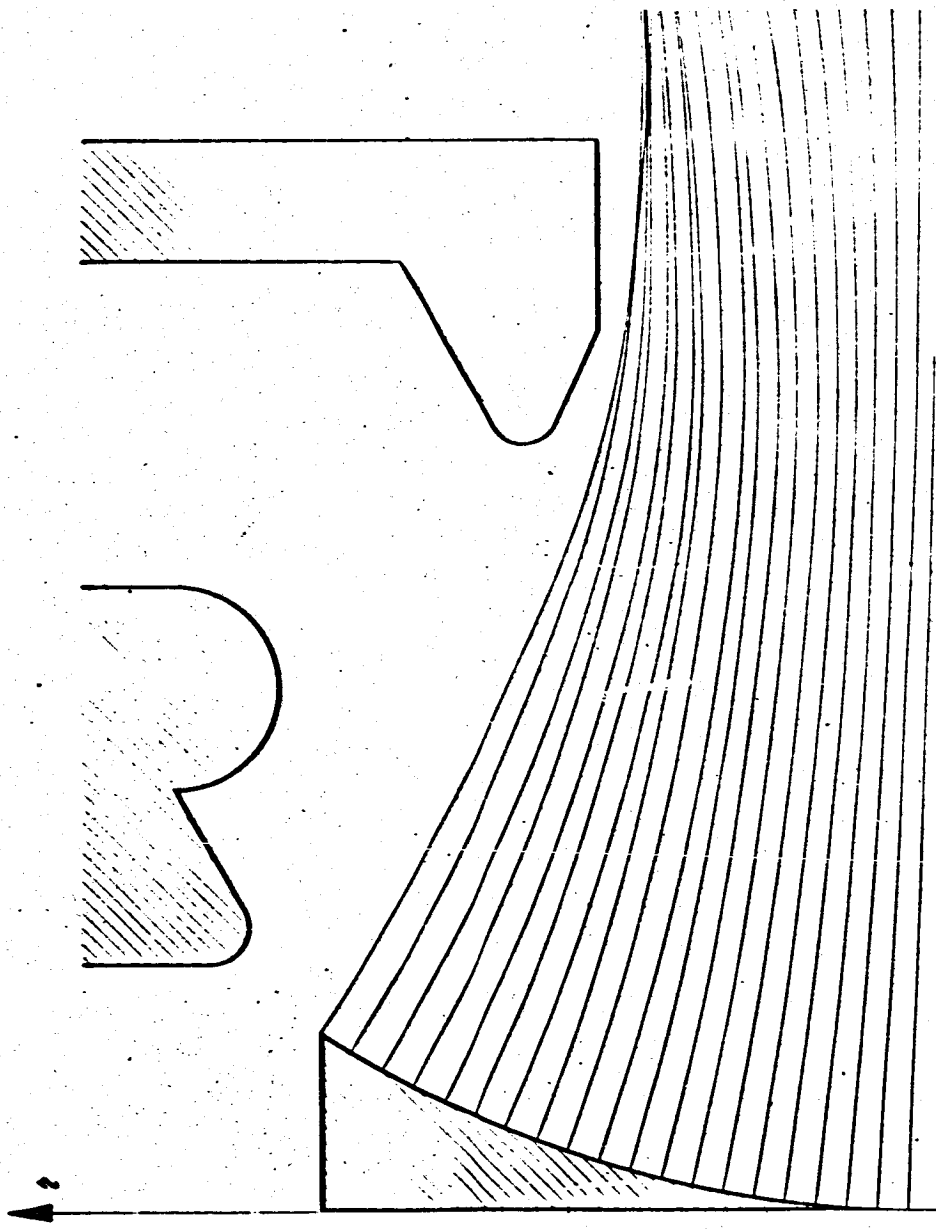
CHART IV₁₁



POISSONIAN FIELD, NETWORK OF EQUIPOTENTIALS

Method No2 4th Approximation $U_0=15 \text{ amp/m}^2$

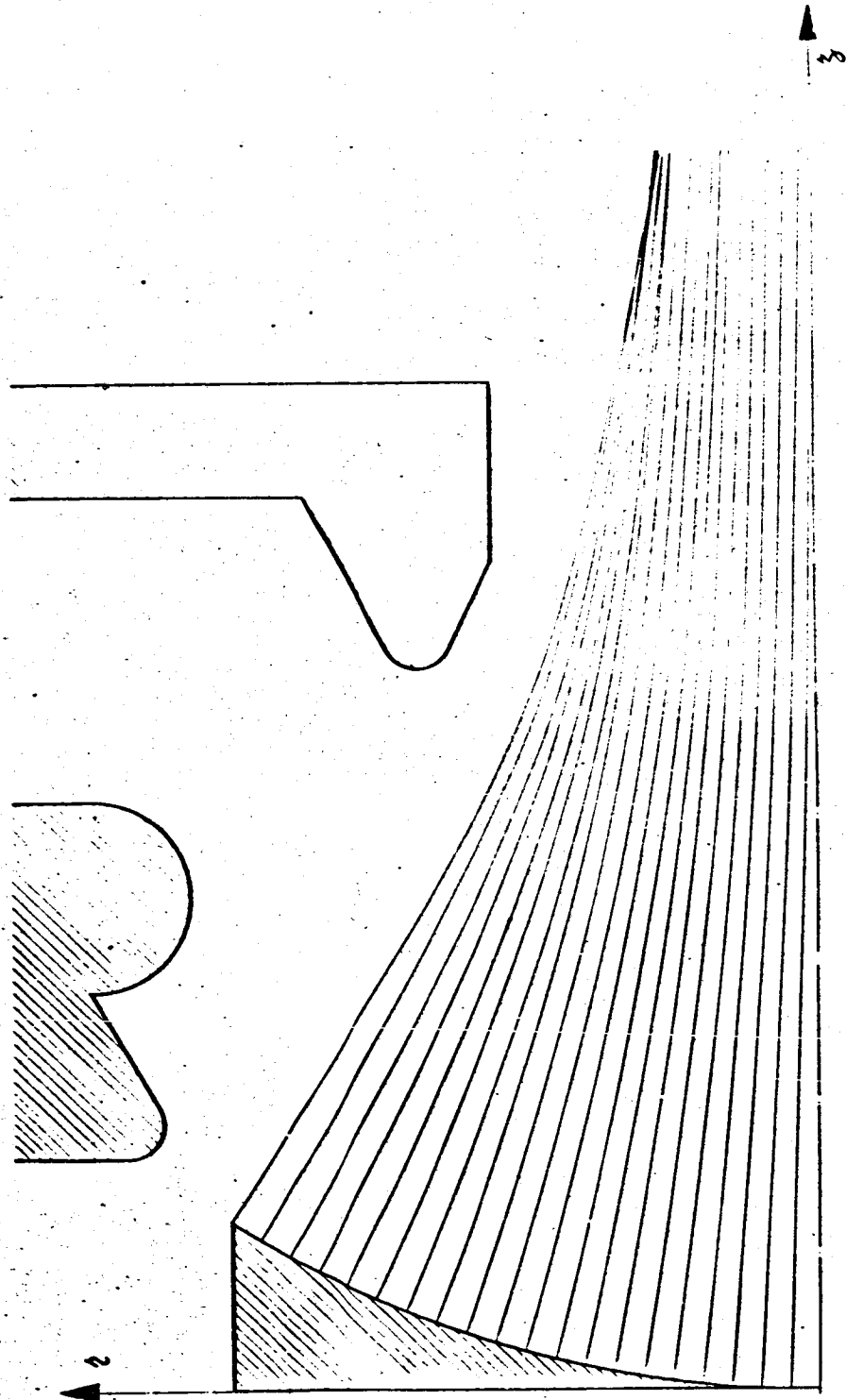
10
11
12
13
14
15
16
17
18
19
20
21
22
23
24
25
26
27
28
29
30
31
32
33
34
35
36
37
38
39
40
41
42
43
44
45
46
47
48
49
50
51
52



NETWORK OF TRAJECTORIES POISSONIAN FIELD

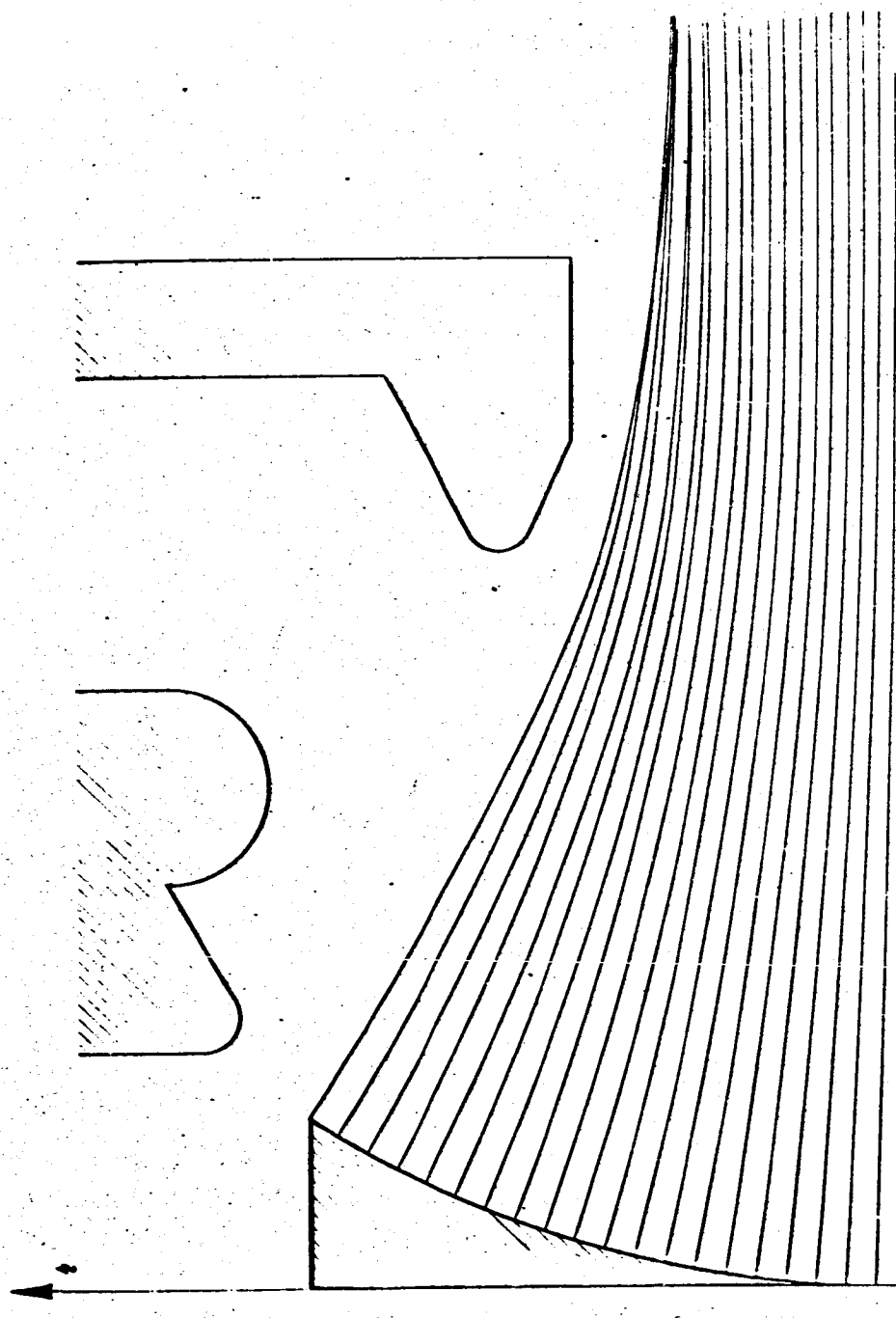
Method No2 1st Approximation $J_0 = 15 \text{ amp/m}^2$

CHART IV₁₃



NETWORK OF TRAJECTORIES - POISSONIAN FIELD Method No. 3
 2nd Approximation $J_0 = 13.55 \text{ amp/m}^2$

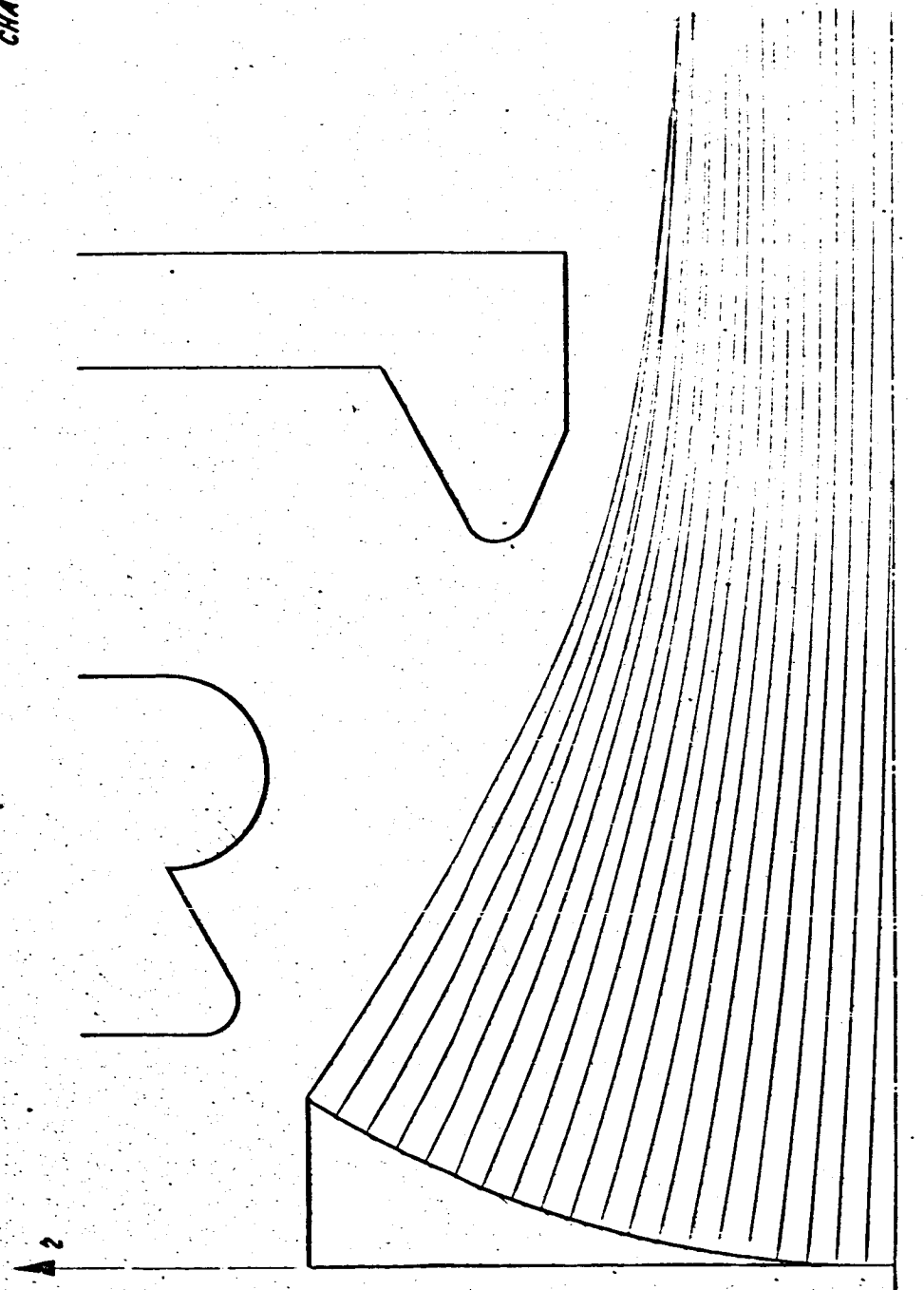
CHART IV₁₄



NETWORK OF TRAJECTORIES-POISSONIAN FIELD

Method №3 3rd Approximation $J_0 = 21 \text{ amp/m}^2$

CHART IV₁₅



NETWORK OF TRAJECTORIES-POISSONIAN FIELD

Method №2 4th Approximation $j_0 = 15 \text{ amp/cm}^2$

CHART IV₁₆

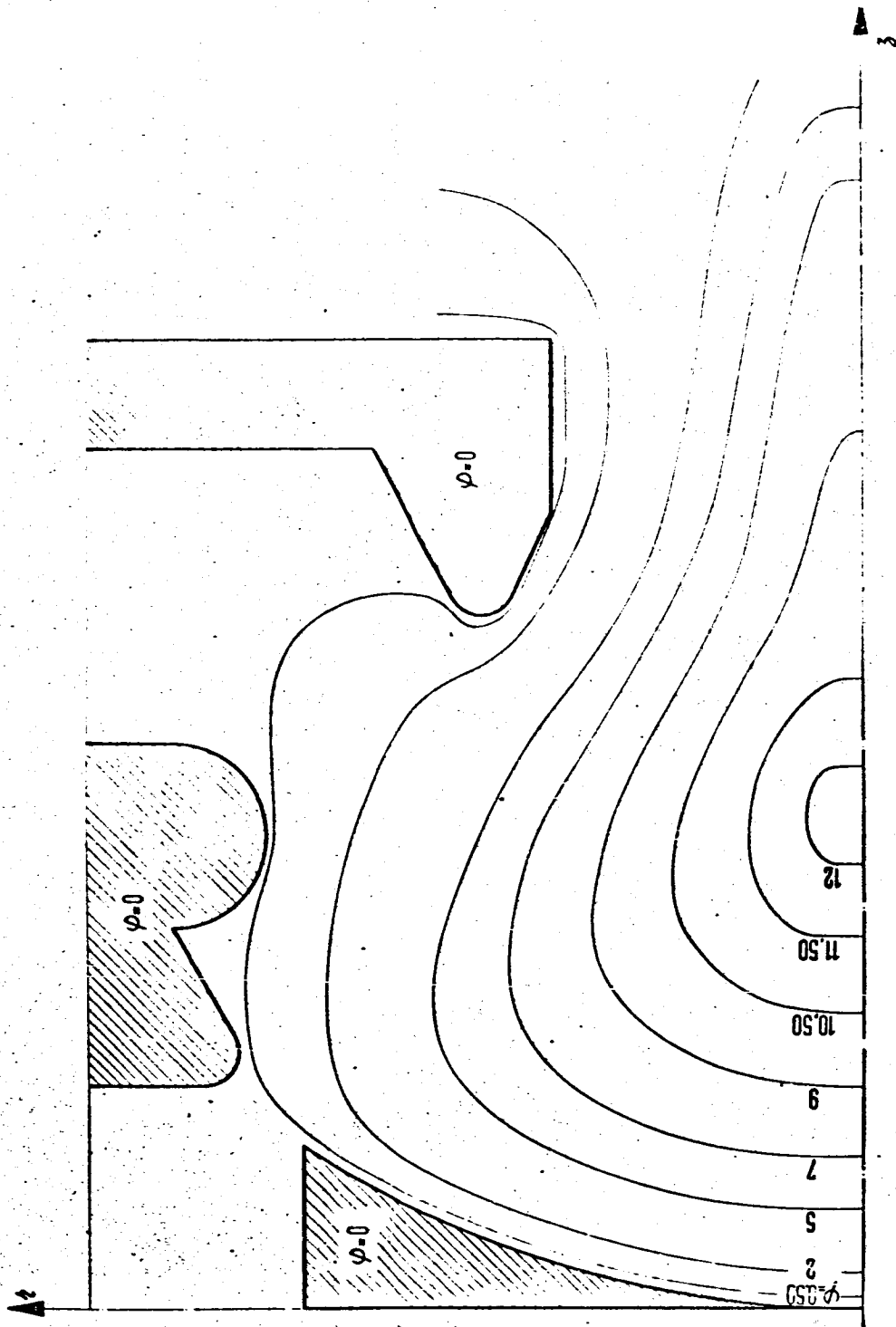


CHART IV_n

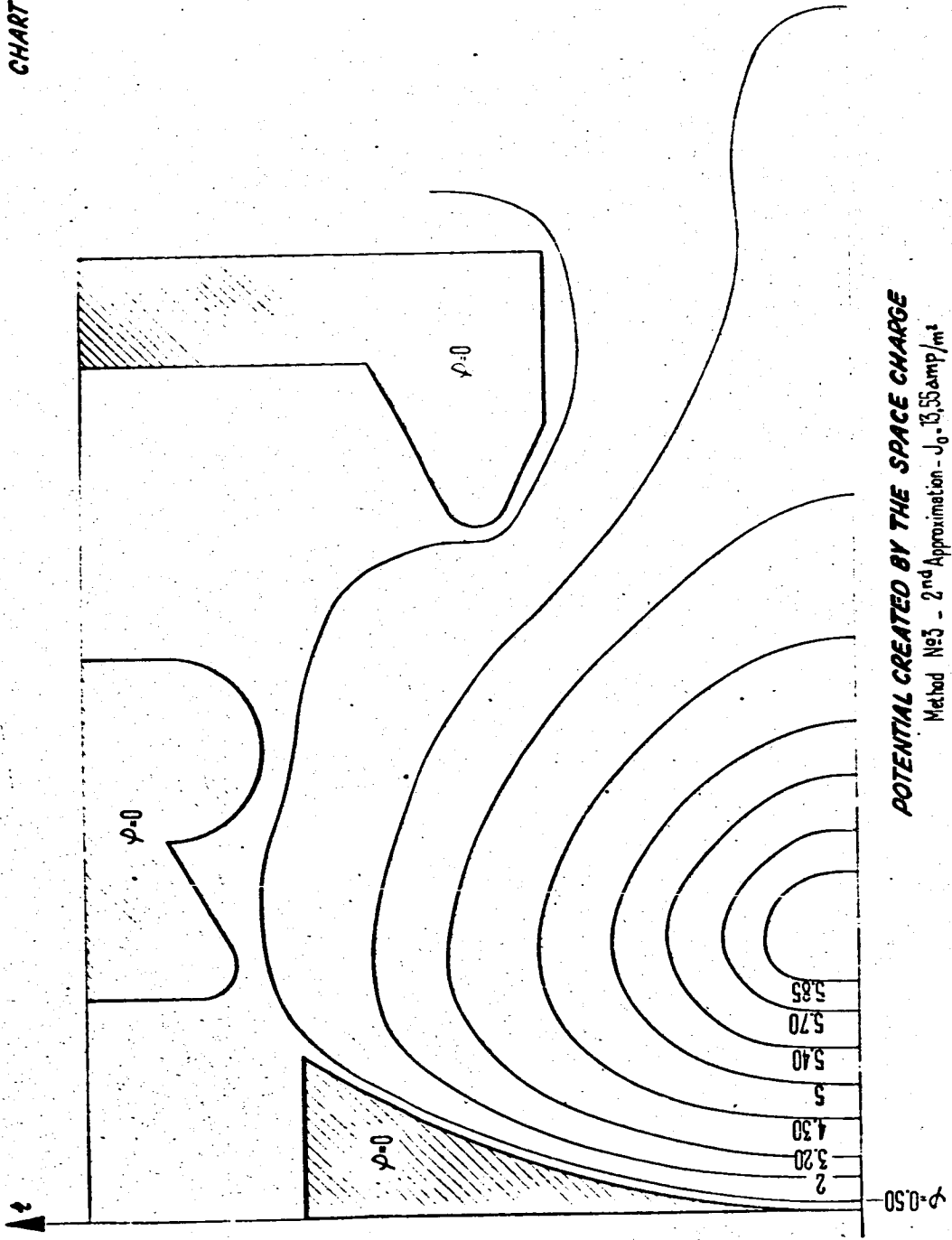


CHART IV₁₈

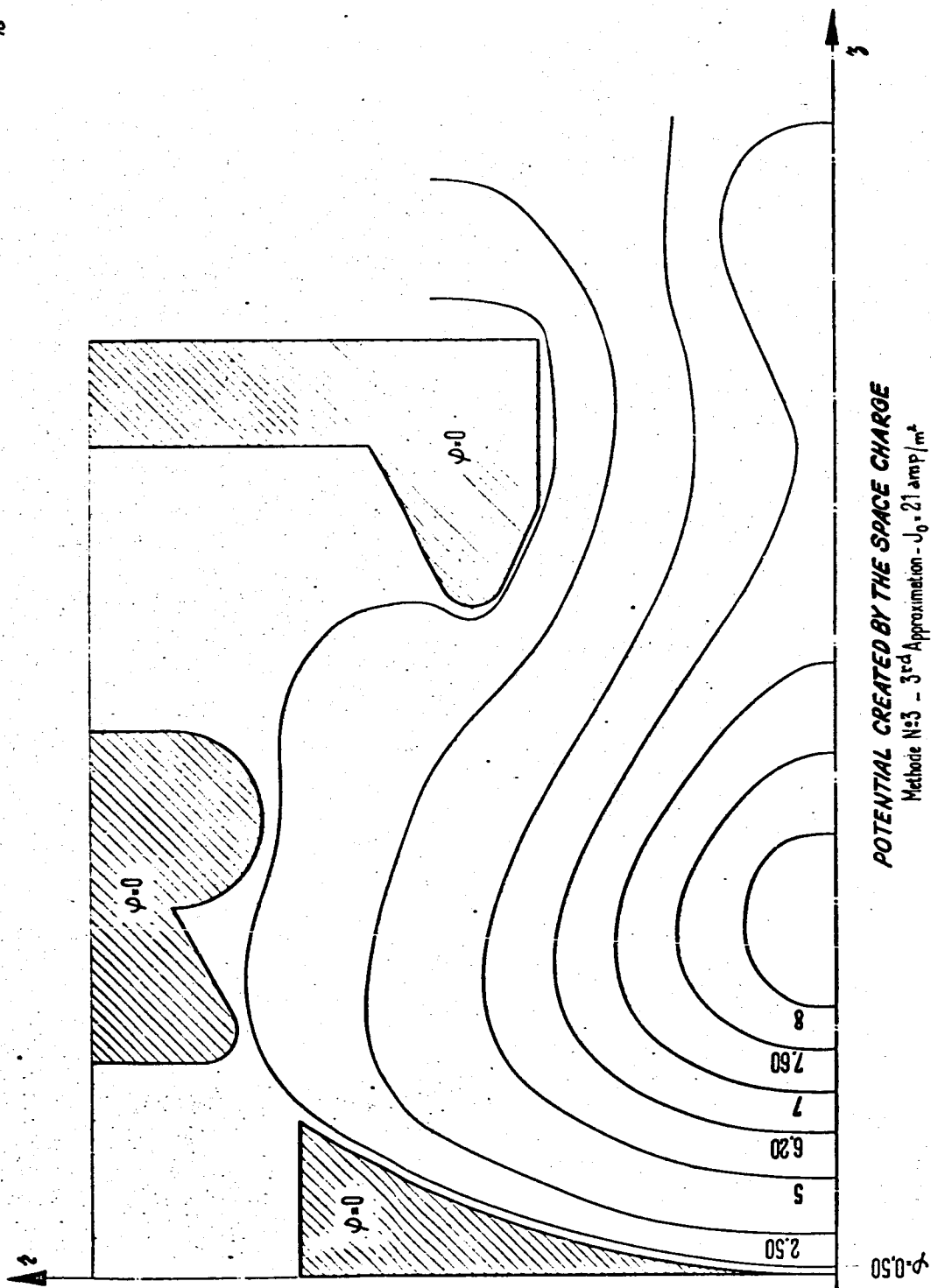
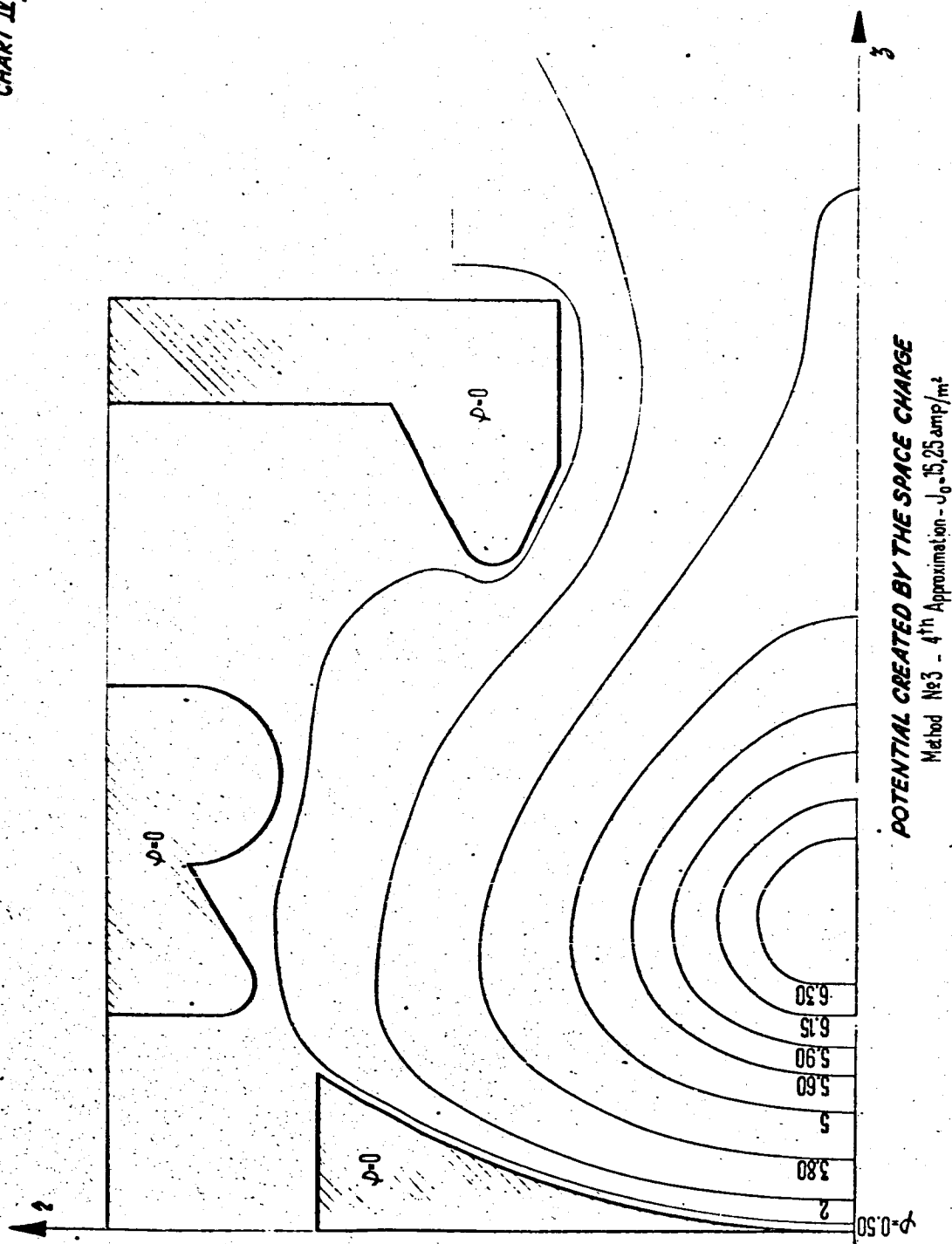


CHART II₉



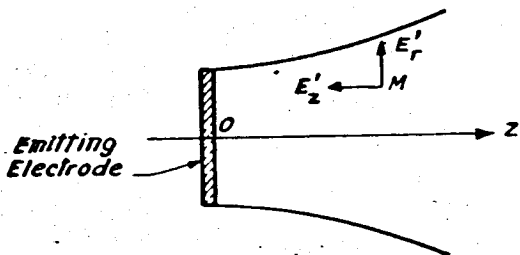


Fig. 1

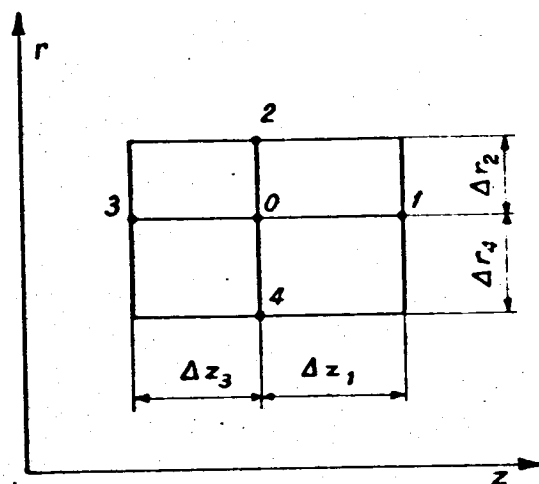


Fig. 2

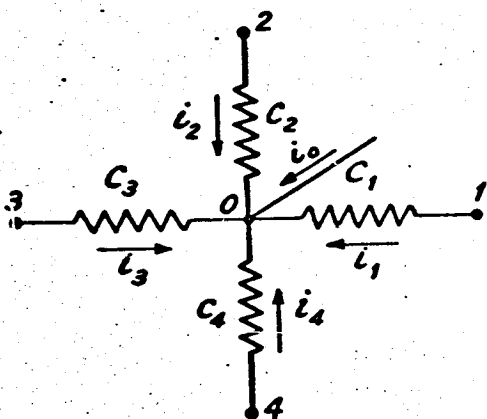


Fig. 3

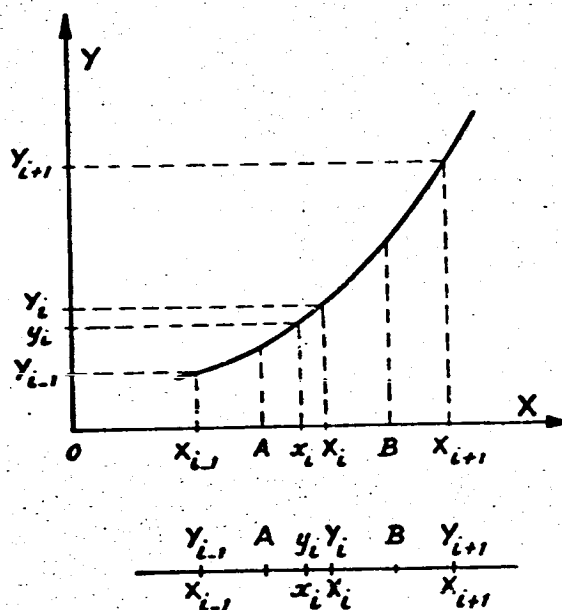


Fig. 4

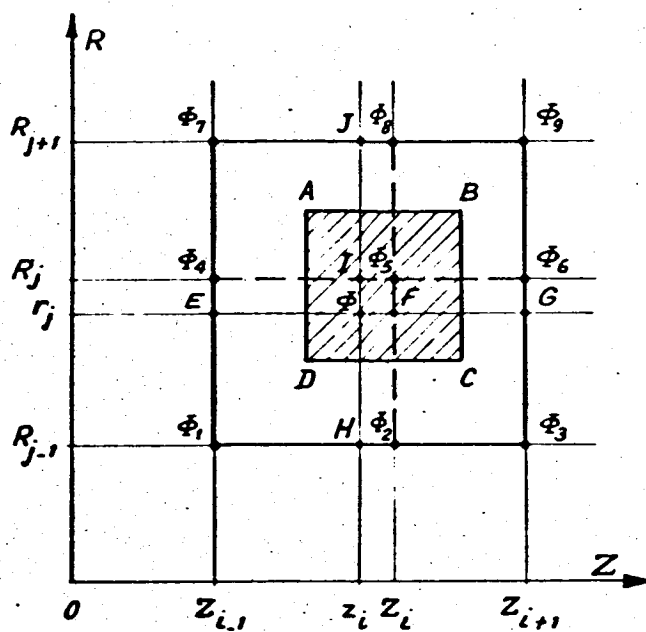


Fig. 5

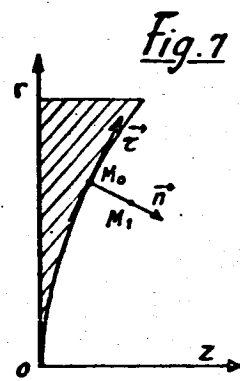


Fig. 7

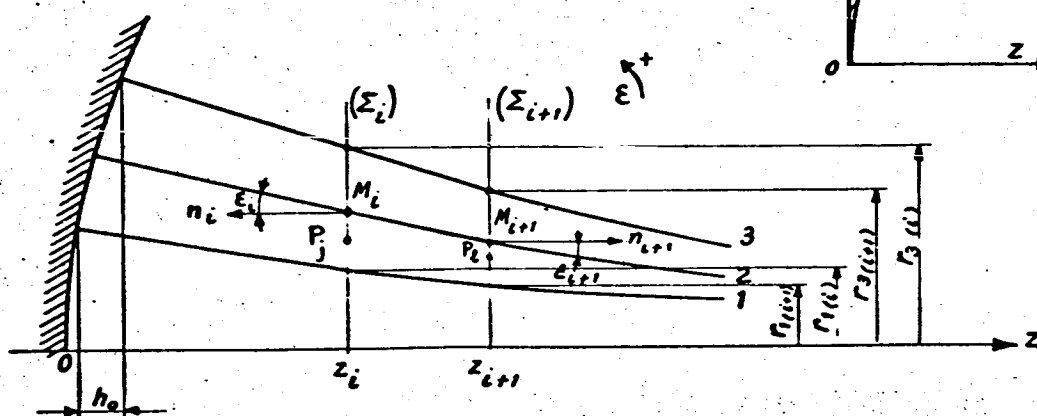


Fig. 6

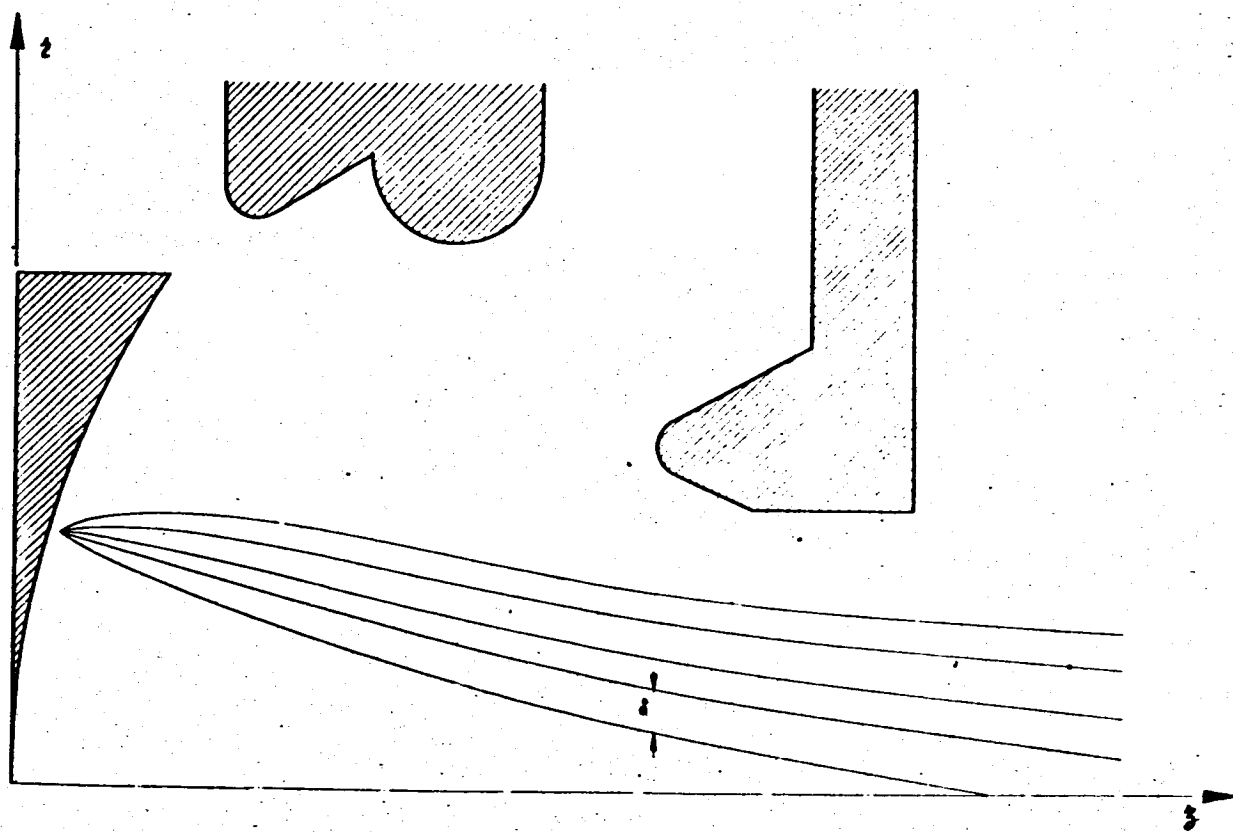


Fig. 8

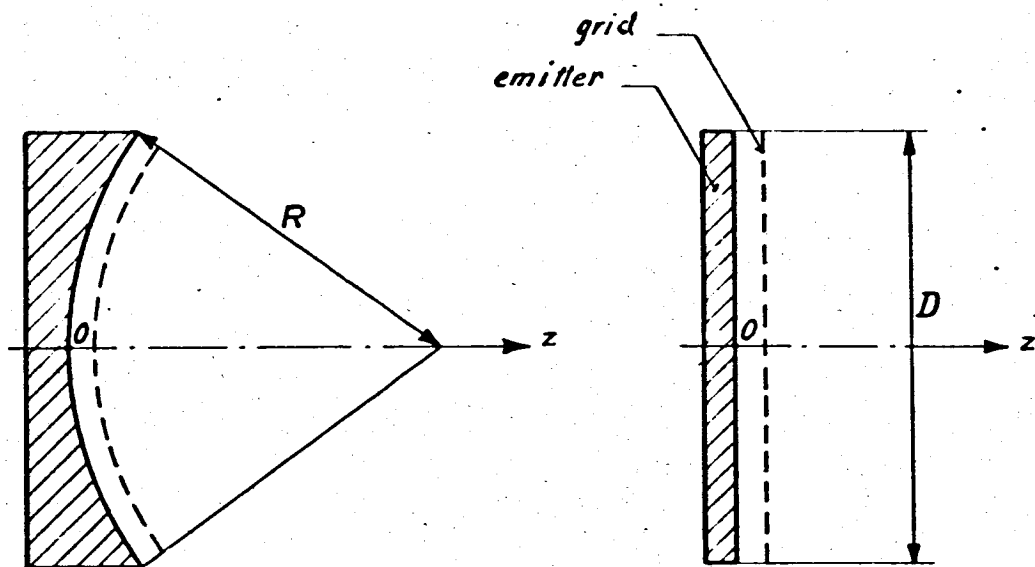


Fig. 9

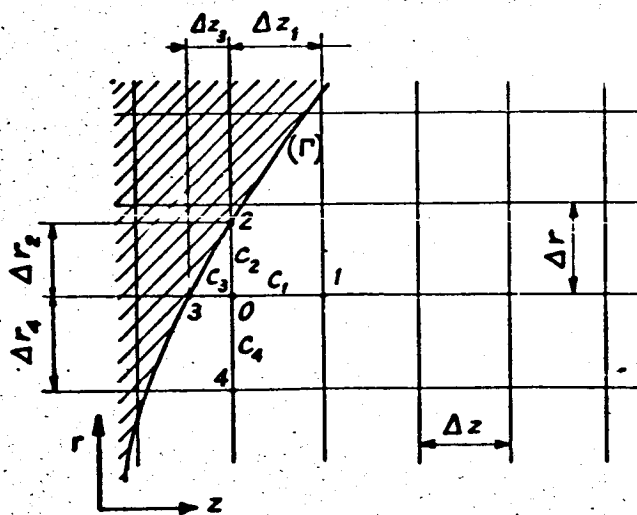


Fig. 10

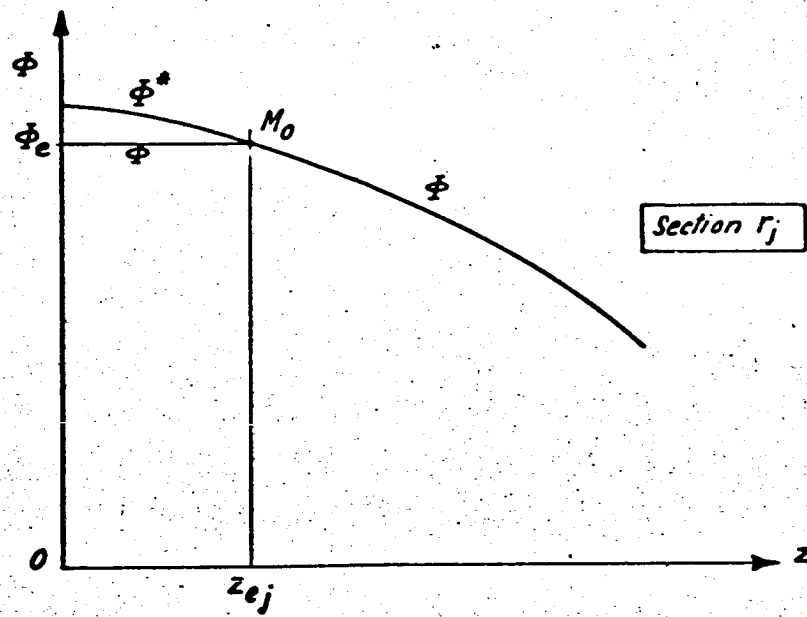
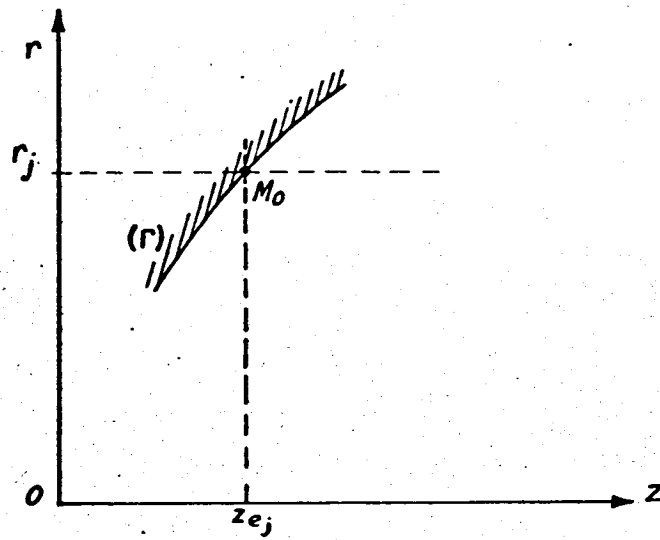


Fig. 11

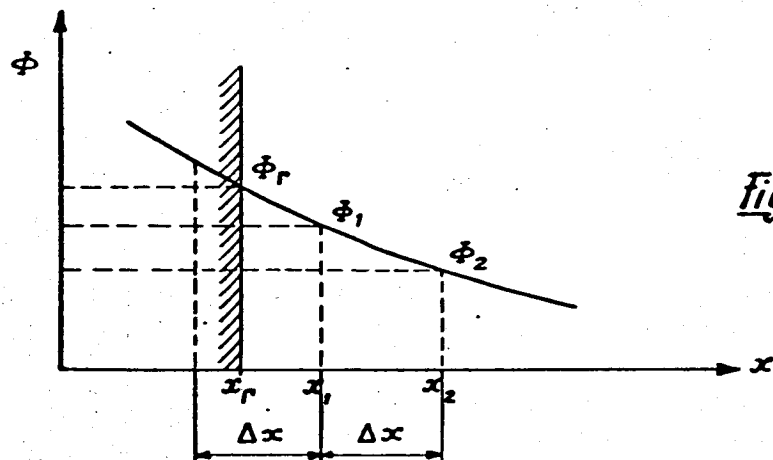


Fig. 12

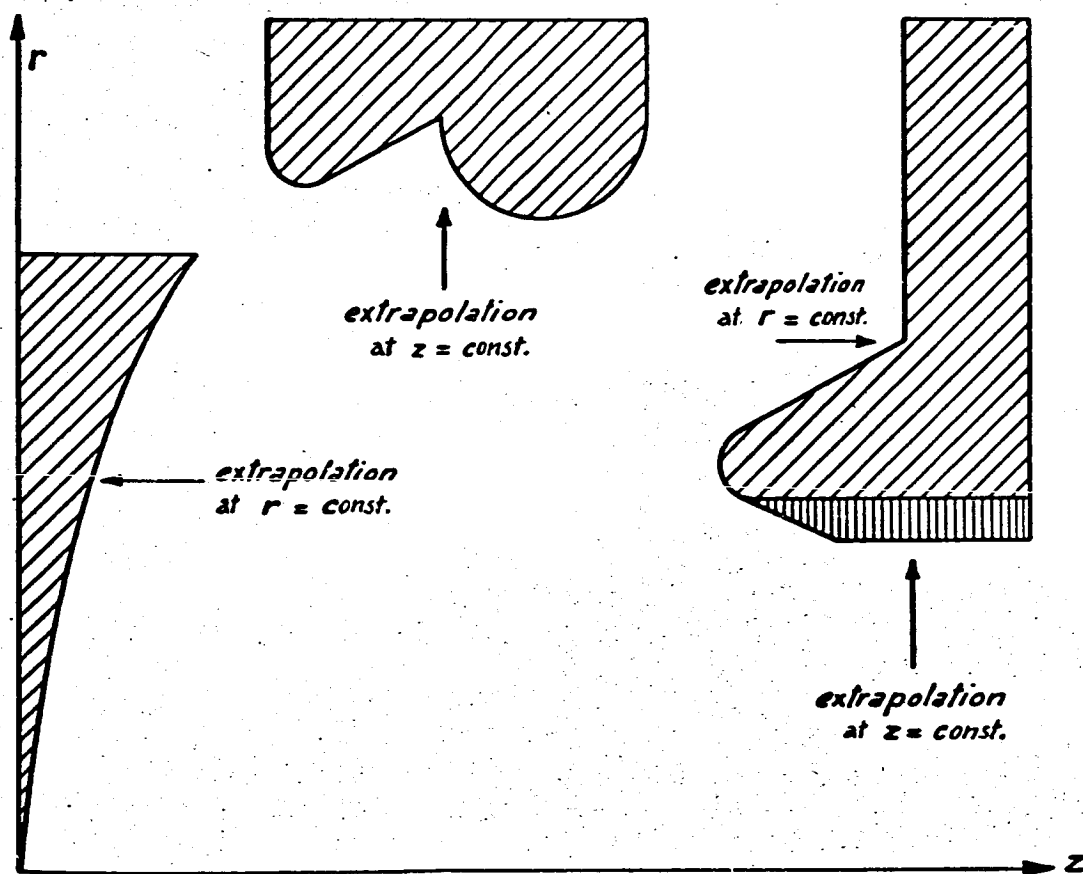
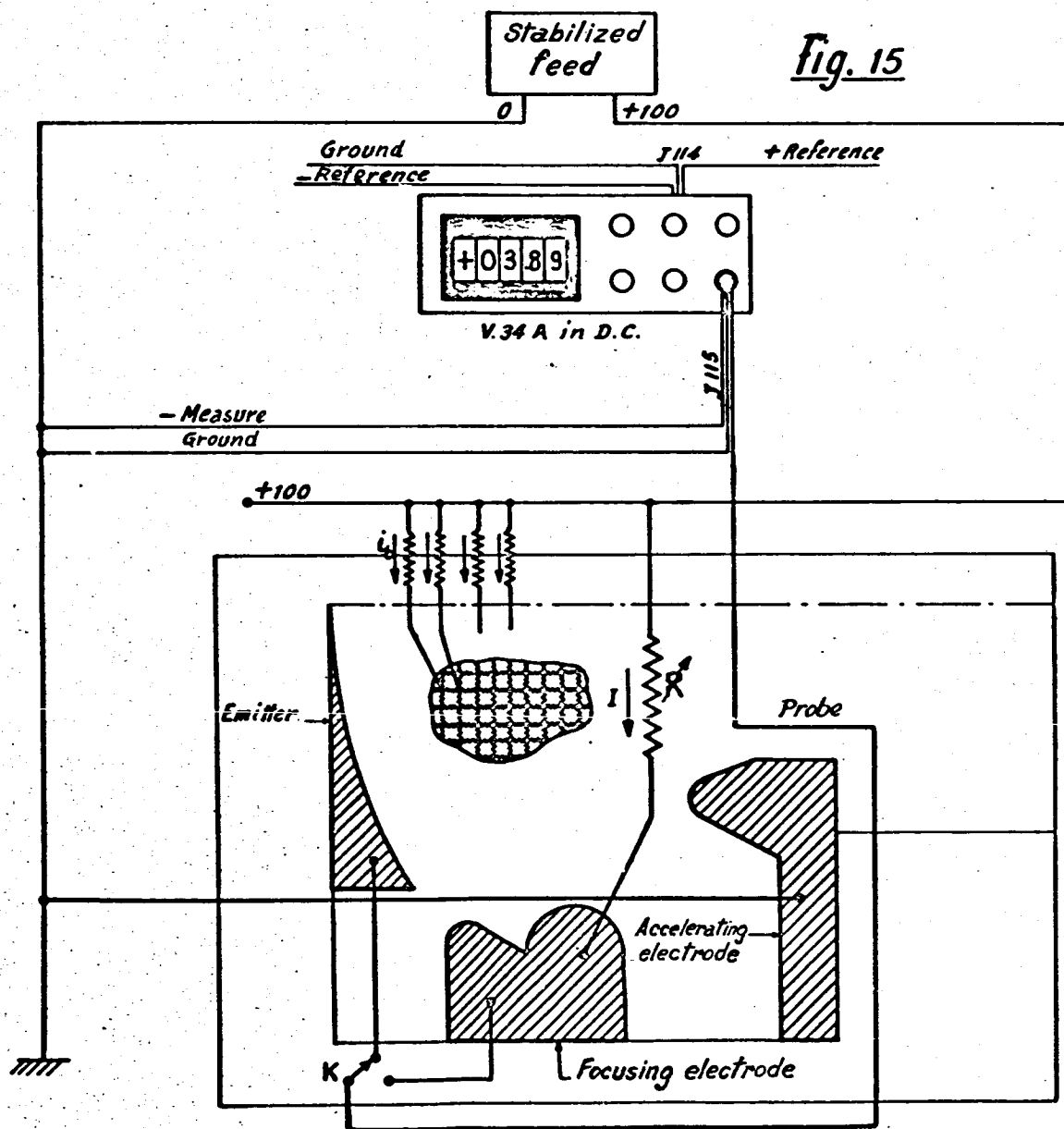
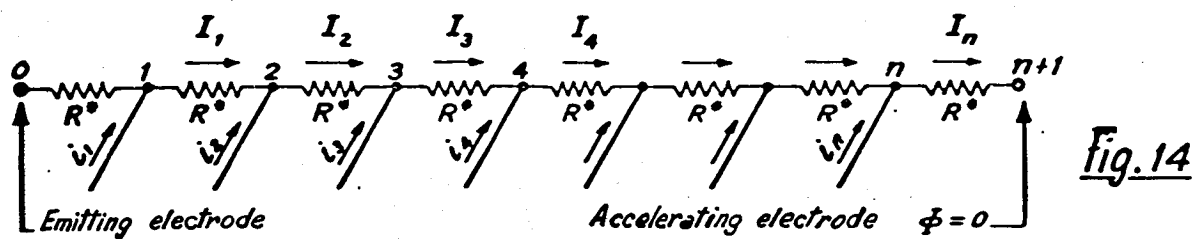


Fig. 13



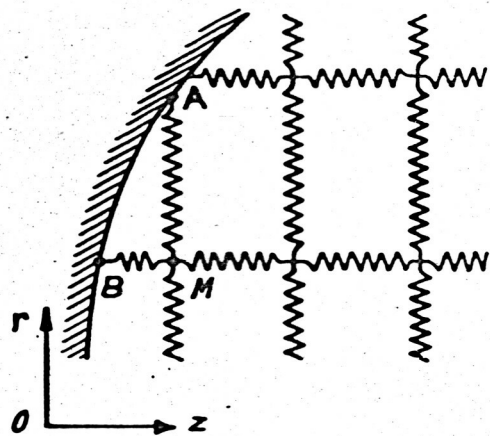


Fig. 16



Fig. 17

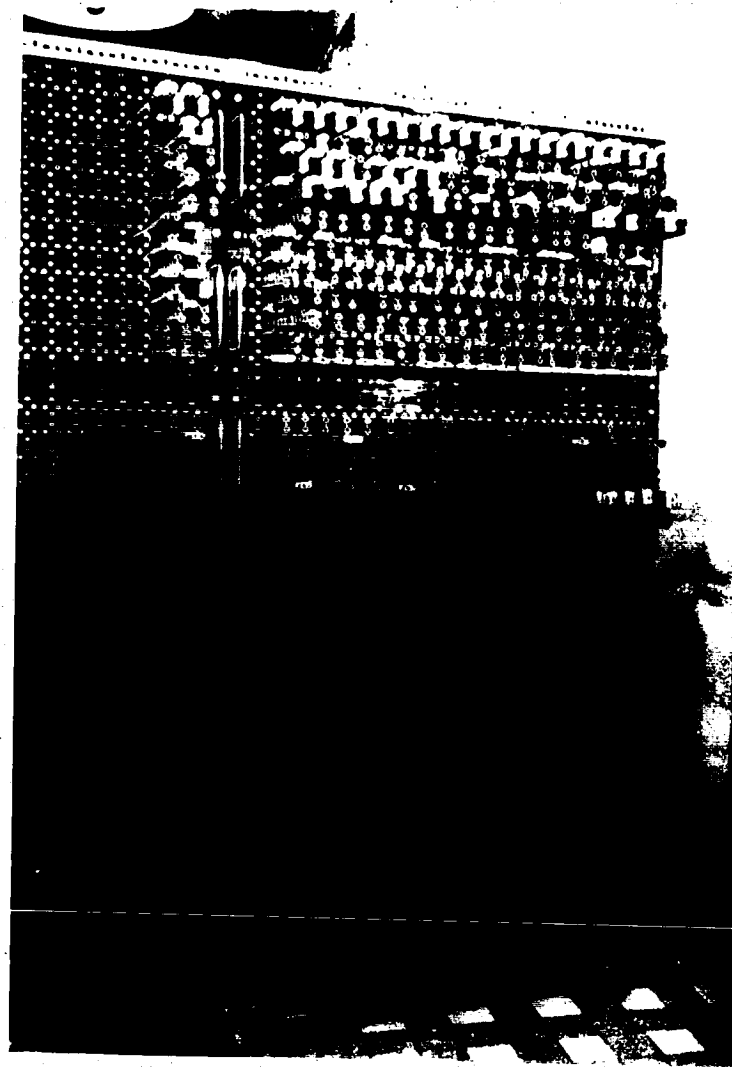


Fig. 18

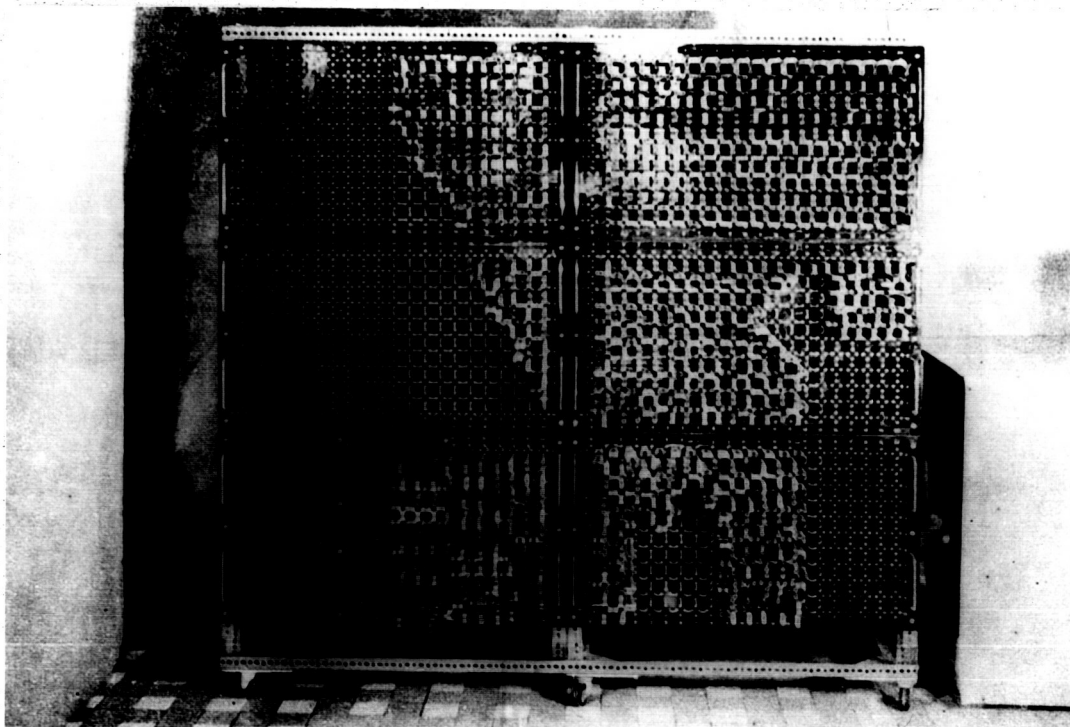


Fig. 18a

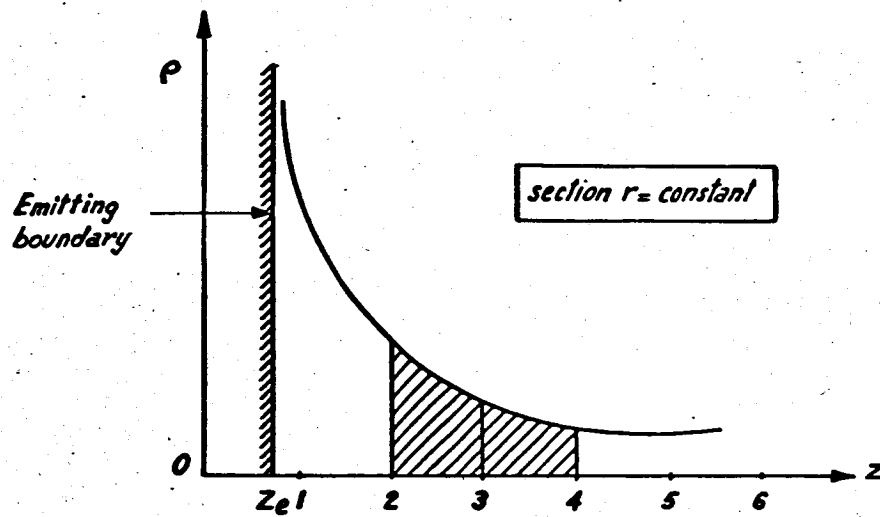


Fig. 19

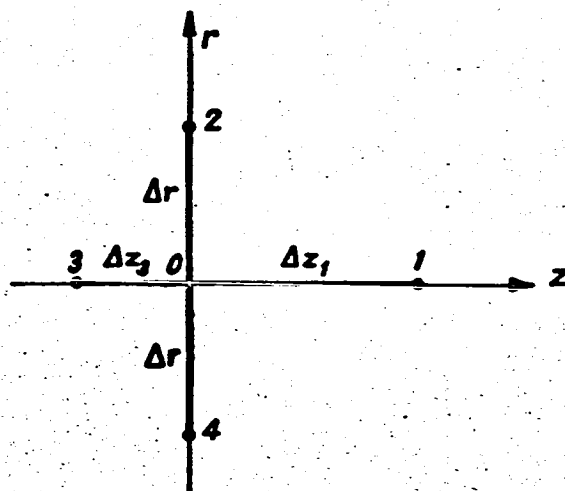
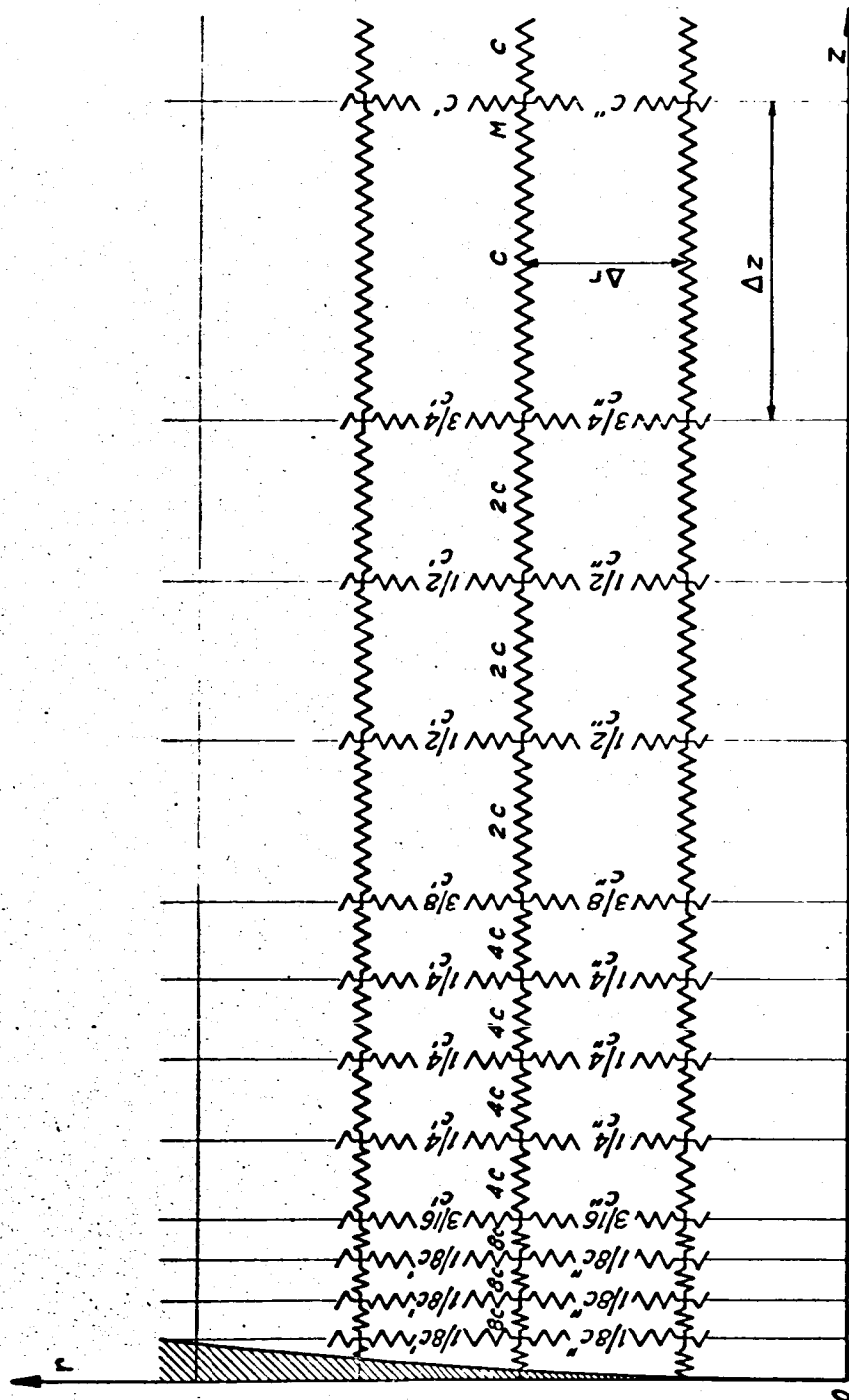


Fig. 20



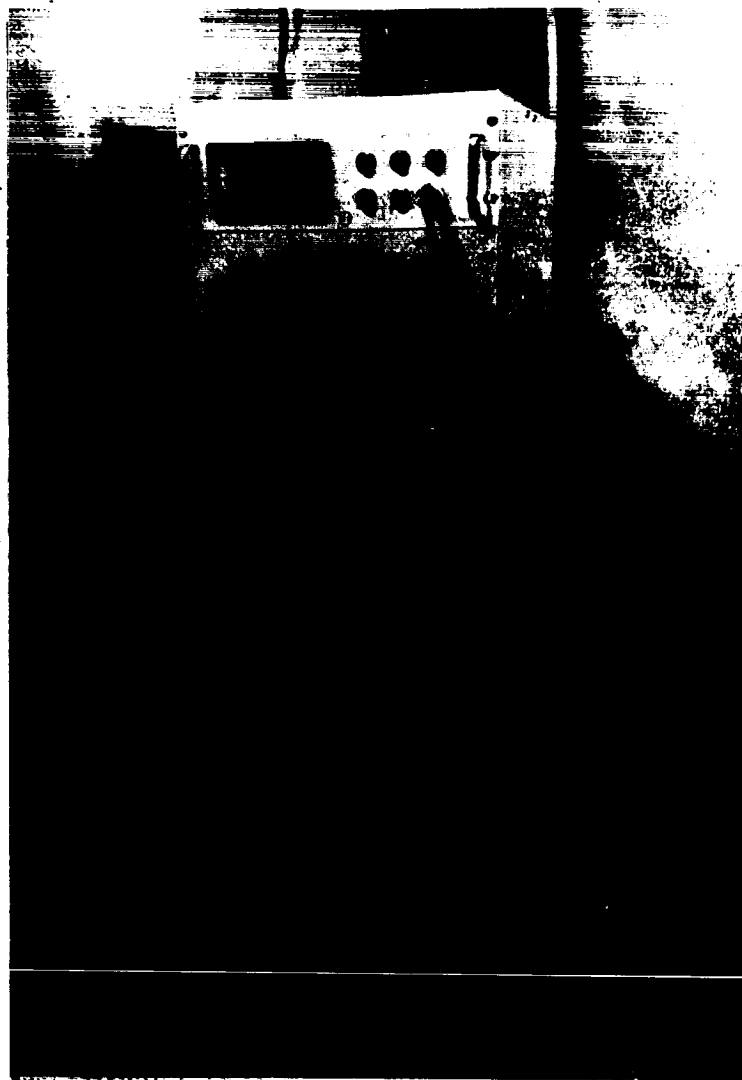


fig. 22

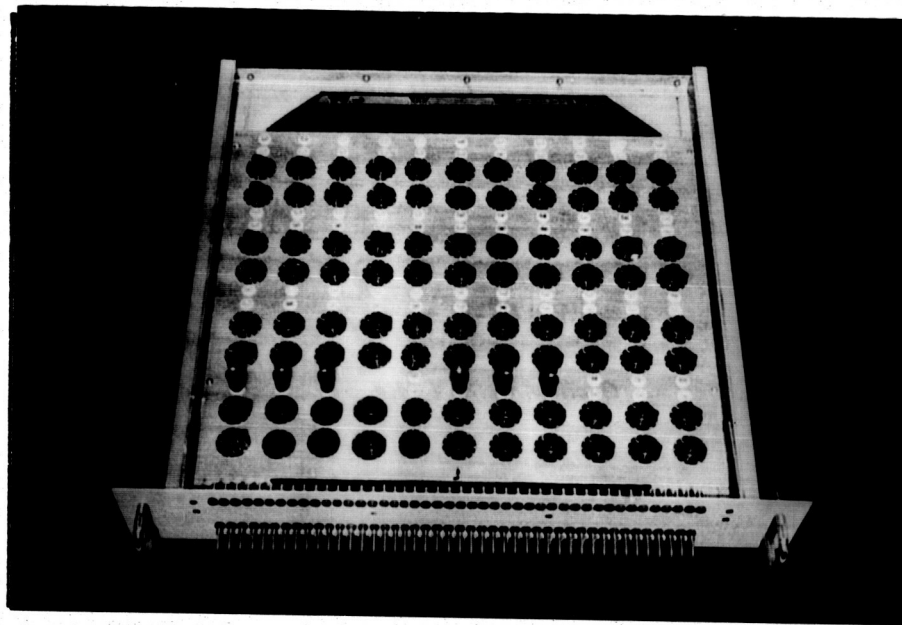


Fig. 23

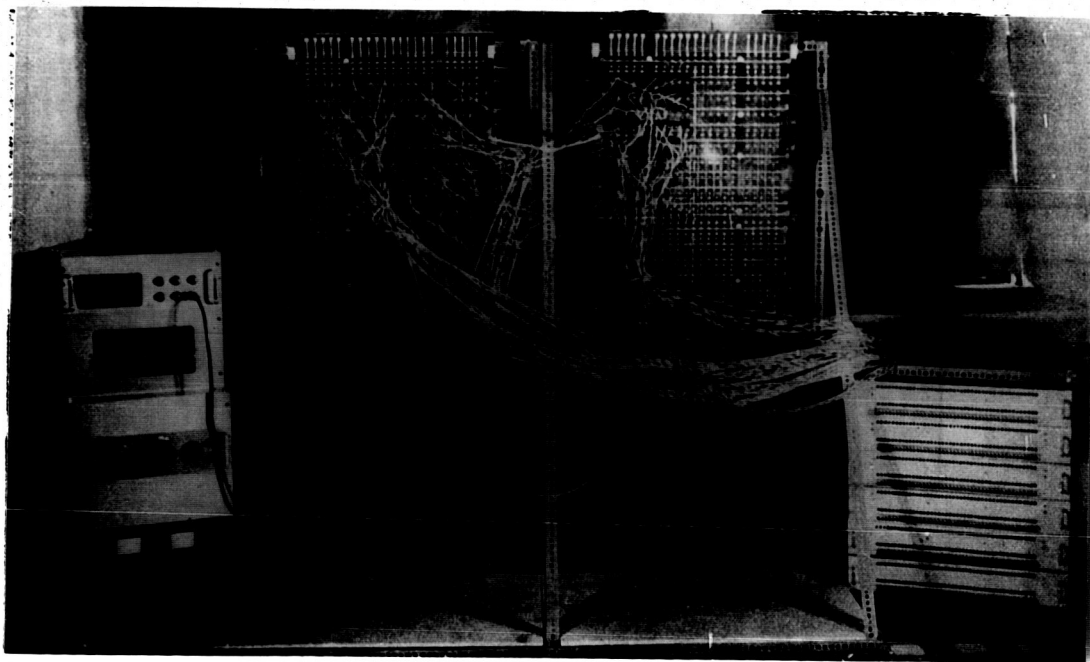


Fig. 25

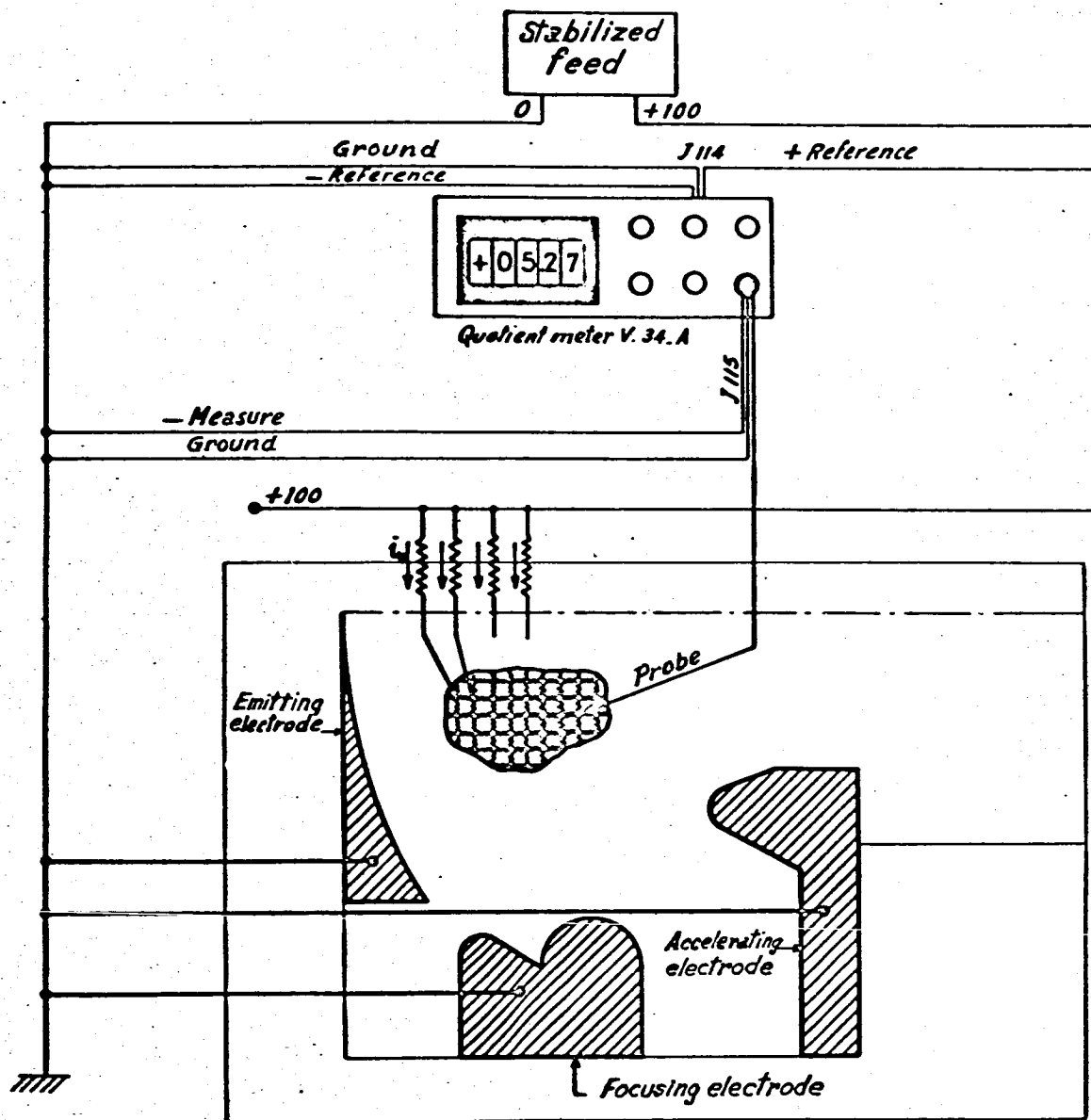


Fig. 24

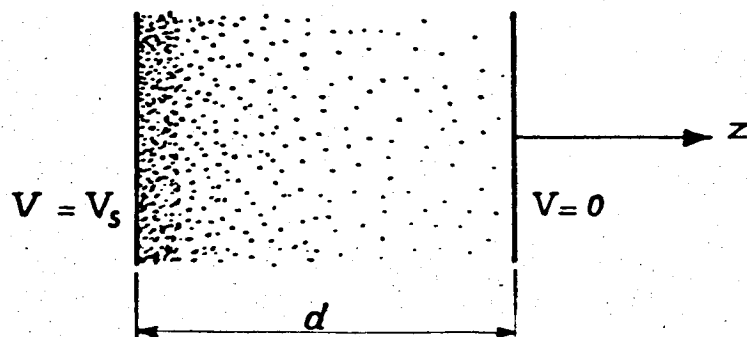


Fig. 26

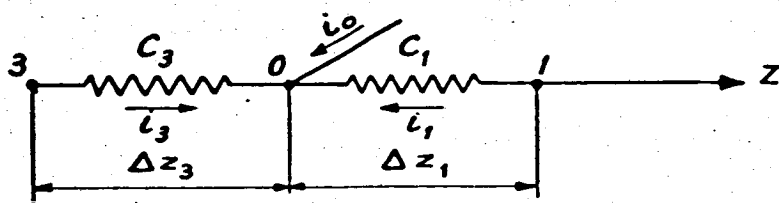


Fig. 27

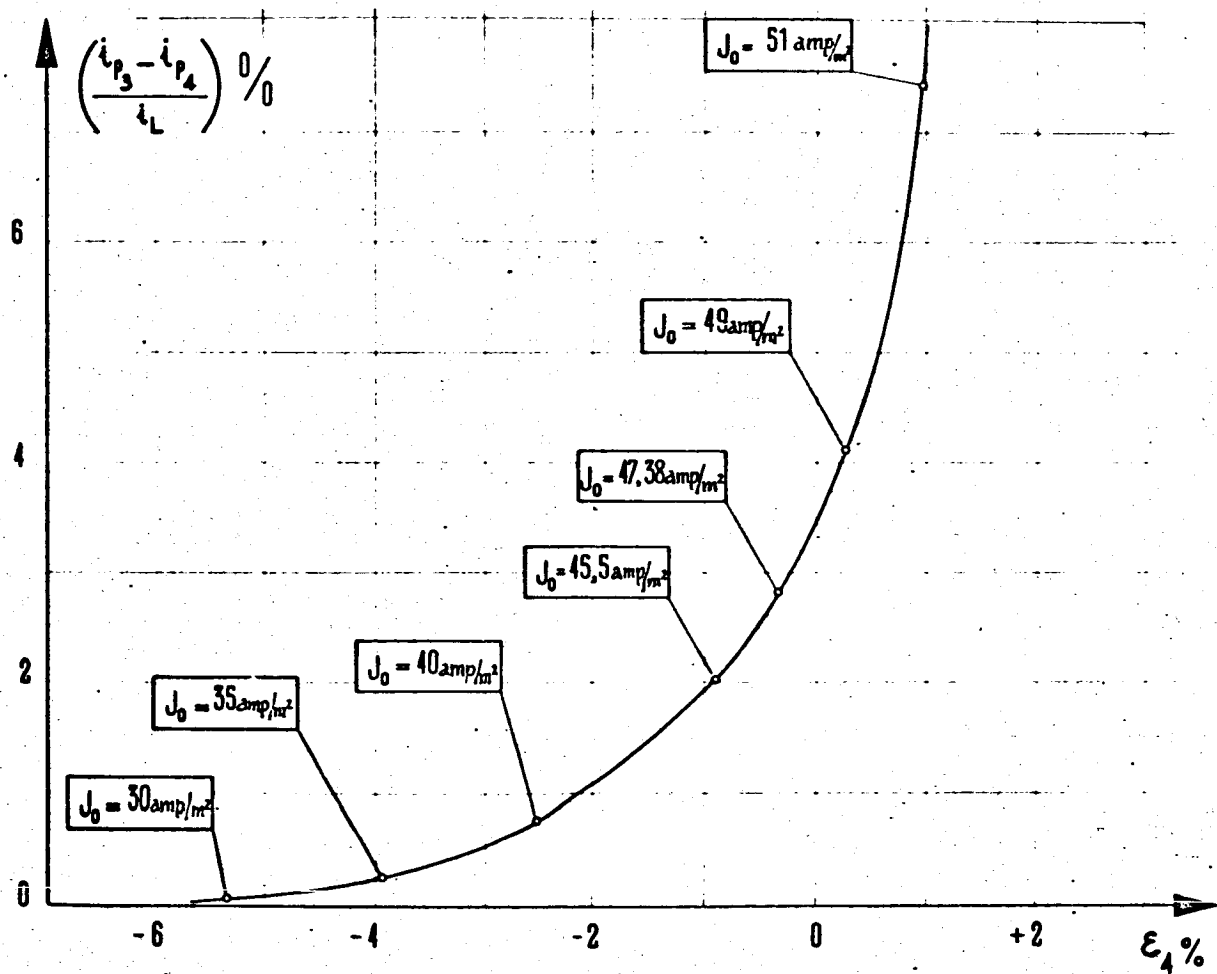
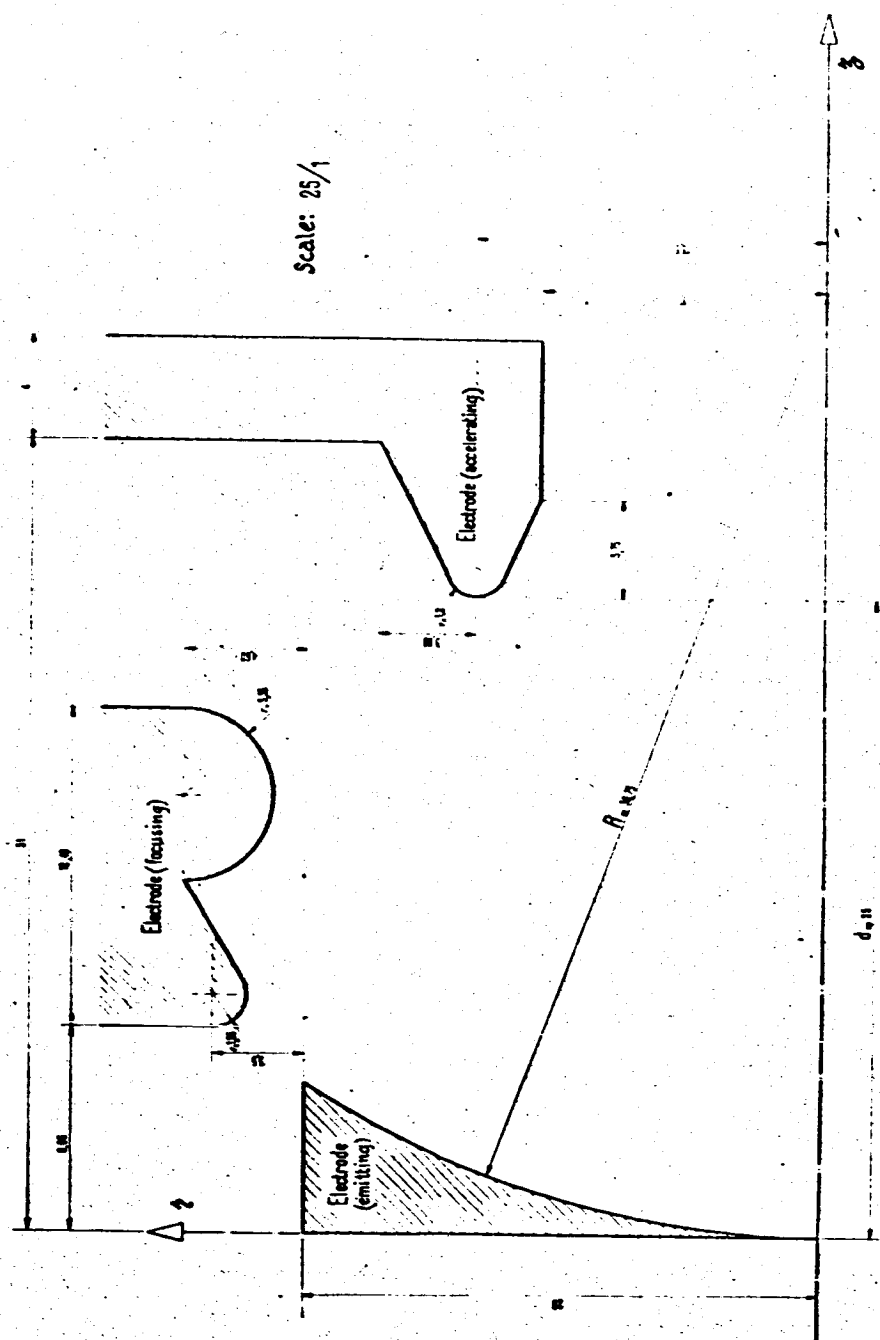
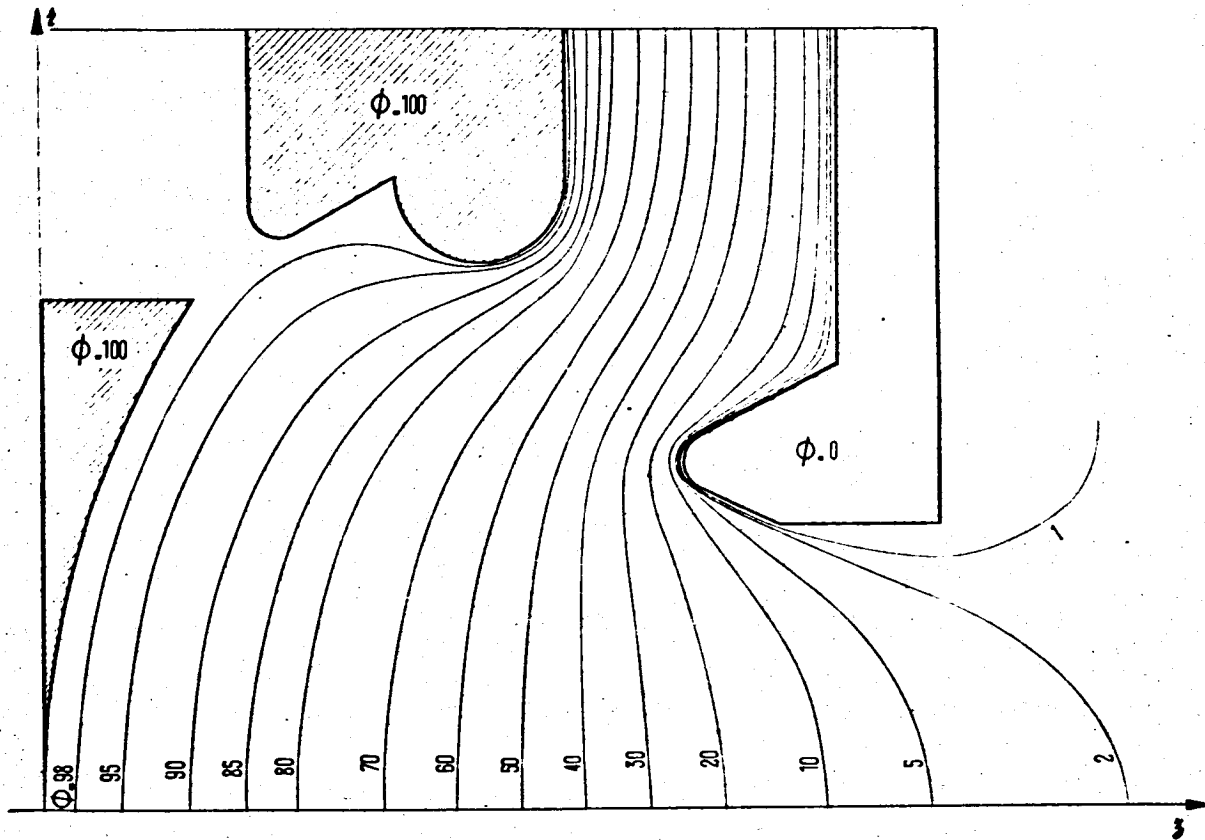


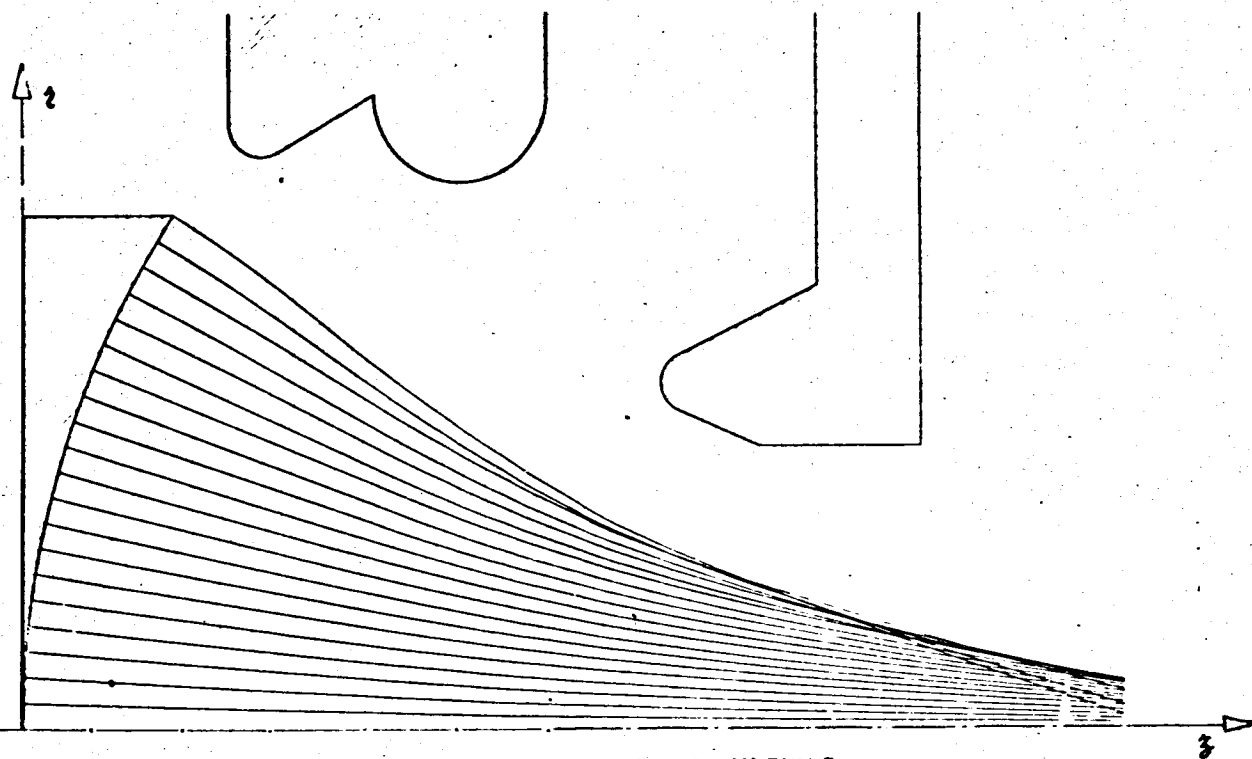
Fig. 28





LAPLACIAN FIELD-NETWORK OF EQUIPOTENTIALS

Fig.30



NETWORK OF TRAJECTORIES-LAPLACIAN FIELD

Fig. 31

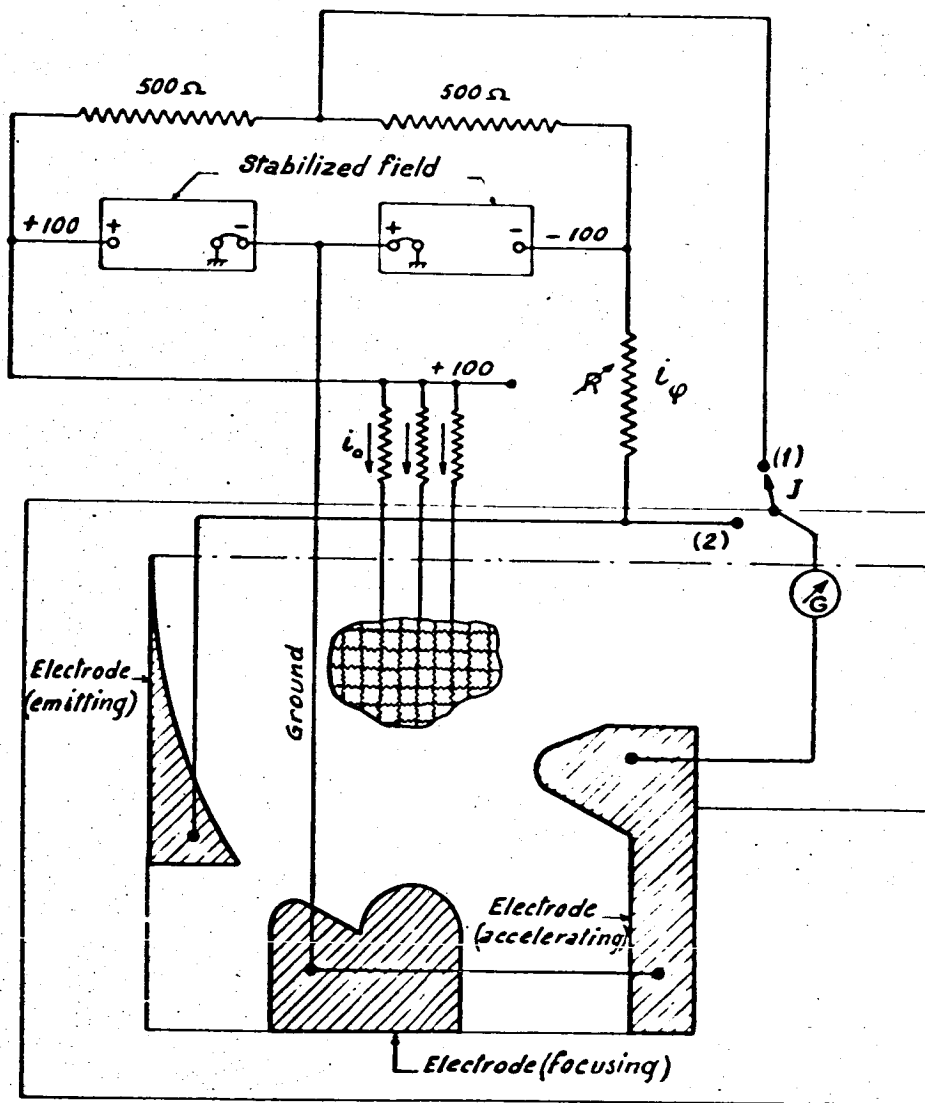


Fig. 32

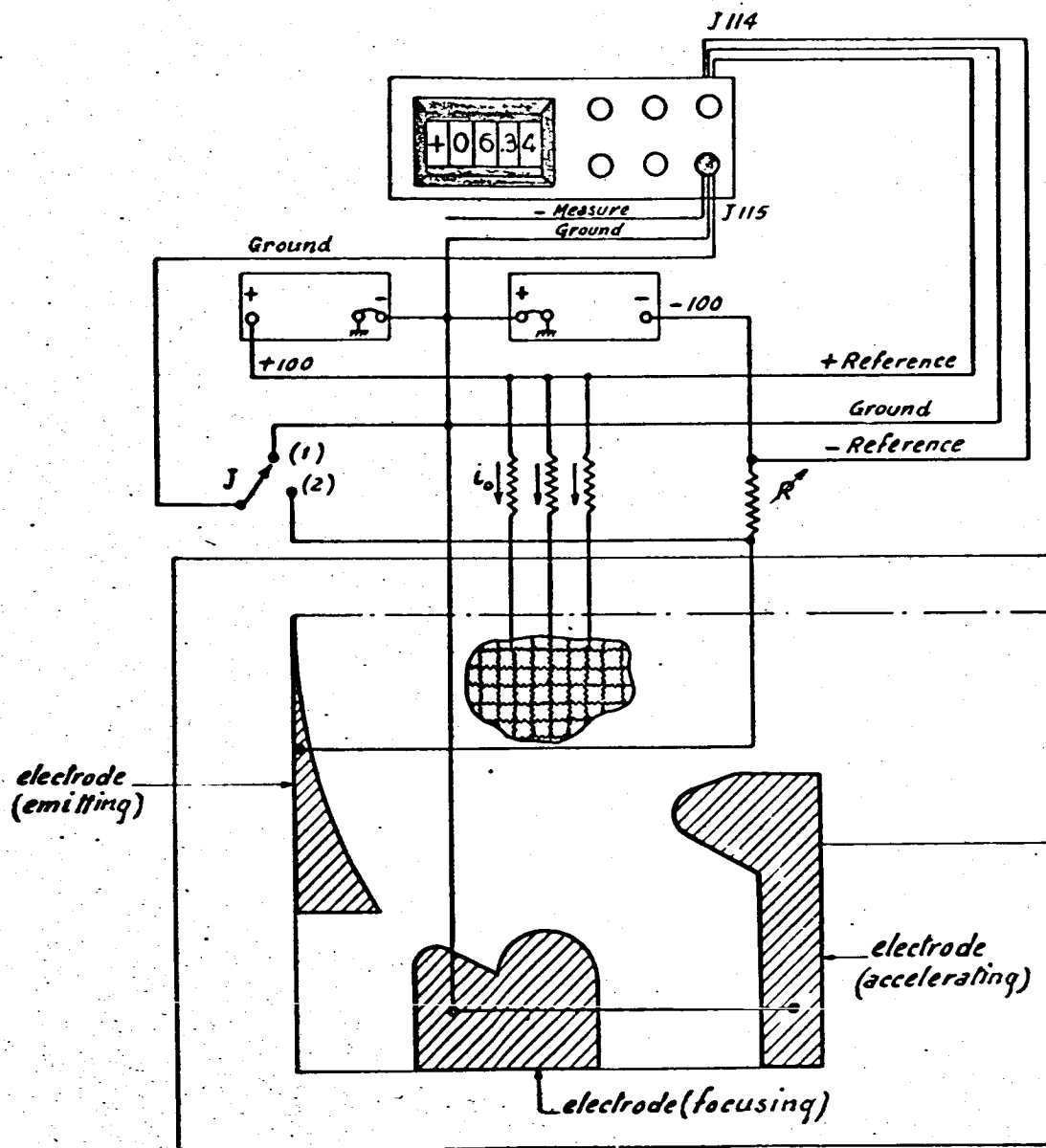
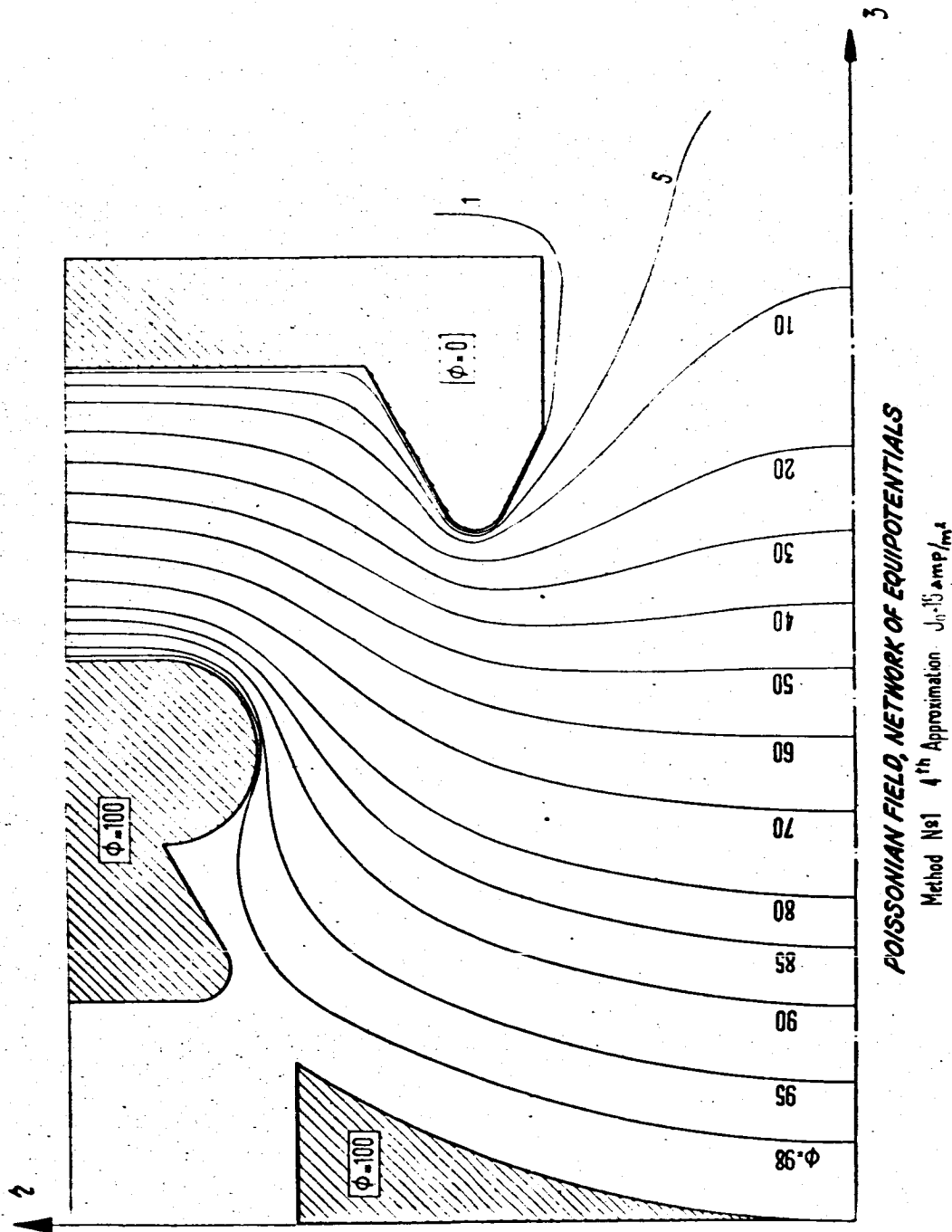


Fig. 33

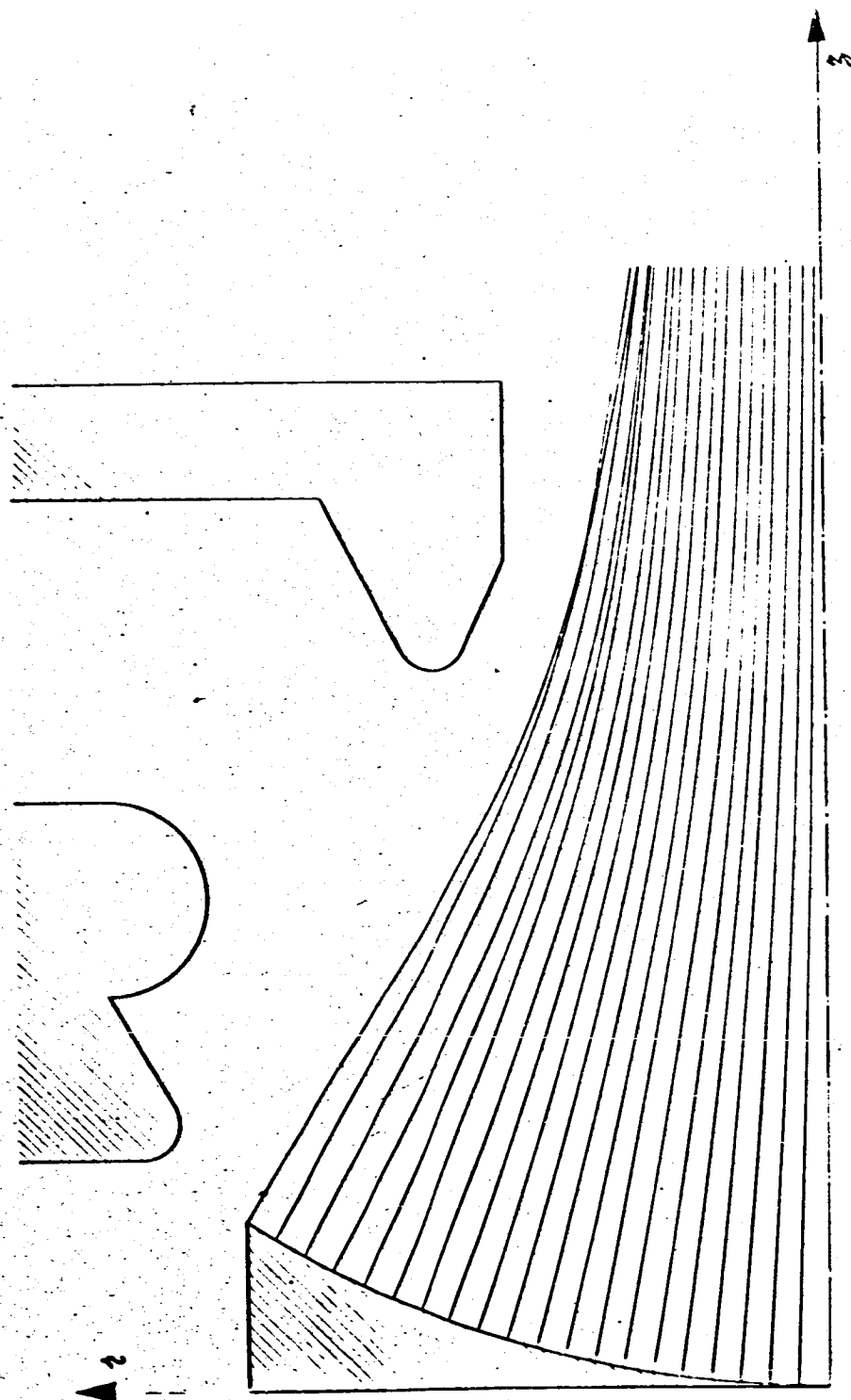


POISSONIAN FIELD, NETWORK OF EQUIPOTENTIALS

Method No 1 4th Approximation $J_0 = 15 \text{ amp/cm}^2$

Fig. 34

32
33
34
35
36
37
38
39
40
41
42
43
44
45
46
47
48
49
50
51
52

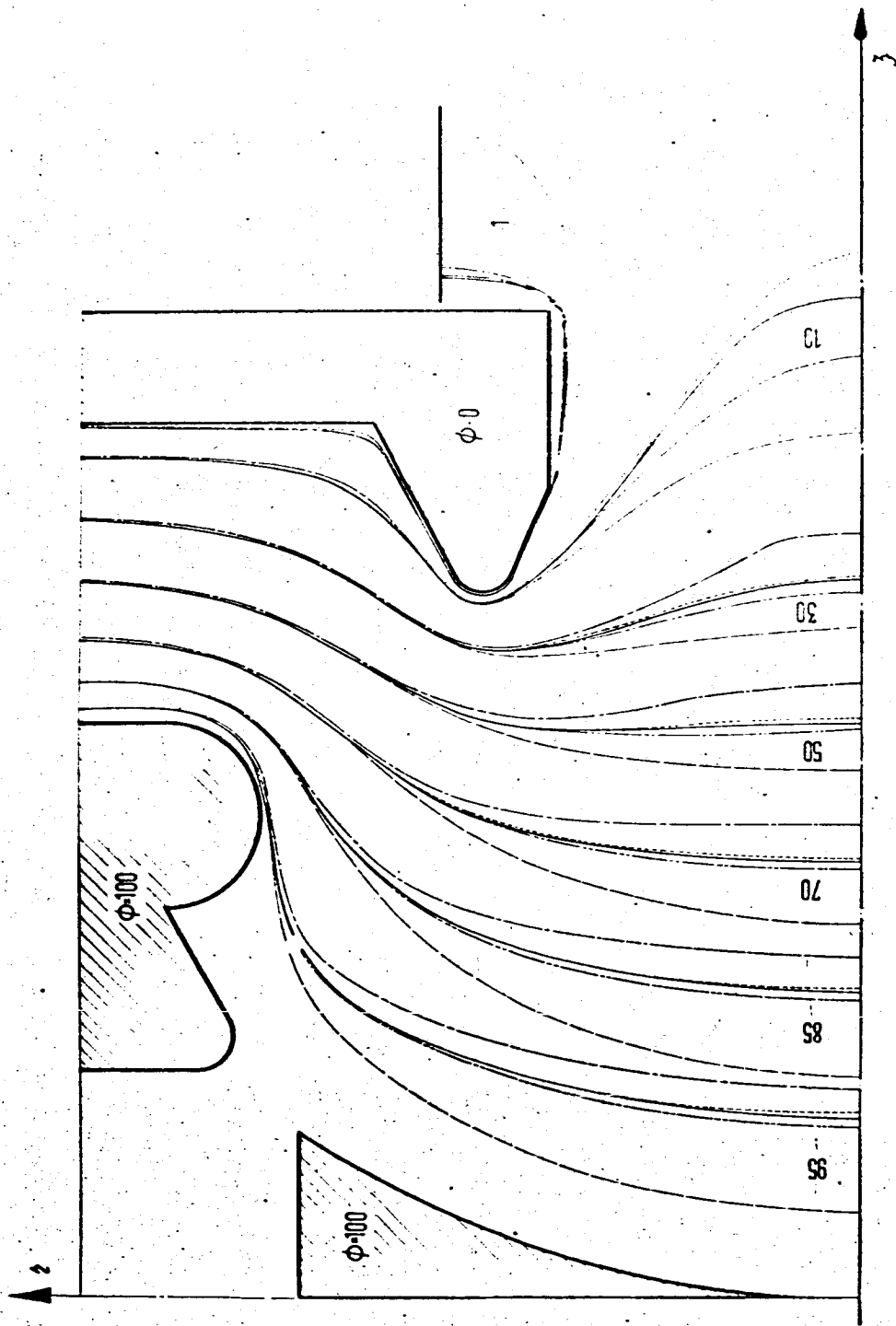


NETWORK OF TRAJECTORIES-POISSONIAN FIELD

Method №1 4th Approximation $J_0 = 15 \text{ amp/m}^2$

Fig. 35

52
51
50
49
48
47
46
45
44
43
42
41
40
39
38
37
36
35
34
33
32
31
30
29
28
27
26
25
24
23
22
21
20
19
18
17
16
15
14
13
12
11
10
9
8
7
6
5
4
3
2
1

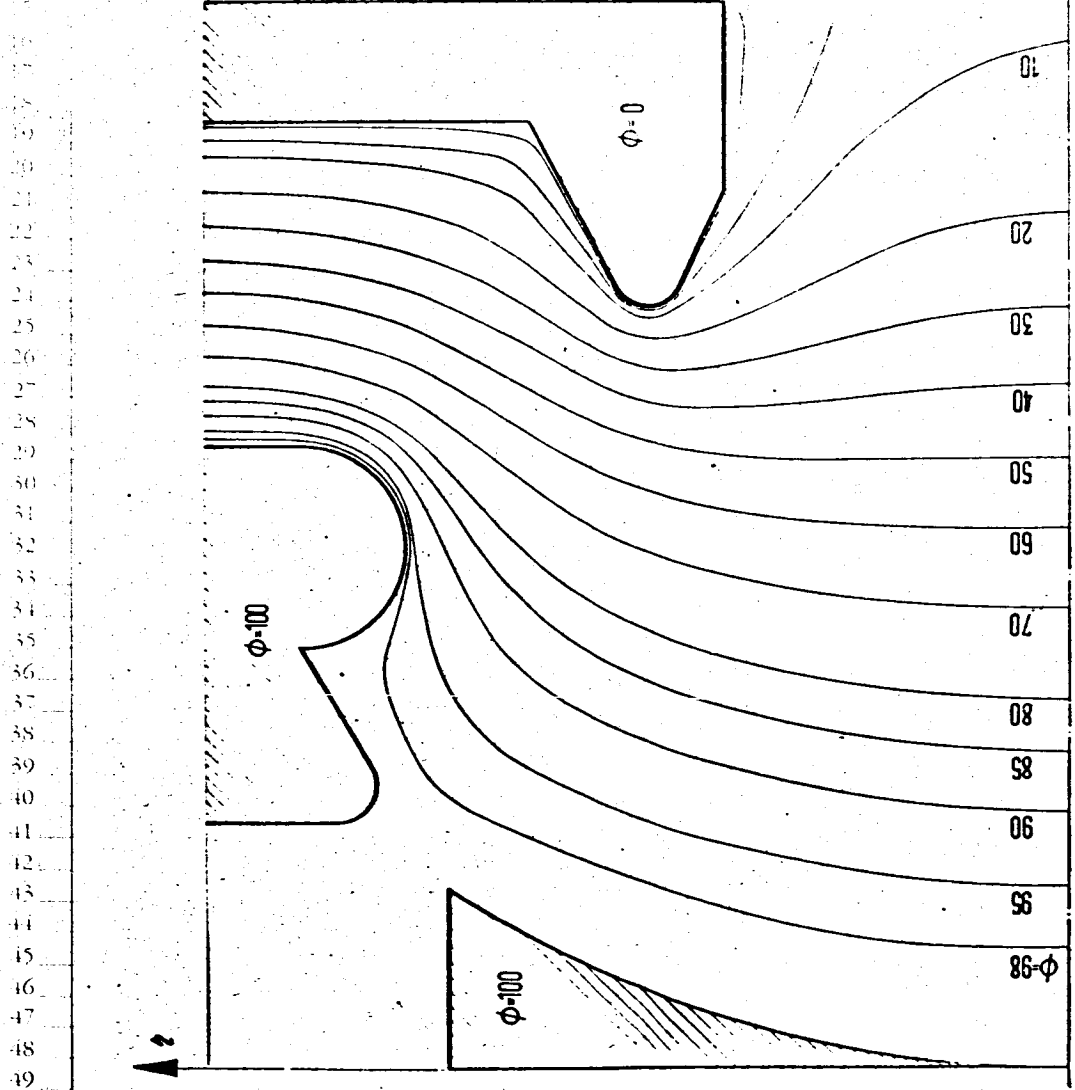


INFLUENCE OF THE SPACE CHARGE

LAPLACIAN FIELD

1 st Approximation		Method №2
2 nd	3 rd	
4 th		

Fig. 36

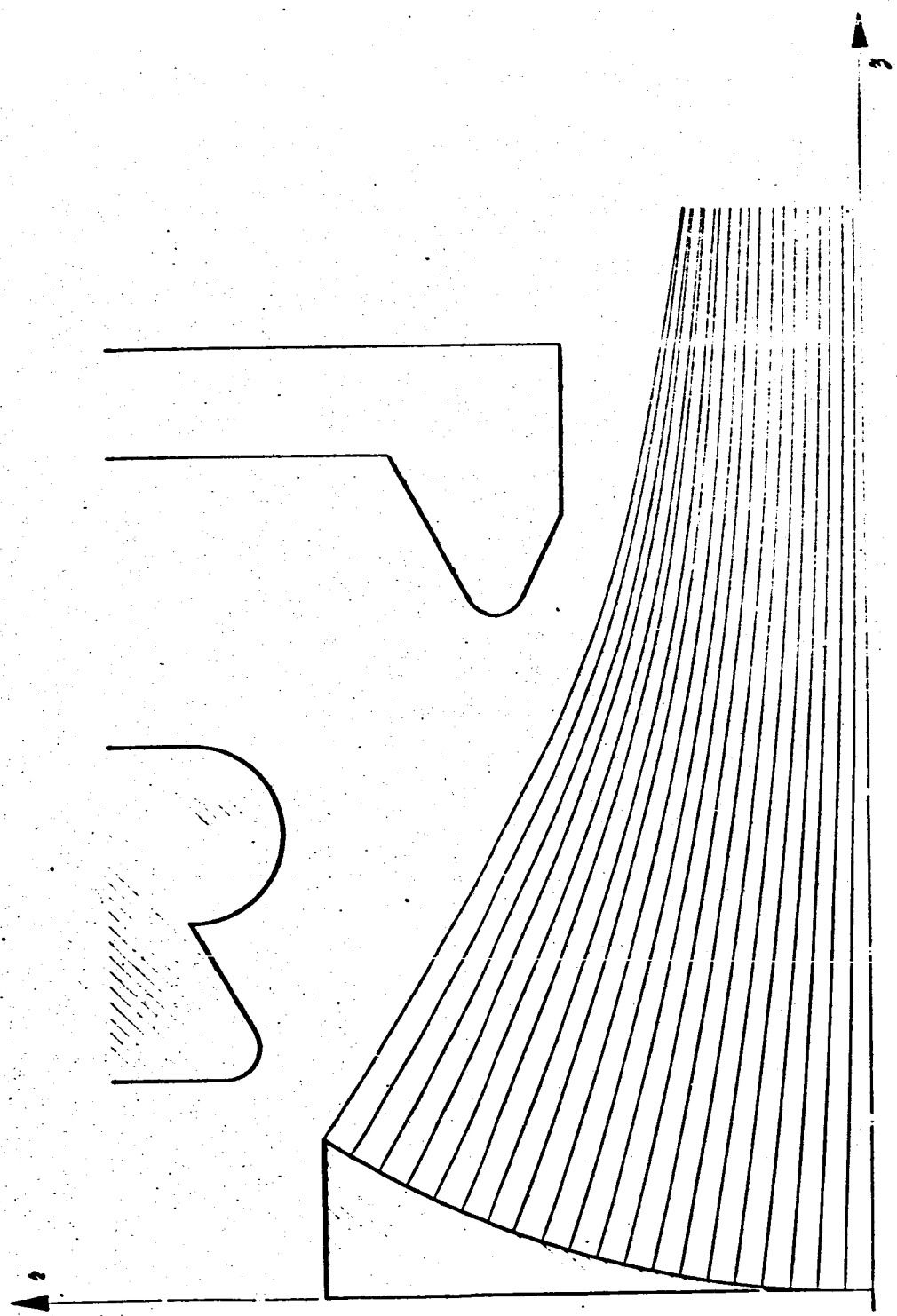


POISSONIAN FIELD NETWORK OF EQUIPOTENTIALS

Method №3 4th Approximation $J_0 = 15.25 \text{ amp/m}^2$

Fig. 37

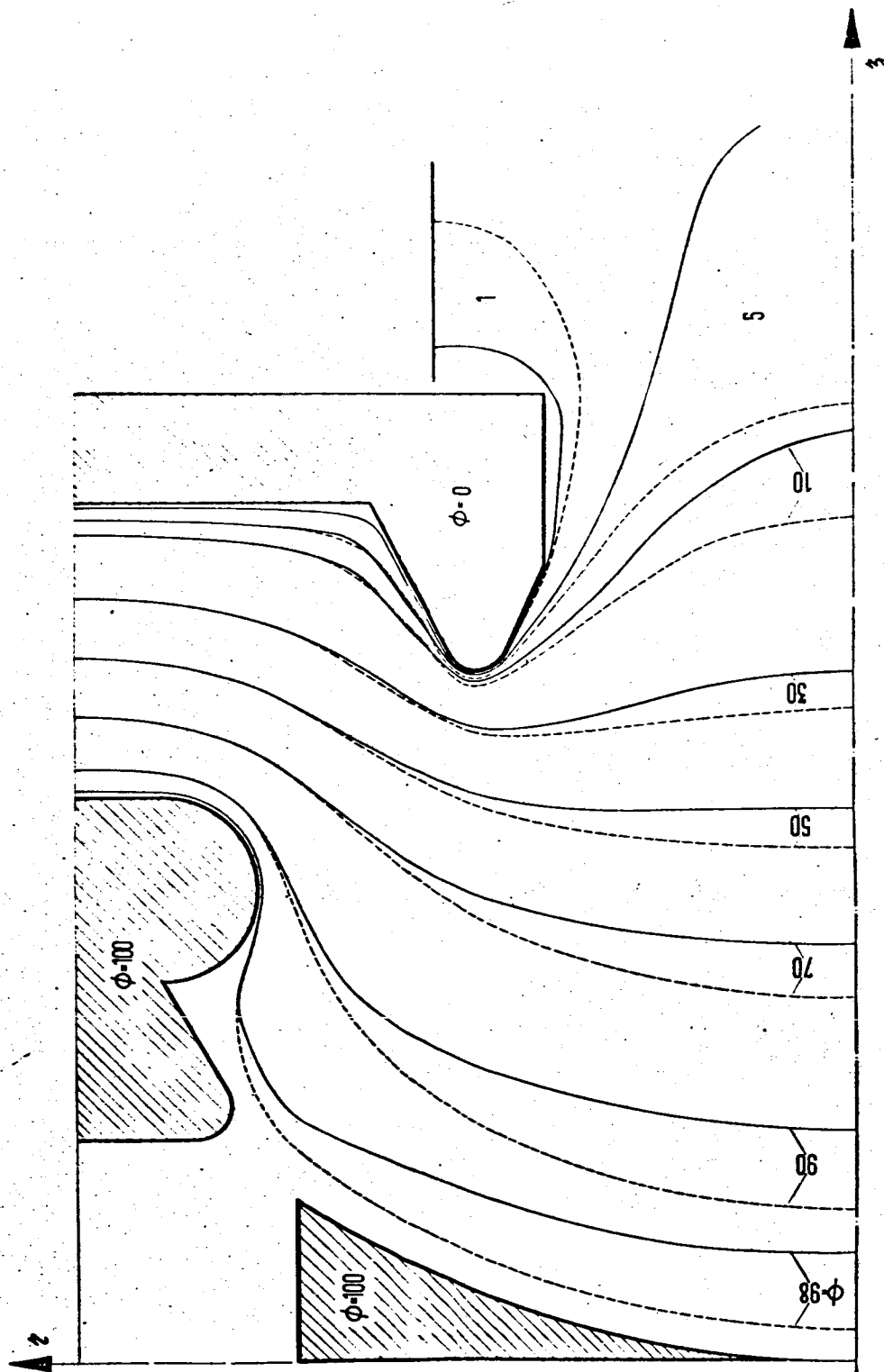
32
33
34
35
36
37
38
39
40
41
42
43
44
45
46
47
48
49
50
51
52



NETWORK OF TRAJECTORIES POISSONIAN FIELD

Method №3 4th Approximation $J_0 = 15,25 \text{ amp/m}^2$

Fig. 38

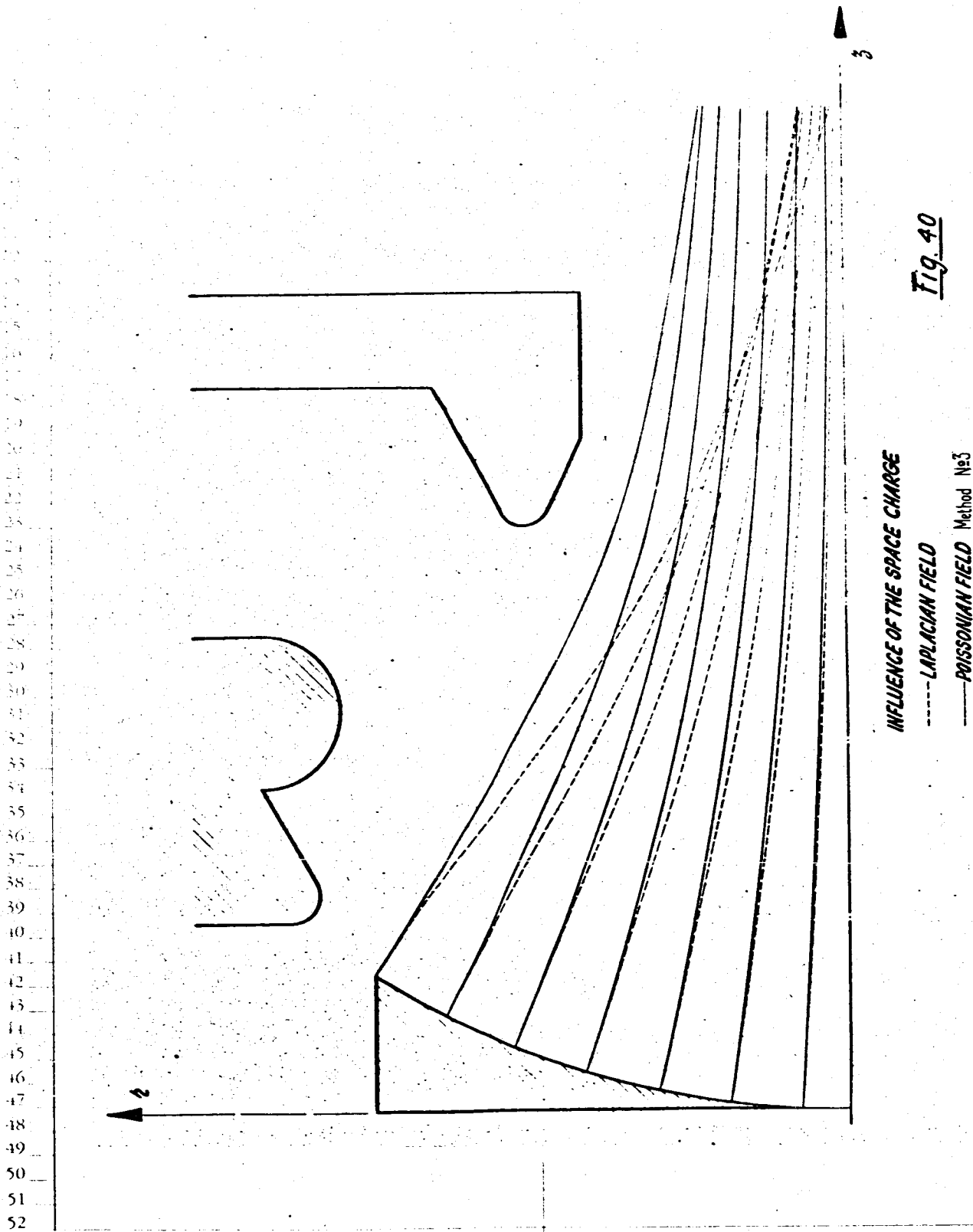


INFLUENCE OF THE SPACE CHARGE

Fig. 39

--- LAPLACIAN FIELD

— POISSONIAN FIELD Method №3



INFLUENCE OF THE SPACE CHARGE

----- LAPLACIAN FIELD

———— POISSONIAN FIELD Method No. 3

Fig. 40

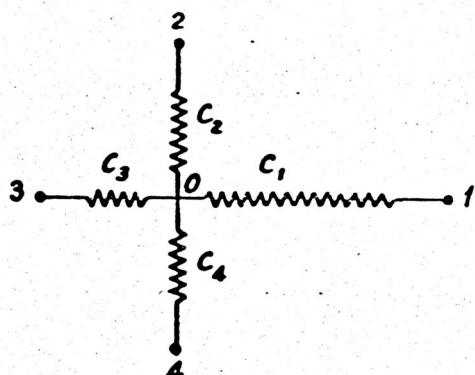


Fig. 41

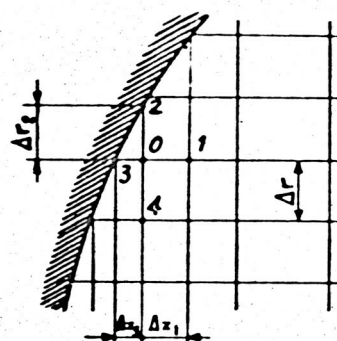


Fig. 42

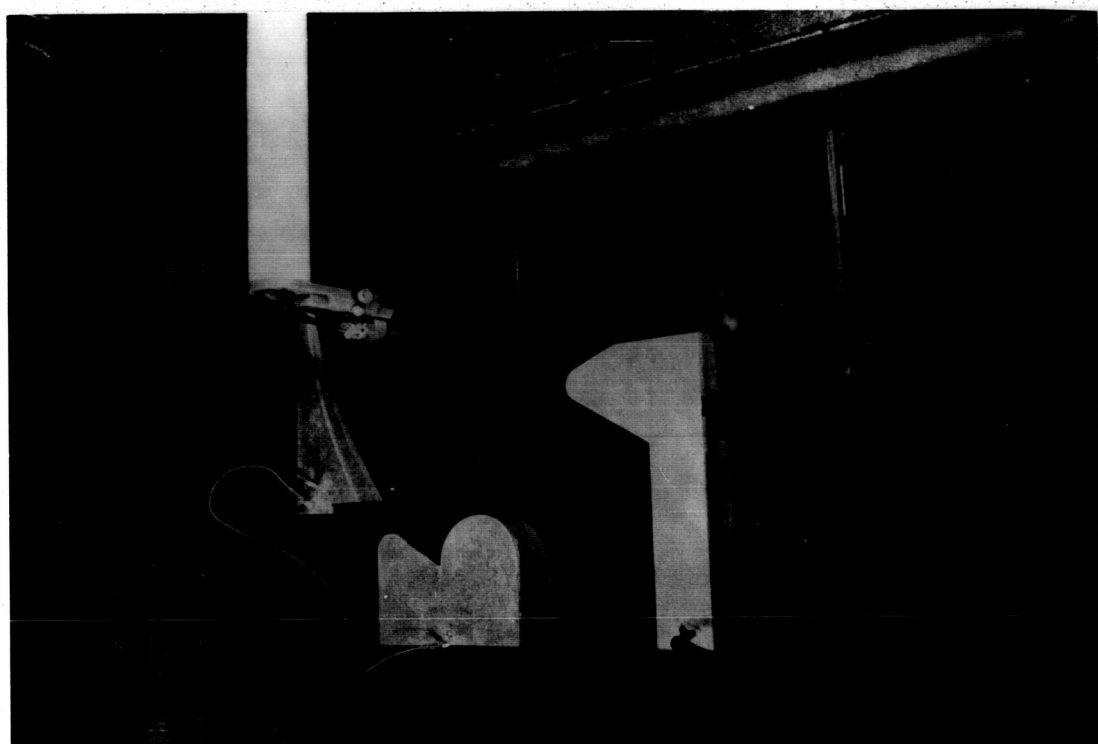


Fig. 43

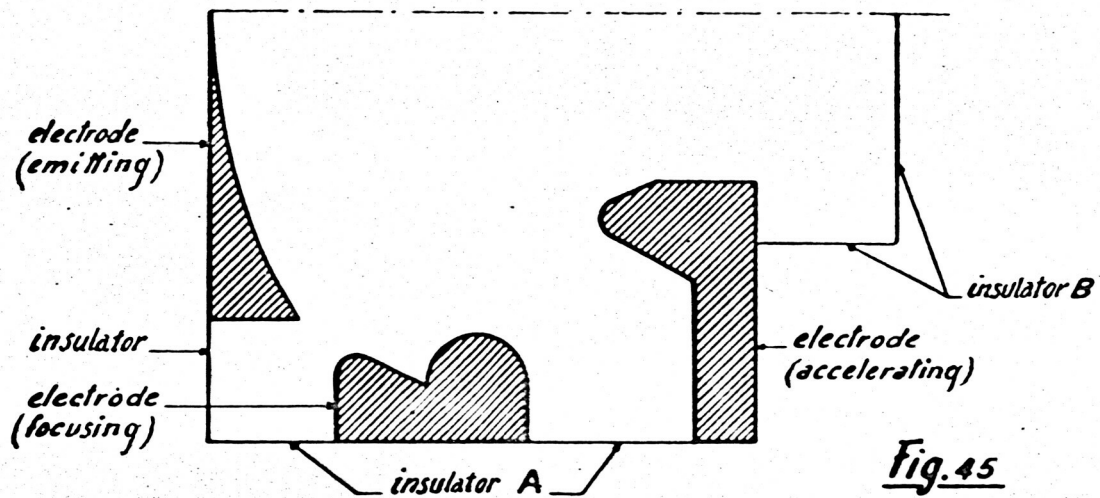


Fig. 45



Fig. 44

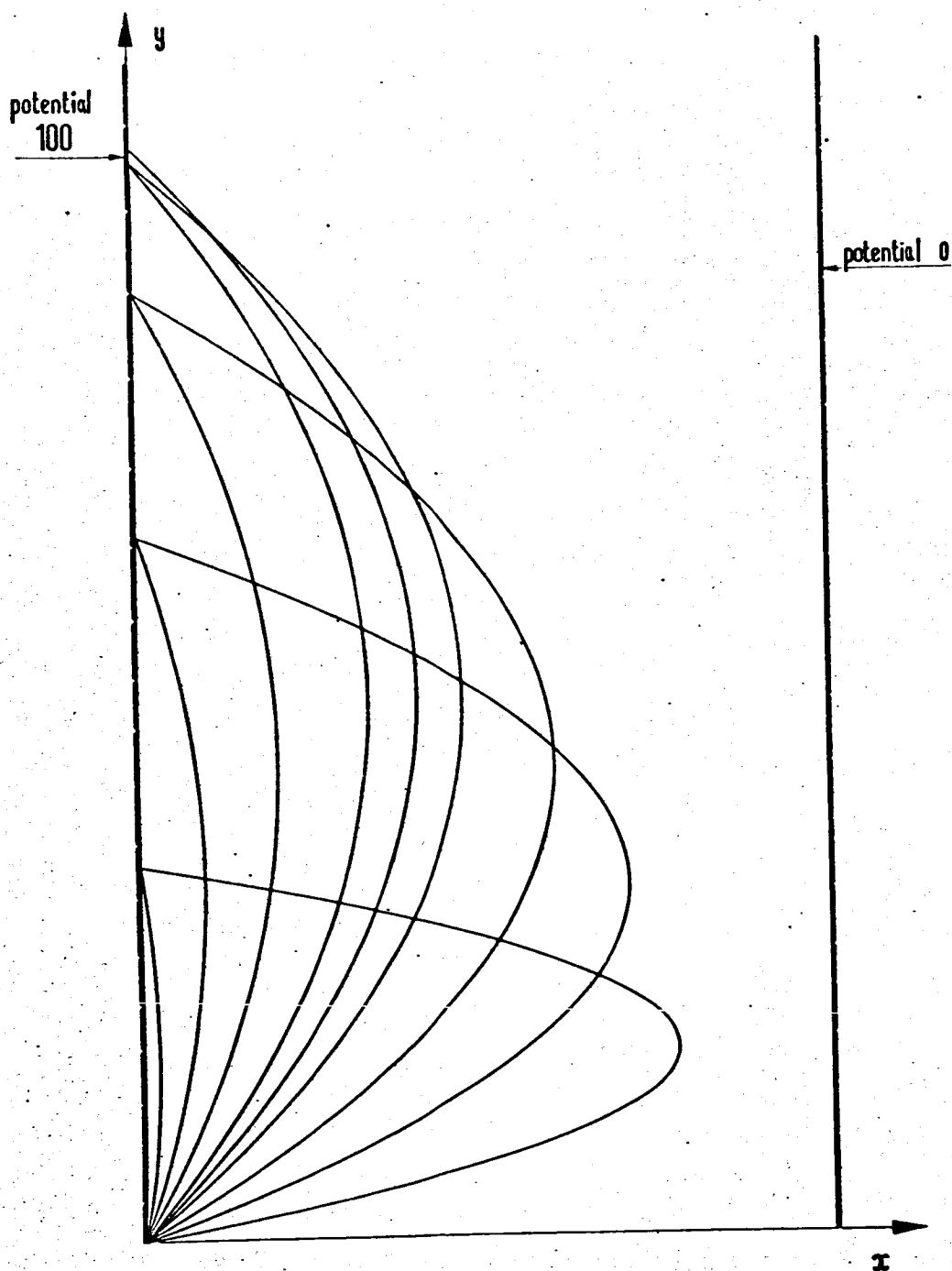


Fig. 46

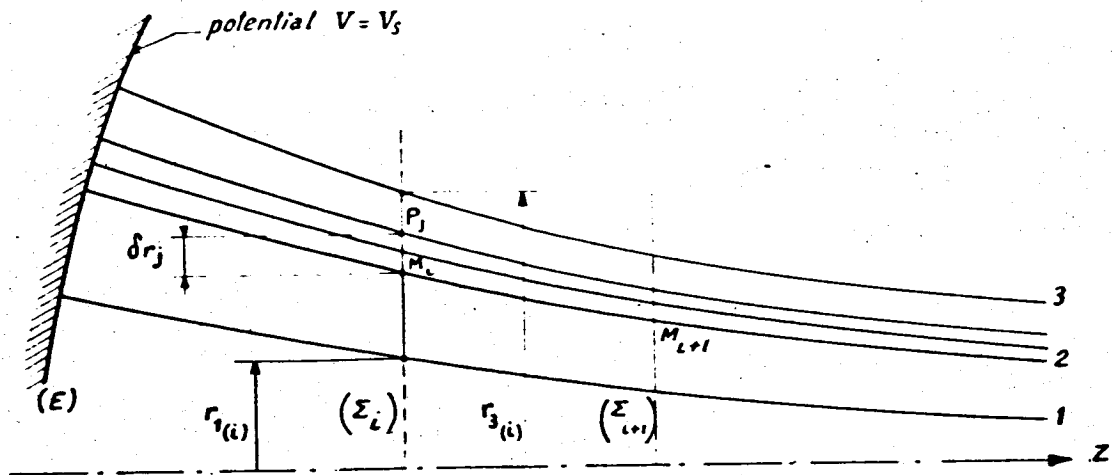


Fig. 47

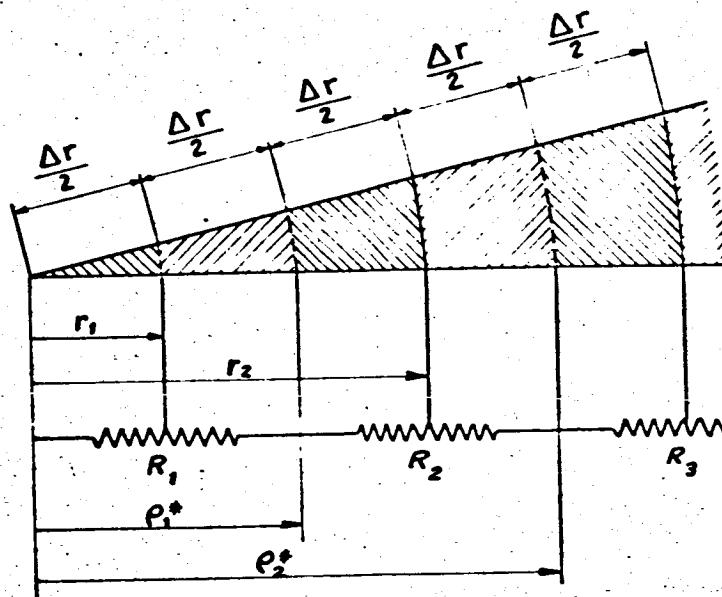
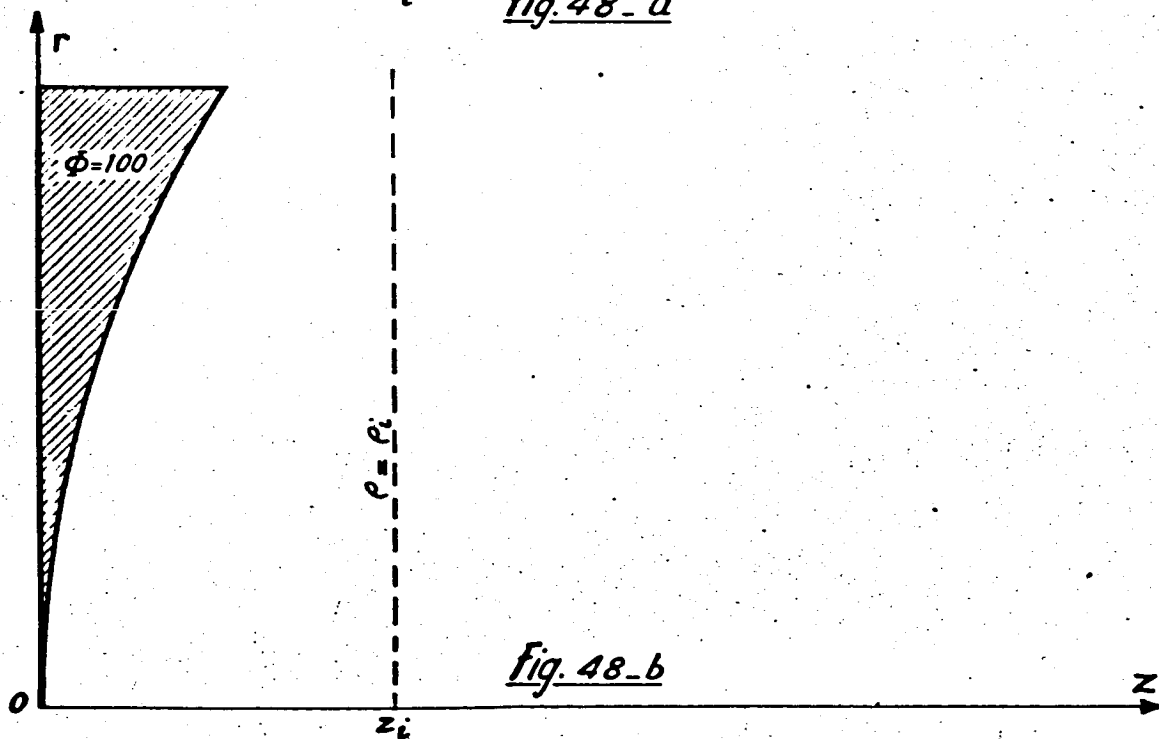
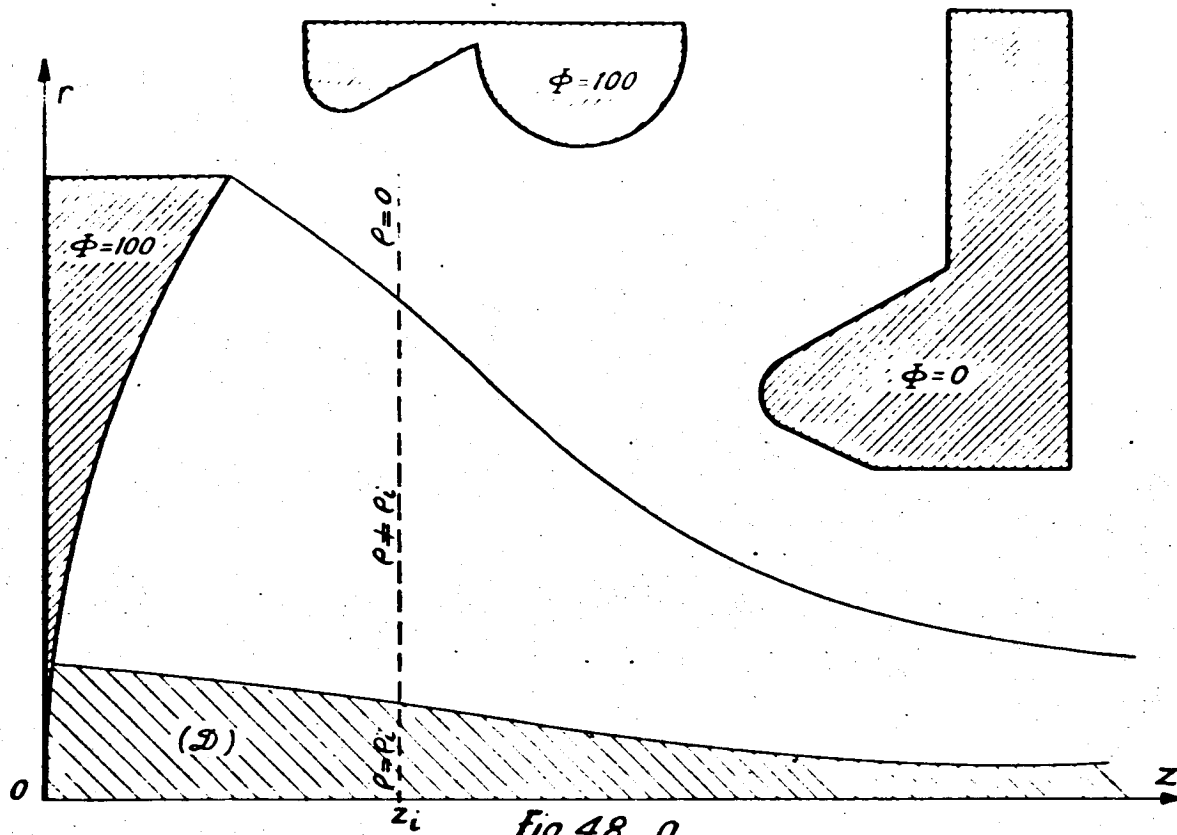
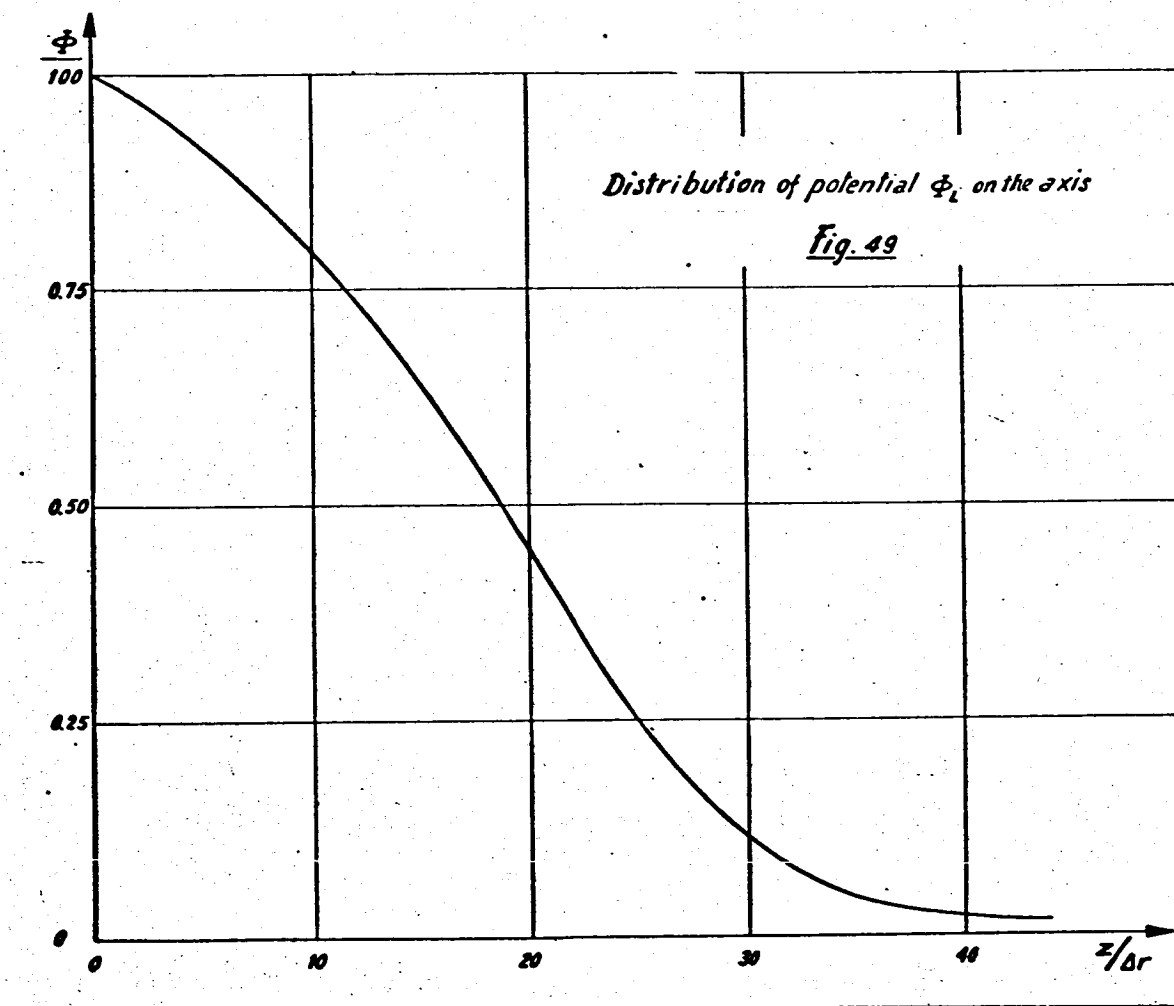


Fig. 50





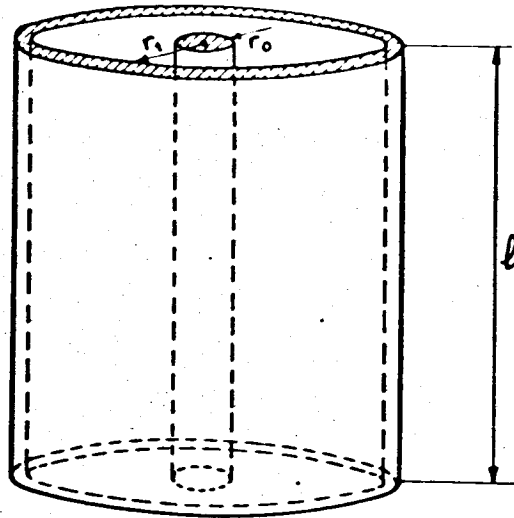


Fig. 51

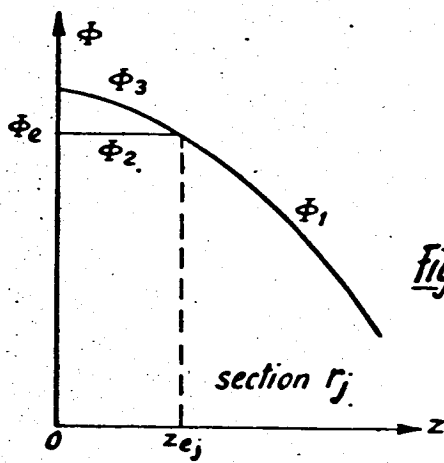


Fig. 52

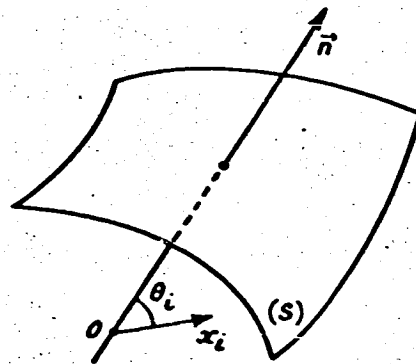
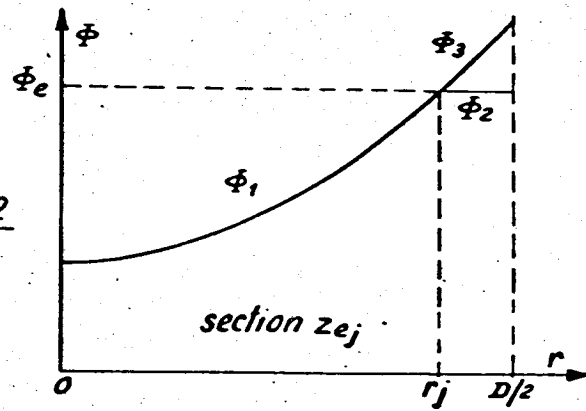


Fig. 53

Note Technique n° 73 -

Office National d'Etudes et de Recherches Aérospatiales.
ASSOCIATION DU RESEAU ELECTRIQUE ET DES
CALCULATRICES ARITHMETIQUES POUR LA
DETERMINATION DES TRAJECTOIRES ELECTRO-
NIQUES. APPLICATION A LA PROPULSION IONI-
QUE, par Christian LERIN, Octobre 1963, 167 p.,
53 fig., 16 tabl.

Dans un propulseur ionique la détermination des trajectoires des particules issues de l'électrode émettrice est nécessaire pour définir les performances et apporter les modifications éventuelles à la disposition relative des électrodes. Pour résoudre ce problème, une méthode de calcul itératif associant calcul analogique et calcul arithmétique est présentée: le potentiel électrique à l'intérieur du propulseur est simulé par la tension d'un réseau de résistances dont les éléments et les conditions aux limites sont

T.S.V.P.



- I. Propulsion ionique
3h 4d 4
2. Calcul analogique:
Applications.
1a 5d 5c

- I. Christian LERIN.
- II. N.T. n° 73 O.N.E.R.A.

Note Technique n° 73 -

Office National d'Etudes et de Recherches Aérospatiales.
ASSOCIATION DU RESEAU ELECTRIQUE ET DES
CALCULATRICES ARITHMETIQUES POUR LA
DETERMINATION DES TRAJECTOIRES ELECTRO-
NIQUES. APPLICATION A LA PROPULSION IONI-
QUE, par Christian LERIN, Octobre 1963, 167 p.,
53 fig., 16 tabl.

Dans un propulseur ionique la détermination des trajectoires des particules issues de l'électrode émettrice est nécessaire pour définir les performances et apporter les modifications éventuelles à la disposition relative des électrodes. Pour résoudre ce problème, une méthode de calcul itératif associant calcul analogique et calcul arithmétique est présentée: le potentiel électrique à l'intérieur du propulseur est simulé par la tension d'un réseau de résistances dont les éléments et les conditions aux limites sont

T.S.V.P.



- I. Propulsion ionique
3h 4d 4
2. Calcul analogique:
Applications.
1a 5d 5c

- I. Christian LERIN.
- II. N.T. n° 73 O.N.E.R.A.

Note Technique n° 73 -

Office National d'Etudes et de Recherches Aérospatiales.
ASSOCIATION DU RESEAU ELECTRIQUE ET DES
CALCULATRICES ARITHMETIQUES POUR LA
DETERMINATION DES TRAJECTOIRES ELECTRO-
NIQUES. APPLICATION A LA PROPULSION IONI-
QUE, par Christian LERIN, Octobre 1963, 167 p.,
53 fig., 16 tabl.

Dans un propulseur ionique la détermination des trajectoires des particules issues de l'électrode émettrice est nécessaire pour définir les performances et apporter les modifications éventuelles à la disposition relative des électrodes. Pour résoudre ce problème, une méthode de calcul itératif associant calcul analogique et calcul arithmétique est présentée: le potentiel électrique à l'intérieur du propulseur est simulé par la tension d'un réseau de résistances dont les éléments et les conditions aux limites sont

T.S.V.P.



- I. Propulsion ionique
3h 4d 4
2. Calcul analogique:
Applications.
1a 5d 5c

- I. Christian LERIN.
- II. N.T. n° 73 O.N.E.R.A.

Note Technique n° 73 -

Office National d'Etudes et de Recherches Aérospatiales.
ASSOCIATION DU RESEAU ELECTRIQUE ET DES
CALCULATRICES ARITHMETIQUES POUR LA
DETERMINATION DES TRAJECTOIRES ELECTRO-
NIQUES. APPLICATION A LA PROPULSION IONI-
QUE, par Christian LERIN, Octobre 1963, 167 p.,
53 fig., 16 tabl.

Dans un propulseur ionique la détermination des trajectoires des particules issues de l'électrode émettrice est nécessaire pour définir les performances et apporter les modifications éventuelles à la disposition relative des électrodes. Pour résoudre ce problème, une méthode de calcul itératif associant calcul analogique et calcul arithmétique est présentée: le potentiel électrique à l'intérieur du propulseur est simulé par la tension d'un réseau de résistances dont les éléments et les conditions aux limites sont

T.S.V.P.



- I. Propulsion ionique
3h 4d 4
2. Calcul analogique:
Applications.
1a 5d 5c

- I. Christian LERIN.
- II. N.T. n° 73 O.N.E.R.A.

ajustés tandis que les trajectoires et la charge d'espace sont définies à partir de la répartition de potentiel à l'aide d'une machine numérique.
Après avoir vérifié le principe de la méthode sur un exemple calculable analytiquement une forme parti- culière de propulseur à symétrie axiale est traitée.



ajustés tandis que les trajectoires et la charge d'espace sont définies à partir de la répartition de potentiel à l'aide d'une machine numérique.
Après avoir vérifié le principe de la méthode sur un exemple calculable analytiquement une forme parti- culière de propulseur à symétrie axiale est traitée.



ajustés tandis que les trajectoires et la charge d'espace sont définies à partir de la répartition de potentiel à l'aide d'une machine numérique.
Après avoir vérifié le principe de la méthode sur un exemple calculable analytiquement une forme parti- culière de propulseur à symétrie axiale est traitée.



ajustés tandis que les trajectoires et la charge d'espace sont définies à partir de la répartition de potentiel à l'aide d'une machine numérique.
Après avoir vérifié le principe de la méthode sur un exemple calculable analytiquement une forme parti- culière de propulseur à symétrie axiale est traitée.



Technical Note N. 73 -

Office National d'Etudes et de Recherches Aéronautiques,
THE ASSOCIATION ELECTRICAL NETWORK-
DIGITAL COMPUTERS FOR THE DETERMINATION
OF ELECTRON TRAJECTORIES. APPLICATION
TO IONIC PROPULSION, by Christian LERIN, Oct.
1963, 167 p., 53 fig., 16 tabl.

In an ionic propulsor it is necessary to determine the trajectories of the particles from the emission electrode to define the efficiency and to modify, if necessary, the relative configuration of the electrodes. For this, an iterative method associating analog and digital computers is presented: the electrical potential inside the propulsor is simulated by the voltage of a resistance network whose boundary conditions and elements are adjusted, while the trajectories and the space charges are defined from the potential distribution by means of a digital computer.

(over)

1. Ionic propulsion

3h 4d 4

2. Analog computation :
Applications.

1a 5d 5c

I. Christian LERIN.

II. T.N. N. 73 O.N.E.R.A.



Technical Note N. 73 -

Office National d'Etudes et de Recherches Aéronautiques,
THE ASSOCIATION ELECTRICAL NETWORK-
DIGITAL COMPUTERS FOR THE DETERMINATION
OF ELECTRON TRAJECTORIES. APPLICATION
TO IONIC PROPULSION, by Christian LERIN, Oct.
1963, 167 p., 53 fig., 16 tabl.

In an ionic propulsor it is necessary to determine the trajectories of the particles from the emission electrode to define the efficiency and to modify, if necessary, the relative configuration of the electrodes. For this, an iterative method associating analog and digital computers is presented: the electrical potential inside the propulsor is simulated by the voltage of a resistance network whose boundary conditions and elements are adjusted, while the trajectories and the space charges are defined from the potential distribution by means of a digital computer.

(over)

1. Ionic propulsion

3h 4d 4

2. Analog computation :
Applications.

1a 5d 5c

I. Christian LERIN.

II. T.N. N. 73 O.N.E.R.A.



Technical Note N. 73 -

Office National d'Etudes et de Recherches Aéronautiques,
THE ASSOCIATION ELECTRICAL NETWORK-
DIGITAL COMPUTERS FOR THE DETERMINATION
OF ELECTRON TRAJECTORIES. APPLICATION
TO IONIC PROPULSION, by Christian LERIN, Oct.
1963, 167 p., 53 fig., 16 tabl.

In an ionic propulsor it is necessary to determine the trajectories of the particles from the emission electrode to define the efficiency and to modify, if necessary, the relative configuration of the electrodes. For this, an iterative method associating analog and digital computers is presented: the electrical potential inside the propulsor is simulated by the voltage of a resistance network whose boundary conditions and elements are adjusted, while the trajectories and the space charges are defined from the potential distribution by means of a digital computer.

(over)

O.N.E.R.A. - Technical Note N. 73

The principle of the method is checked with an example analytically computable and then a particular form of axially symmetrical propulsor is treated.



O.N.E.R.A. - Technical Note N. 73

The principle of the method is checked with an example analytically computable and then a particular form of axially symmetrical propulsor is treated.



O.N.E.R.A. - Technical Note N. 73

The principle of the method is checked with an example analytically computable and then a particular form of axially symmetrical propulsor is treated.



Service des Relations Extérieures
et de la Documentation

1. Subject: [redacted]
 2. Re: [redacted]
 3. Date: 11/10/2010
 4. Time: 11:10 AM
 5. Location: [redacted]
 6. Officer: [redacted]
 7. Unit: [redacted]
 8. Vehicle: [redacted]
 9. Witness: [redacted]
 10. Notes: [redacted]

N/envoi du 2.12.63

1 ex. : NOTE TECHNIQUE N° 73 :

: Association du réseau électrique et des calculatrices arithmétiques
: pour la détermination des trajectoires électroniques
: Application à la propulsion ionique, par Ch. LERIN